Modeling and Design of Novel Bioreactors and Fermentation Processes

Kold, David; Hobley, Timothy John

Publication date:
2010

Document Version
Publisher's PDF, also known as Version of record

Study of Mass Transfer in Viscous Fermentations

- using a Rotating Jet Head Mixing System

David Kold

Ph.D. Thesis

April 2010

Center for Microbial Biotechnology

Department of Systems Biology

Technical University
of Denmark

Study of Mass Transfer in Viscous Fermentations

- using a Rotating Jet Head Mixing System

David Kold
PhD Thesis

Center for Microbial Biotechnology
Department of Systems Biology

Frontpage: Broth from two Aspergillus oryzae fermentations.
Left: Fermentation conducted in a Rotating Jet Head fermenter system.
Right: Fermentation conducted in a impeller mixed tank

ISBN-9788791494918

Printed in Denmark by
WWW.FRYDENBERG.DK
Baldersgade 12 - 16
DK-2200 Copenhagen N

Abstract

Modern industrial biotechnology has paved the way for a range of new bio-based chemicals, food additives, enzymes and pharmaceuticals. However, for many of these products to be economically competitive, the capital and running costs of the production equipment must be kept at a minimum.

In this thesis, the performance of a Rotary Jet Head mixing system (model IM15 from ISO-MIX optimised for fungal broth) is evaluated as the sole means of mixing and mass transfer during a range of different aerobic fermentations with viscous broths. In contrast to traditional impeller mixed fermenters, mixing in the Rotary Jet Head system is achieved by recirculation of the fermentation broth from the bottom of the tank, through an external loop and back into the tank through the four nozzles of the rotating Jet Head. Air and substrates can be introduced immediately prior to the jet head ensuring that they are rapidly dispersed into the bulk liquid. The need for an impeller with a drive shaft and motor as well as sparging in the tank bottom is thus eliminated.

The mixing and mass transfer capabilities of a given fermentation setup are highly dependant on the rheological properties of the broth. A precise, robust and simple method for broth rheology characterisation is therefore needed when evaluating the performance of a mixing system. In this thesis, a range of different rheometers (Cone-Plate, Parallel-Plate, Cone-Plate with gap, two Wide-Gap rheometers, three different Impeller rheometers and an in-line vibrating rod sensor) were tested using both bacterial and fungal fermentation broth in combination with model solutions consisting of different concentrations of xanthan gum. Of the tested rheometers the Cone-Plate with gap (Carrimed CSL 100) gave the most consistent and precise results when using model solutions and non-pelleted fungal broth. However, the setup was susceptible to mycelium pellets and trapped air bubbles. For broth with complex rheological properties, such as sedimenting fungi growing as a mixture of freely dispersed and pelleted mycelium, a large (L/D 60mm/40mm) Impeller rheometer (Haake FL10 vane spindle) was found to be the best suited. The large size was necessary to continuously resuspend the mycelium, but required a sample volume of 1.4L. Frequent sampling is

therefore only possible in large scale fermentations. To facilitate an online measurement of the viscosity and reduce the volume needed for samples, an in-line vibrating rod sensor (Marimex VA-300) was tested. The signal output was found to closely follow the viscosity measured at-line for both fungal and bacterial broths. By combining the on-line and at-line data, a precise and robust method for characterisation of the rheological properties of a fermentation broth was established.

To evaluate the mass transfer capabilities of the Rotary Jet Head mixing system, and whether it could be use for fungal fermentations, its performance was compared to a fermenter of similar size equipped with a set of Intermig impellers during fed-batch *Aspergillus oryzae* fermentations. When using a complex soy based medium, the Rotary Jet Head did not affect the growth rate, average size distribution or intracellular stress levels negatively (estimated based on mRNA transcription data). The Rotary Jet Head did, however, significantly increase the oxygen transfer rate, and was able to reach a k_La approximately 2.4 times higher per kW used than the Intermig system.

In fermentations with a chemically defined minimal medium, a clear difference in mycelium morphology was observed between the two mixing systems. In the Rotary Jet Head fermenter, the fungi grew in a loosely associated mycelium, whereas pellets more than 1mm in diameter could be seen in the reference system. The difference in morphology resulted in a viscosity, in the Rotary Jet Head fermenter, one fourth of that of the impeller mixed system (0.8Pas vs. 3.2Pas, 51h after inoculation). The reduced viscosity facilitated a 20-60% higher dissolved oxygen tension in the broth at half the power input. It was anticipated that the Jet Head would lead to an elevated intracellular stress level in the fungi, but this hypothesis could not be confirmed. On the contrary, the mRNA transcription data indicated elevated levels of stress related genes in the impeller mixed system.

To further characterise the Rotary Jet Head fermenter, batch fermentations with the bacterium *Xanthomonas campestris* were conducted. During the fermentations xanthan gum (a natural emulsifier) was excreted by the cells, thereby increasing the viscosity of the broth. The Jet Head did not affect the maximum growth rate of the cells, which was identical to that found in literature using the same media ($0.13h^{-1}$). Furthermore, the

system was able to sustain a k_La of 0.15s^{-1} at a power input of 1.1kWm^{-3} and an air flow of 0.1VVM. The following correlation for the k_La with the superficial gas velocity (u_s), power input (P_t), volume of the tank (V), viscosity (η_{app}) and a constant (k) was determined:

$$k_L a = k u_s^{0.4} \left(\frac{P_t}{V} \right)^{0.122} \left(\eta_{app} \right)^{-0.8}$$

The equation indicates that the effect of viscosity on the k_La is in the range typically seen for conventional mixed systems (-0.6 to -1). The Rotary Jet Head fermenter is thus able to achieve high k_La values at relatively low power inputs, but the k_La decreases as the viscosity increases, as for impeller mixed systems.

Dansk Resumé

Moderne bioteknologi har skabt mulighed for at producere en række nye bio-baserede kemikalier, fødevareingredienser, enzymer og lægemidler. For mange af disse produkter er det dog nødvendigt at holde investerings- og produktionsomkostningerne på et minimum for at gøre dem økonomisk konkurrencedygtige.

I denne afhandling bliver ydeevnen af et roterende jet-hoved opblandingssystem (model IM15 fra ISO-MIX, optimeret til svampefermenteringer) evalueret, gennem en række aerobe viskøse fermenteringer, hvor systemet bliver brugt som den eneste kilde til opblanding og massetransport. I modsætning til traditionelle fermentorer er der i det roterende jet-hoved opblandingssystem ikke et røreværk. Opblanding sker ved at recirkulere fermenteringsvæsken fra bunden af tanken, gennem et eksternt rør, og tilbage ind i tanken gennem det roterende jet-hoveds fire dyser. Luft og substrat kan blive tilsat umiddelbart før jet-hovedet, hvilket sikrer en hurtig opblanding. Behovet for et røreværk med aksel og motor samt lufttilførsel i tanken bliver derfor elimineret.

Ydeevnen mht. opblanding og massetransport af en given fermentor er i høj grad afhængig af rheologien af fermenteringsvæsken. En præcis, robust og simpel metode til at karakterisere fermenteringsvæskens rheologi er derfor nødvendigt, når ydeevnen af et opblandingssystem skal evalueres. I denne afhandling blev en række forskellige rheometre undersøgt (Kegle-Plade, Parallel-Plade, Kegle-Plade med mellemrum, to forskellige rheometre med et stort mellemrum, tre forskellige røreværk rheometre og en in-line sensor bestående af en ossilerende stav) ved brug af væske fra både bakterie- og svampefermenteringer kombineret med modelopløsninger bestående af forskellige koncentrationer af xanthangummi. Ud af de testede rheometre gav Kegle-Plade med mellemrum modellen (Carrimed CSL 100) de mest konsistente og præcise resultater, når der blev anvendt modelopløsninger og svampefermenteringsvæske uden klumper. Præcisionen af udstyret blev dog kraftigt forringet, når svampemyceliet klumpede sammen, eller når der var luftbobler i fermenteringsvæsken. For fermenteringsvæske med kompleks rheologi, såsom sedimenterende svampe, der voksede som en blanding af frit opløst og sammenfiltret mycelium, var rheometeret opbygget som et røreværk

(Haake FL10, H/D 60mm/40mm) det mest velegnede. Den relativt store størrelse var nødvendig for at undgå, at væsken bundfaldt, men krævede et prøvevolumen på 1,4L. Det er derfor kun muligt at udføre hyppige målinger under storskalafermenteringer. For at muliggøre online målinger af viskositeten og reducere volumen, der blev brugt til prøver, blev en sensor bestående af en ossilerende stav (Marimex VA-300) sat ind i systemet. Udgangssignalet fulgte med stor præcision viskositeten, der blev målt med rheometeret. Ved at kombinere dataene var det muligt at udvikle en præcis og robust metode til at karakterisere de rheologiske egenskaber af fermenteringsvæske.

For at kunne evaluere massetransporten i det roterende jet-hoved system, og bedømme hvorvidt det kunne bruges til svampefermenteringer, blev ydeevnen sammenlignet med en fermentor af lignende størrelse udstyret med et intermig røreværk under fed-batch fermenteringer af *Aspergillus oryzae*. Når der blev brugt et kompleks sojabaseret medie, påvirkede brugen af det roterende jet-hoved ikke vækstraten, den gennemsnitlige størrelsesfordeling eller det intracellulære stressniveau (målt vha. mRNA transskriptionsdata) negativt. Det roterende jet-hoved forøgede derimod ilttransporten og var i stand til at nå en k_La ca. 2,4 gange højere per forbrugt kW i forhold til Intermig systemet.

Under fermenteringer med et kemisk veldefineret minimalmedie, kunne der observeres en klar forskel i morfologien af myceliet mellem de to opblandingssystemer. I det roterende jet-hoveds fermentor voksede svampen som løst associerede mycelium, hvorimod der blev set hårde klumper på mere end 1mm i referencesystemet. Forskellen i morfologi resulterede i, at viskositeten i det roterende jet-hoveds fermentor var en fjerdedel af systemet med røreværk (0.8Pas mod 3.2Pas 51 timer efter inokulering). Den reducerede viskositet muliggjorde en 20-60% højere iltmætning i væsken selv ved det halve energi-input. Det var forventet, at jet-hovedet ville forårsage et forhøjet stressniveau i svampecellerne, men teorien blev ikke bekræftet. Tværtimod indikerede mRNA transskriptionsdataen, at svampene i systemet med røreværket udtrykte flere stressrelaterede gener.

For yderligere at karakteriserer fermentoren med det roterende jet-hoved blev der foretaget en række batch-fermenteringer med bakterien *Xanthomonas campestris.*

Under fermenteringerne udskiller cellerne xanthangummi (et naturligt fortykningsmiddel), hvilket øger viskositeten af væsken. Jet-hovedet påvirkede ikke den maksimale vækstrate, som blev fundet til at være identisk med værdier fra litteraturen (0.13 per time). Endvidere var systemet i stand til at opretholde en k_La på 0,15s^{-1} ved et energi input på 1,1kWm^{-3} og et luftflow på 0.1VVM. Den følgende korrelation mellem k_La og superficial gas velocity (u_s), energi-input (P_t), volumen af tanken (V), viskositeten (η_{app}) og konstanten (k) blev bestemt.

$$k_L a = k u_s^{0.4} \left(\frac{P_t}{V} \right)^{0.122} \left(\eta_{app} \right)^{-0.8}$$

Ligningen indikerer, at effekten af stigende viskositet på k_La er i samme område som for konventionelle opblandingssystemer (fra -0,6 til -1). Det roterende jet-hoved er således i stand til at levere en høj k_La ved et forholdsvist lavt energiforbrug, men når viskositeten stiger, falder k_La i samme grad som for opblandingssystemer med et røreværk.

Preface

In this thesis, the main results from my Ph.D. project carried out in the period February 2006 to March 2009 are presented. The majority of the work, consisting of approximately 24 pilot scale fermentations, was conducted at the Center for Microbial Biotechnology, Department of Systems Biology, Technical University of Denmark, and in part at the pilot plant facilities of Chr. Hansen A/S (Nienburg, Germany) and Novozymes A/S (Bagsværd, Denmark). The study was financed by the research consortium "Innovative Bioprocess Technology" comprised of the Technical University of Denmark, Chr. Hansen A/S, Novozymes A/S, Danisco A/S and the Danish Research Council for Technology and Production (FTP).

During my Ph.D. study, I have received help and good advice from numerous people. I would especially like to thank my supervisors, Timothy John Hobley, for his support throughout the project, and Karsten Hellmuth, who was my external supervisor during the majority of the project.

I am also grateful for the help I received from my other supervisors from Chr. Hansen A/S. Henrik Rømer, who supervised the initial phase of the project. Susanne Grøn is also thanked for taking over the role as external supervisor after Henrik. Her engagement and interest, which continued throughout the project, was of great help, both in form of good advice and in tackling practical challenges.

I would also like to thank the staff at the pilot plant of Chr. Hansen A/S in Nienburg, who made my stay during a cold wet winter an enjoyable experience.
Stuart Michael Stocks from Novozymes A/S for his advice and guidance concerning the complex matter of determining broth rheology.
Mikkel Nordkvist from ISO-MIX A/S (now a part of Alfa Laval) for practical advice with the Rotary Jet Head and the lending of equipment.
Peter Stubbe for help with the initial programming of the control unit of the fermenter system.

Master student Mikkel Adolph, who did some of the initial *Xanthomonas campestris* test fermentations.
Claus Lindvald Johansen from Danisco A/S for practical advice on running pilot scale *Xanthomonas campestris* fermentations.
Hans van den Brink from Chr. Hansen A/S for providing transcriptome data from two *Aspergillus niger* fermentations.

Also tanks to Linda Lehmann for her great help during the sample preparation and mRNA extraction, and also her bachelor student Tilde Jordal's assistance during the *Trichoderma reesei* fermentation.
Mikael Rørdam Andersen for his extensive help with the analysis of the transcriptome data, his quirky sense of humour and numerous cups of life saving coffee during my long fermentations.

All of my other great colleagues at the Center for Microbial Biotechnology for contributing to providing an inspiring and welcoming atmosphere making my time (even the weeklong fermentations non-stop at DTU) both interesting and enjoyable.

And last, but not least, my family, friends and fiancée for showing extraordinary patience and support during all phases of the project.

David Kold

Copenhagen, 2010

Nomenclature

Roman Letters

a	specific intercaial area	m^2m^{-3}
c	Impeller constant	-
c(x)	Concentration of x	mol l^{-1}
c*	Equilibrium Concentration	mol l^{-1}
D	Diameter	m
D_R	Impeller diameter	m
F_g	Gas flow	Mol s^{-1}
h	Height	m
K	Consistency index	Ns^nm^{-2}
k	Constant	-
k_L	Mass transfer coefficient for liquid film	-
k_La	Volumetri mass transfer coeficient	
L	Length	m
M	Torque	Nm
n	Power-law index	-
N	Rotation speed	RPS
$\mathbf{N_{FI}}$	Flow number	
N_P	Power Number	-
P	Power input	W
p	Pressure	bar
Po	Power number	
q	Volumetric rate	mol l^{-1} h^{-1}
Q_{GV}	Gas flow rate	VVM
Q_i	Impeller liquid pumping rate	m^3 s^{-1}
Q_L	Flow	Kg s^{-1}
r	Radius / rim	m / -
R	Ideal Gas Constant	J K^{-1} mol^{-1}

r(x)	Specific production rate of x	mol h^{-1}
Re	Reynolds number	-
T	Temperature	K
t_c	Circulation time	s
u_s	Superficial gas velocity	M s^{-1}

Greek Letters

α	Exponent factor	-
β	Exponent factor	-
$\dot{\gamma}$	Shear rate	s^{-1}
$\dot{\gamma}_a$	Average shear rate	s^{-1}
η	Viscosity	Pa s
η_a	Apparent viscosity	Pa s
θ_0	Gap angle	rad
ρ	Density	kg m^{-3}
ρ_a	Average density	kg m^{-3}
τ	Shear stress	Pa
τ_0	Yield stress	Pa
Ω	Angular velocity	rad s^{-1}
ω	Exponent factor	-

Subscripts

i	Impeller
I	Inner
O	Outer

Contents

Chapter 1

Introduction

Chapter 1

Introduction

Over the last decades, highly efficient enzyme producing *Aspergillus* and *Trichoderma* strains have been engineered, able to secrete more than $30gL^{-1}$ enzyme during a fermentation.[1] To achieve these high yields at a fast production rate requires bioreactors with high mass and heat transfer capacities, which may prove difficult and highly energy consuming in traditional industrial impeller mixed fermenters; especially during fermentations with viscous broths. For industrial processes with a "low value added" end-product, the expenses from energy consumption used for mixing must be kept at a minimum to lower the production costs. These conflicting requirements drive the quest for new energy efficient fermenter systems.

1.1 Impeller Mixed Fermenters

In a fermenter, the agitation of the broth has multiple purposes:

- To keep insoluble particles suspended in the fermentation broth.
- Achieve convective heat transfer by ensuring bulk flow at the cooling coils of the fermenter.
- Reduce the bubble diameter of the sparged air thereby increasing the gas/liquid interface area.
- Disperse components added to the fermenter – e.g. media and acid/base used for pH regulation.
- Blend the content of the fermenter to ensure uniform conditions.

In most industrial fermenters, the agitation is performed by one or more impellers. A large variety of different impellers have been developed for different mixing tasks; for detailed descriptions see bioreactor engineering textbooks such as Nielsen et al. [2] or equipment reviews e.g. Nienow [3] . The majority of the impellers can be divided in two main categories: the 'axial and mixed flow' and the 'radial flow' impellers. The axial and mixed flow impellers, such as the Pitched blade or Intermig impeller, are suited for particle suspensions and high volume flow. For fermentations where a high convective flow is important, e.g. due to heat transfer or to suspend particles, these types of impellers are efficient. The energy dissipation region of a radial flow impeller is small

compared to that of an axial or mixed flow impeller, which results in large velocity gradients in the broth. As the bubble/droplet size in a fluid is dictated by these velocity gradients, the radial flow impellers, such as the Rushton turbine, are commonly used in fermentations where gas dispersion and fast local mixing of substances added to the fermenter are important.[4] The performance of the different impeller types are significantly affected by the viscosity of the broth, and as the viscosity of the broth may increase significantly during a fermentation, an impeller suitable for mixing of the broth in the beginning of the fermentation may prove inefficient at the end. Apart from changing viscosity, the requirements in terms of mass and heat transfer often changes during a fermentation, and the choice of impeller is therefore often a compromise of several conflicting performance requirements. [3, 5] The effect of changing viscosity during a fermentation will be described in detail in later chapters. During oxygen transfer limited fermentations, special care must be taken when choosing impeller type, as the system ideally should promote both mixing and bubble break up.

Essential for choosing the right impeller for a given process is the power number 'Po' and Reynolds number 'Re' for the impeller.

The power number for an impeller can be calculated using equation 1.1.

$$Po = \frac{P}{\rho_a N^3 D_R^5} \qquad \textbf{Eq. 1.1}$$

Where P is the power dissipated by the impeller, ρ_a is the average broth density, N is the impeller speed and D_R is the impeller diameter. P is highly dependent of the liquid properties, impeller type and dimensions. Due to the differences in P for different impellers the Po varies from impeller to impeller as illustrated in table 1.1.

Table 1.1: Power number for four impellers under turbulent flow regime. Adapted from Nienow [3].

Impeller type	Po
Rushton turbine (6 blade)	5.2
Scaba (3 blade)	1.70
Pitch blade turbine (6 blade , 45 °)	1.45
Intermig (per stage)	0.31

The Reynolds number can be use to identify in which regime mixing is taking place. Generally Re>10^4 is characterised as turbulent flow, where rapid mixing occurs. If the Re drops below 10, laminar flow dominates severely impairing the mixing of the system. For 10<Re<10^4 is defined as Transitional flow. [2]

The Reynolds number for an impeller mixed system is affected by the properties of the liquid in the vessel (liquid density and apparent viscosity 'η_a'), the impeller diameter, and impeller rotation speed, as demonstrated in equation 1.2.

$$\mathrm{Re}_a = \frac{\rho_a N D_R^2}{\eta_a} \qquad \textbf{Eq. 1.2}$$

From equation 1.2 it is evident that the liquid viscosity is a key component when looking for reasons for impaired mixing during a fermentation. The effect and a detail method for determining the apparent viscosity will be presented in chapter 2.

1.2 Mixing with Jets

Stationary jets are a well known low power input alternative for mixing in large tanks. [4, 6] Jets are mainly used in waste water treatment and in storage tanks to avoid stratification. In contrast to traditional impellers, where the liquid flow is mediated by the movement of the impeller, the main mixing with jets is caused by the jet stream as it entrains fluid at the boundaries of the stream forming eddies. The jet stream is achieved by recirculation of the fermentation broth through an external loop and back into the liquid. For stationary jet systems the flow patterns are constant which may lead to stagnant zones in the tank resulting in compartmentalization and poor mixing in the tank.[4] To avoid these stationary flow patterns, a novel mixing system with rotating jets has been developed by the Danish company ISO-MIX A/S.

1.3 The Rotary Jet Head System

The Rotary jet head (RJH) mixing system was patented by Hummer [7] and was developed based on a fermenter tank 'cleaning in place' (CIP) machine produced by Toftejorg, Denmark. The first thorough characterisation was conducted by Nordkvist [8]. The system has found a range of mixing applications especially within the food and beverage industry. [9]

Mixing in the RJH system is achieved, as for traditional stationary jet mixing systems, by recirculation of the fermentation broth through an external loop. The broth is pumped out from the bottom of the tank and fed back through the four nozzles of the RJH. A simplified schematic model of the RJH system can be seen in figure 1.1 where the green arrows indicate the direction of the liquid flow.

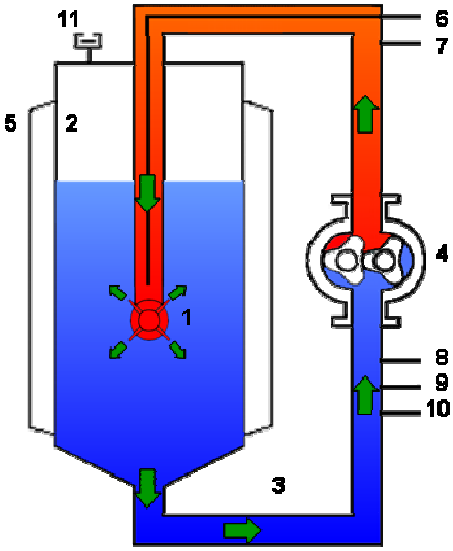

Figure 1.1:
Simplified model of a Rotary jet head mixing system. The green arrows indicate liquid flow.

1: Rotary jet head
2: Fermenter tank
3: Recirculation loop
4: Lobe pump
5: Cooling jacket
6: Feed inlet tube
7: Gas inlet
8: Base inlet
9: Acid inlet
10: Antifoam inlet
11: Gas exhaust.

As the recirculated fermentation broth is distributed by the four nozzles of the RJH into the tank, the liquid drives a small turbine. The force from the turbine is used to power a horizontal rotation of the system and a vertical rotation of the distributor arms, see figure 1.2. As the horizontal rotation speed is slightly lower than in the vertical axis (43/45), the directions of the four jet streams continuously change direction, thereby avoiding compartmentalization and development of a stationary flow field in the tank.

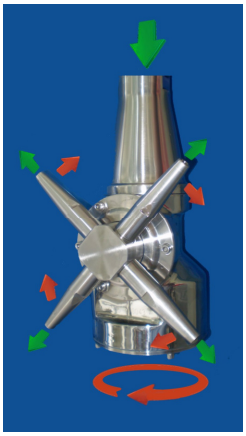

Figure 1.2: RJH of the type IM15 with 7mm nozzles. Green arrows indicate liquid flow, red arrows motion.

The mixing process in the RJH system can be divided into separate mechanisms: A high shear intense mixing zone in the circulation pump and jet head, and the bulk mixing where the jet streams blend the broth. The highly energetic zones are efficient for rapid blending and dispersion of e.g. feed during a fed-batch fermentation or base used for pH control. The RJH system may be especially suited to handle media with particles which sediment rapidly. In the RJH system, liquid and any insoluble particles are continuously removed from the bottom of the fermentation tank and redistributed with the jet nozzles. Using a conical tank will thereby hinder deposits from being formed.

Apart from facilitating heat and mass transfer for the process, the fermenter must also ensure that the cultivation is run under aseptic conditions to avoid contaminations with unwanted microorganisms. For impeller agitated fermenter systems, baffles are often used to break-up laminar flow patterns, and for processes with high conversion rates, internal cooling-coils may be necessary to achieve a sufficiently large interfacial surface. Both baffles and internal cooling coils increase the risk of contamination, as they make efficient cleaning and sterilizing in place (CIP and SIP) difficult. In the RJH system, baffles are not necessary as the liquid flow is continuously changed by the jets. Furthermore, cooling aggregates inside the tank are unnecessary as the heat transfer can be performed using heat exchangers inserted in the recirculation loop.

1.3.1 System Setup

The work presented in this thesis was, if not stated otherwise, conducted in a 310l stainless steel fermenter (see figure 1.3, #2) with a working volume of 200-250l, retrofitted with a RJH mixing system (model IM15 with D=7mm nozzles and isolated gear, ISO-MIX A/S, Denmark). Figure 1.3 is a picture of the fermenter setup used for the work presented in this thesis.

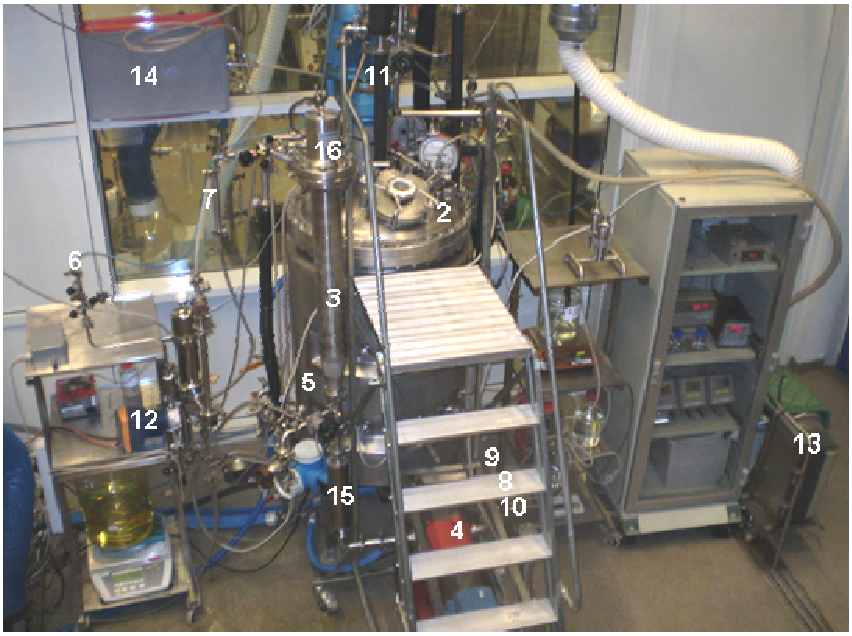

Figure 1.3: The Rotary Jet head system developed as a part of this thesis. 2: Fermenter tank, 3: Recirculation loop, 4: Lobe pump, 5: Cooling jacket, 6: Feed inlet tube, 7: Gas inlet, 8: Base inlet (below stairs), 9: Acid inlet, 10: Antifoam inlet, 11: Gas exhaust, 12: Feed-pump, 13: Frequency-transformer, 14: Gas mass flow controller, 15: Mass flow measurement system, 16: In-line viscosity probe.

The broth was circulated from the bottom of the tank through an external loop (figure 1.3, #3), with a volume of approximately 12L, and back into the fermenter through the RJH, using a stainless steel positive displacement lobe pump (model 3/0054, Johnson Pump, United Kingdom, figure 1.3, #4). The speed of the pump was regulated with a frequency converter (figure 1.3, #13), and the flow rate was measured with a promass 60M mass flow measurement system (Endress + Hauser, Switzerland, figure 1.3, #15). The broth viscosity was measured in-line with a vibrating rod sensor (Marimex VA-300,

Marimex Industries Corp, Canada), placed on the pressure side of the lobe pump. The dissolved oxygen tension (DOT) was measured in three locations in the system; 1. in the loop, 2. at the surface of the tank, 3. approximately 20cm from the tank wall beneath the RJH. If not stated otherwise, the third sensor was used for DOT measurement as Nordkvist *et al.* [10] demonstrated that the mixing in the RJH system was poorest close to the RJH itself.

The system was developed specifically for microbial fermentation, as long fed-batch fermentations necessitate strictly aseptically conditions. Furthermore, special care was taken to facilitate CIP and SIP. pH control and antifoam addition were conducted on the low pressure side of the loop. The inlets were placed shortly before the lobe pump to ensure the acid and base were rapidly mixed into a larger volume of broth by the pump. In this way, stress on the cells due to high pH gradients was minimised, while the low pressure minimised the risk of the tubes connected to the base or acid from being dislodged or ruptured.

The air and feed was added immediately before the RJH resulting in fast and efficient mixing. During fed-batch fermentations, the feed was added using a ProMinent gamma/L solenoid metering pump (GALA 0708PVT, ProMinent Dosiertechnik, Germany, figure 1.3, #12). This pump controlled feed rates unaffected by the pressure in the recirculation loop. The pump speed was monitored and controlled using a computer enabling constant feed rates as well as exponential increasing flows and oxygen saturation controlled flow profiles. The gas flow rate was controlled using a gas mass flow controller (Mass Flow Controller Model 5853 S, Brooks Instruments, United States).

1.3.2 Power Input Calculation

In this thesis the power input for the RJH system has been estimated using two simple methods, partly adapted from Nordkvist [8].

1. As the kinetic energy of the broth as it leaves the jet nozzles
2. As the difference in pressure energy between the loop and the fermenter.

In the kinetic power input model, the kinetic energy of the broth is assumed to fully dissipate in the fermenter, see equation 1.3. Furthermore, the flow velocity of the liquid is assumed to be equal to the average flow velocity in the loop, which is only valid for liquids with uniformly dispersed gas.

$$P_{kin} = \tfrac{1}{2} F_L v^2 \qquad \textbf{Eq. 1.3}$$

Where F_L is the mass flow in kgs^{-1} and v is the flow velocity in ms^{-1} defined as:

$$v = \frac{\frac{F_L}{\rho} + F_g\left(\frac{p_{ferm}}{p_{loop}}\right)}{A_n} \qquad \textbf{Eq. 1.4}$$

Here, ρ is the liquid density in kgm^{-3}, F_g is the gas flow in m^3s^{-1}, p_{ferm} and p_{loop} is the pressure in the headspace of the tank and loop in Pa, and A_n is the total cross section of the nozzles in m^2. As the gas flow or mass flow increases, so does the flow velocity and thus the power input. Unfortunately, the calculated value relies heavily on an exact measurement of the mass flow which can be difficult to obtain in gas/liquid mixed systems. In figure 1.4, the mass flow in the loop of the RJH system is plotted at different pump speeds varying from 60RPM to 420RPM. The average mass flow in the system without any airflow is plotted as black circles (**●**) with the standard variation of the measurement points as error bars. The corresponding average mass flows with a gas flow of $3.76ls^{-1}$, equivalent to 1VVM, are plotted as circles (○), and the mass flow based on the volume displaced per revolution of the pump is plotted as a solid line. From the error bars in the plot, it is evident that the precision of mass flow measurements is significantly reduced as air is added to the system and begins to be drawn back into the recirculation loop. Furthermore, the mass flow, and thereby the pump efficiency, is reduced due to the recirculation of bubbles. Also, when no air is added to the system, the mass flow is close to that displaced by the pump, which indicates an efficient energy transfer.

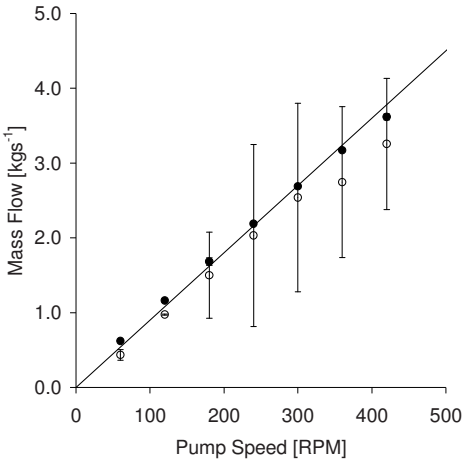

Figure 1.4: Average mass flow at different pump speeds (60-420RMP). F_L with F_g=0; ●. F_L with F_g=3.76ls^{-1}; ○. The line illustrates the volume displaced per revolution of the pump, assuming a liquid density of 1000kgm^{-3}.

Due to the use of equation 1.3 and 1.4, even a slightly inaccurate measurement of the mass flow results in large errors in the calculated power input. The kinetic power input model is therefore only applicable for fermentations without any gas flow.

The 'pressure' power input model is somewhat simpler, and is less vulnerable to inaccurate measurements of the mass flow. In this model, the pressure difference between the loop and the fermenter is assumed to completely dissipate into the broth, see equation 1.5.

$$P_{pump} = \left(p_{loop} - p_{ferm}\right)\frac{F_L}{\rho} \qquad \textbf{Eq. 1.5}$$

As the pressure in the loop increases either due to increased rotation speed of the pump or air flow, so does energy input to the broth. Equation **1.5** thus gives an estimate of the work performed by the pump, which can be compared to the torque measured on the shaft of a traditional impeller mixed fermenter. These values can be used when comparing the power consumptions of the RJH fermenter with other systems.

When inserting the measured pressures with their resulting mass flows in equation 1.3 and 1.5, the power input from the pump can be determined, see figure 1.5. In the figure, the power input at different pump speeds are plotted: pressure model, circles (without

gas flow ●, with gas flow of 3.76ls^{-1} ○), kinetic model, squares (without gas flow ■). From the figure, it can, not surprisingly, be seen that the power input calculated both with the kinetic model and the pressure model increases with the pump speed. Furthermore, sparging with gas results in an increased power input as the pressure in the loop increases. It can also be deduced from the plot that, at the flow rates and viscosity investigated, the recirculating air bubbles do not significantly reduce the efficiency of the pump.

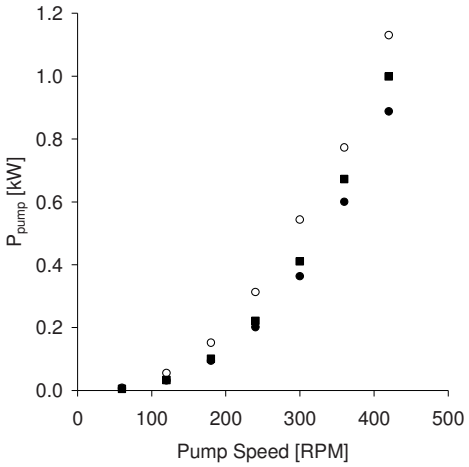

Figure 1.5 Power input at different pump speeds (60-420RMP) calculated using equation 1.3 and 1.5 assuming a liquid density of 1000kgm^{-3}. P(kinetic model), ■; P(pressure model, without gas flow), ●; P(pressure model, without gas flow), ○.

Apart from the energy added to the loop, the gas sparged into the fermenter also contributes to the total power input. The power input from the air was estimated as an isothermal expansion of the gas flow (F_g) from pressure at the air inlet (p_i) to the pressure in the head space of the tank (p_{ferm}) as in a traditional impeller mixed fermenter described by Cooke [11], see equation 1.6.

$$P_g = F_g RT \ln \frac{p_i}{p_{ferm}} \qquad \textbf{Eq. 1.6}$$

Here, R is the ideal gas constant and T is the temperature in Kelvin. The total power can thus be calculated by summing up the power input from the loop and the gas, see equation 1.7.

$$P_{RJH} = P_g + P_{pump} \qquad \text{Eq. 1.7}$$

Equation 1.7 was used to estimate the power input of the RJH system throughout this thesis if not stated otherwise.

The maximum Reynolds number for the RJH was assessed to be in the jet nozzles, and the Reynolds number for each of the 4 nozzles was therefore estimated using equation 1.8.

$$\mathrm{Re}_{RJH} = \frac{\rho_a v D}{\eta_a} \qquad \textbf{Eq. 1.8}$$

Where D is the hydraulic diameter of the nozzle.

1.4 References

1. Gouka, R.J., P.J. Punt, and C.A.v.d. Hondel, *Efficient production of secreted proteins by Aspergillus: progress, limitations and prospects.*, in *Applied Microbiology and Biotechnology*. 1997, Springer-Verlag. p. 1.
2. Nielsen, J., J. Villadsen, and G. Lidén, *Bioreaction Engineering Principles*, ed. 2. 2003, New York: Kluwer Acedemic/Plenum Publishers. 528.
3. Nienow, A.W., *Hydrodynamics of Stirred Bioreactors.* Applied Mechanics Reviews, 1998. **51**(1): p. 3.
4. BHR-Group, *Improving Mixing Processes (Course Notes)*. 2008, BRG Group.
5. Amanullah, A., et al., *The influence of impeller type in pilot scale Xanthan fermentations.* Biotechnology and Bioengineering, 1998. **57**(1): p. 95-108.
6. Zaidi, A., et al., *Xanthan production in a plunging jet reactor*, in *Applied Microbiology and Biotechnology*. 1991. p. 330.
7. Hummer, J.S., *A method and a process plant for treating a batch of liquids*, W.I.P. Organization, Editor. 2002.
8. Nordkvist, M., *Mixing and mass transfer by rotating jets: Fundamentals and applications*, in *BioCentrum-DTU*. 2005, Technical University of Denmark: Kgs. Lyngby. p. 151.
9. www.ISO-MIX.com, *www.iso-mix.com*. 2010.
10. Nordkvist, M., et al., *Mixing by rotary jet heads: Indications of the benefits of head rotation under turbulent and transitional flow conditions.* Chemical Engineering Research and Design, 2008. **86**(12): p. 1454.
11. Cooke, M., J.C. Middleton, and J. Bush, *Mixing and mass transfer in filamentous fermentations.* King R (ed) 2nd Int. Conf. on Bioreactor Fluid Dynamics, 1988: p. 37–64.

Chapter 2

Rheological Characterization of Fermentation Broths

Chapter 2

Rheological Characterization of Fermentation Broths

2.1 Introduction

During the time course of a fermentation, the rheological properties of the broth may change significantly as biomass increases, morphology changes and medium components are depleted. As discussed in the previous chapter, increased viscosity results in longer mixing times (lower Re), which may cause undesirable nutrient and oxygen concentration gradients. Thus, in insufficiently mixed fermentations, the microorganisms may experience nutrient or oxygen starvation in some zones of the tank, reducing the overall efficiency of the fermenter.[1] In the case of fed-batch fermentations, poor mixing can result in high nutrient concentrations near the feed inlet, which may lead to unwanted overflow metabolism or catabolite repression. [1-3] When the viscosity increases, the broth becomes more coalescing further limiting the oxygen transfer due to a reduced gas-liquid interfacial area.[1] Good mixing is also essential for efficient heat transfer. In viscous fermentations, stagnant zones are prone to form in regions with low shear rate, such as behind cooling aggregates and in the periphery of the tank. In these zones, the broth can come to a complete standstill severely limiting heat transfer.[1, 2] As mass and heat transfer are often the limiting parameters in fermentation processes, changes in the rheological properties of the fermentation broth may significantly impair the overall performance of the bioreactor. An accurate description of the broth rheology is therefore necessary when evaluating data from different fermentations. However, determining the rheological properties of a fermentation broth may not be a trivial task. Fungal fermentations are especially challenging due to the presence of large pellets which have a tendency to settle and the shear thinning properties of the broth.

In light of the above, and given the general objectives of this thesis to characterise mixing and mass transfer during fungal and bacterial fermentations, several methods for broth rheology characterization are described and evaluated experimentally in this

chapter. The methods are compared with respect to precision, robustness and complexity, in order to develop an easily applicable method for broth characterization. A number of different types of broths were used and were obtained from *Aspergillus oryzae* fermentations with or without pellet formation, *Aspergillus niger*, *Trichoderma reesei* as well as from the exopolysaccharide producing bacterium *Xanthomonas campestris*. It was concluded that a combination of in-line measurements with a Marimex VA-300 vibrating rod sensor and at-line data from a Haake FL10 vane spindle rheometer gave a precise and robust method for determining the rheological properties of the various shear thinning fermentation broths examined.

2.2 Theory

2.2.1 Viscosity and Rheological Models

The viscosity η of a fluid can be described as the relationship between the shear stress τ and a velocity gradient (shear rate) $\dot{\gamma}$ of a fluid as written in equation 2.1:

$$\tau = \eta \dot{\gamma} \qquad \textbf{Eq. 2.1}$$

The rheological properties of Newtonian and most non-Newtonian fluids can be described by equation 2.2.

$$\tau = \tau_0 + K(\dot{\gamma})^n \qquad \textbf{Eq. 2.2}$$

Where, τ_0 is the yield stress, K is the consistency index, and n is the flow behaviour index. For Newtonian fluids (n= 1 and τ_0= 0) e.g. non-shear thinning bacterial fermentations, the viscosity is constant (K= η) and can be readily measured using a conventional rheometer. However, fermentation broths are often highly non-Newtonian (n ≠ 1 and/or $\tau_0 \neq$ 0), hence the viscosity is a function of the shear rate. The shear dependent viscosity is often called the shear viscosity or apparent viscosity η_a.[2] Fluids with non-Newtonian flow behaviour can be divided into two subgroups; fluids which can be described by the two-parameter model of Ostwald and de Waele (power-law fluids) and fluids with a yield point, as defined in equations 2.3-2.6 and shown schematically in figure 2.1.

	With respect to equation 2.2		
Power-law fluids	$n \neq 1$ and $\tau_0 = 0$		
Dilatant	$n > 1$	$\tau = K(\dot{\gamma})^n$	**Eq. 2.3**
Pseudoplastic	$n < 1$	$\tau = K(\dot{\gamma})^n$	**Eq. 2.4**
Fluids with yield point	$\tau_0 > 0$		
Bingham plastic	$\tau_0 > 0$ and $n = 1$	$\tau = \tau_0 + K(\dot{\gamma})$	**Eq. 2.5**
Pseudoplastic with yield point	$\tau_0 > 0$ and $n \neq 1$	$\tau = \tau_0 + K(\dot{\gamma})^n$	**Eq. 2.6**

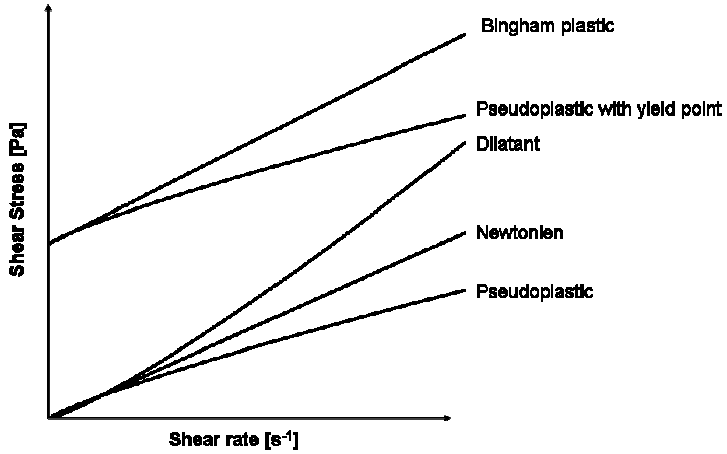

Figure 2.1: Representation of the behaviour of liquids according to 5 different models

Dilatant or shear thickening broths can be encountered when working with mediums containing high concentrations of small insoluble particles such as corn starch.[2, 4] When the shear rate is increased (e.g. during fermenter start-up), this type of flow behaviour can cause the broth viscosity to abruptly increase as much as two or three orders of magnitude.[2, 4] The increase in viscosity affects power consumption and causes strain on the shaft, gear and motor of the fermenter. A low shear mixing system is therefore preferable when working with dilatant fluids. In many shear thickening liquids, a certain amount of mixing is needed to avoid sedimentation or to draw down

floating particles. A rheological characterisation of the medium is therefore important to ensure the fermenter setup is able to handle the maximum stress encountered during the fermentation.

Fermentation broths are often shear thinning. At shear rates relevant for large stirred fermenters (10-25s^{-1}), the pseudoplastic model has been successfully used to describe the rheology of both fungal fermentations and those where exopolysaccharides were produced.[2, 5] The pseudoplastic model does not include a yield stress term, which may be of importance e.g. to determine start-up power requirements. [6]

The Bingham plastic model does include yield stress, but fails to describe shear thinning. To describe pseudoplastic fluids with a yield point, the Herschel-Bulkley model can be used. This model gives an accurate description of the rheological properties of a range of fermentation broths.[2, 7, 8] In some cases, an estimation of the yield stress may prove highly valuable to predict e.g. the formation of unmixed “caverns” in a fermenter or, when determining the power input, the capacity needed at start up. During most industrial fermentations, cavern formation is unacceptable as mass and heat transfer is greatly reduced and is therefore avoided. Allen and Robinson, [9] and Reuss *et al.* [10] demonstrated that no significant difference between the power-law and Herschel-Bulkley models could be observed over the shear rate range encountered during fermentations. As the yield point is determined at very low shear rates, extremely sensitive equipment is needed for a precise determination. In this thesis, a robust method for characterization of the broth rheology for pilot scale fermentations is developed. Thus the pseudoplastic model is used as it is simpler and less susceptible to equipment inaccuracy. Furthermore, constant broth motion is assumed ($\eta>0$).

2.2.2 Effect of temperature on viscosity

The viscosity of a fluid is temperature dependent, and generally the viscosity decreases as the temperature increases. Shear heating during a rheological measurement can therefore cause the measured viscosity to decrease if the rheometer is not equipped with accurate temperature control. [5]

2.2.3 Conventional Rheometers

Measurement of the viscosity in fungal fermentations is often challenging due to the complex nature of the broth. The rheological properties are affected by the interaction of a number of different parameters such as cell morphology, biomass concentration and medium components, and even small changes can cause significant increases in broth viscosity. [11] For conventional rheometers with well defined geometries such as a Cone-Plate, Parallel-Plate or concentric cylinder type, the shear rate and shear stress for power-law fluids can be calculated using the equations listed in table 2.1.

Table 2.1: Shear rate and shear stress relationships for four different rheometer geometries. Ω - Angular velocity, θ - Gap angle, M - torque, r - radius , L - length of cylinder and h - gap.

Cone-Plate [5]	
$\dot{\gamma} = \frac{\Omega}{\theta}$	**Eq. 2.7**
$\tau = \frac{3M}{2\pi r^3}$	**Eq. 2.8**
Narrow-Gap Concentric Cylinder [5]	
$\dot{\gamma} = \frac{r_O \Omega}{r_O - r_I}$	**Eq. 2.9**
$\tau = \frac{M}{2\pi r_O^2 L}$	**Eq. 2.10**
Wide Gap Concentric Cylinder [5]	
$\dot{\gamma} = \frac{2\Omega}{n\left(1 - \left(\frac{r_I}{r_O}\right)^{2/n}\right)}$	**Eq. 2.11**
$\tau = \frac{M}{2\pi r_I^2 L}$	**Eq. 2.12**
Parallel-Plate [4]	
$\dot{\gamma}_r = \frac{r\Omega}{h}$	**Eq. 2.13**
$\tau = \frac{3M}{2\pi r^3}\left(1 + \frac{n}{3}\right)$	**Eq. 2.14**
Cone-Plate with Gap [12, 13]	
$\dot{\gamma}_r = \frac{r\Omega}{h}$	**Eq. 2.15**
$\tau = \frac{3M}{2\pi r^3}\left(1 + \frac{h_0 n}{3h}\right)$	**Eq. 2.16**

For the Cone-Plate and the Narrow-Gap Concentric Cylinder rheometers, the shear rate can be calculated independently of the properties of the fluid being measured. Hence the shear rate can be controlled by varying the angular velocity. The shear stress is in both cases directly proportional to the torque. [5] When measuring the viscosity of fungal fermentations, the morphology of the cells may hinder a precise rheological characterisation of the broth as the diameter of pellets in the broth can exceed the annulus of the apparatus leading to large errors in the measured torque. Pellets may also be destroyed during the measurement in both systems thereby altering the rheology of the broth. [1, 14]

To accommodate pellets, the Parallel-Plate or the Wide Gap Concentric Cylinder rheometer can be used. Both rheometers can have a larger annulus thereby minimizing the problems associated with particles in the broth.[1] When using these types of rheometers, the flow behaviour index for the fluid must be calculated before the shear stress and rate can be found. [5] Special caution must be used if the shear rate control and subsequent data analysis are automated, and Newtonian flow behaviour is assumed. This assumption is only acceptable for pseudoplastic fluids if $(r_i/r_O)<0.97$. [5]

Due to the macro morphology of fungal fermentation broth, air bubbles are prone to become trapped in the Parallel-Plate rheometer leading to errors in the measured apparent viscosity. To avoid air bubbles, the Cone-Plate with a gap such as described by Jackson and Kaye [12] may be used. This type of setup has successfully been used to characterise fluids with complex rheology, e.g. shear thinning elastic fluids with settling particles. [13] Pedersen [15] used this setup to measure the rheological properties of *Aspergillus* fermentation broth and got what they reported as “fairly” reproducible results using a system setup with a 2° cone as top plate and a gap of 1.5-2.0mm. Though this setup minimises the error caused by particles and air bubbles, some problematic issues due to fungal fermentation broths remain.

2.2.4 The Impeller Rheometer

In addition to the problems associated with annula size and large pellets, Bongenaar *et al.* [14] reported two additional hurdles to overcome when determining the rheological properties of fungal fermentation broths with traditional rheometers.

1. The formation of a less dense layer at the interaction surfaces.
2. Samples become inhomogeneous during the measurement due to settling and particle interaction.

Bongenaar *et al.* [14] proposed a method of characterizing the rheological properties of fungal suspensions by measuring the torque on a submerged impeller at different rotation speeds. The power consumption of an impeller P, can be expressed as a function of the power number N_P, the density of the fluid ρ, the diameter of the impeller D_R and the rotation speed N as stated in equation 2.17. [16]

$$P = N_P \rho N^3 D_R^5 \qquad \textbf{Eq. 2.17}$$

In the Laminar flow regime (Re<10), the power number is proportional to the Reynolds number. [1]

$$N_P = \frac{c}{Re} \qquad \textbf{Eq. 2.18}$$

Where c is a constant depending on the tank and impeller geometry. The Reynolds number can be defined as a function of the power number, in the same way as for a normal impeller:

$$Re = \frac{\rho N D_R^2}{\eta} \qquad \textbf{Eq. 2.19}$$

The power consumption can be correlated to the torque on the impeller using equation 2.20. [1]

$$P = 2\pi NM \qquad \textbf{Eq. 2.20}$$

By combining equations 2.17, 2.18, 2.19 and 2.20, the relationship between torque and impeller speed can be determined using equation 2.21.

$$M = \frac{c}{2\pi} \eta D_R^3 N \qquad \textbf{Eq. 2.21}$$

c can be calculated by measuring the torque and rotation speeds of the impeller in a Newtonian fluid with known viscosity.

The average shear rate $\dot{\gamma}_a$ for an impeller in the laminar flow regime is proportional to the impeller speed. [1]

$$\dot{\gamma}_a = kN \qquad \textbf{Eq. 2.22}$$

For a fluid that follows the power-law, equations 2.1, 2.4 and 2.22 can be combined resulting in:

$$\eta_a = K(kN)^{n-1} \qquad \textbf{Eq. 2.23}$$

Combining equation 2.21 and 2.23 the impeller specific constant k can be isolated:

$$k = \frac{1}{N}\left(\frac{M\,2\pi}{cKND_R^3}\right)^{\frac{1}{(n-1)}} \qquad \textbf{Eq. 2.24}$$

By measuring the torque of the impeller at different rotation speeds submerged in a fluid with known n and K values, k can then be determined.

2.2.5 Online Rheometers

To completely circumvent the problems with settling particles in samples and other inaccuracies associated with off-line measurements, a number of on- and in-line methods have been proposed. Olsvik and Kristiansen [17] demonstrated how an impeller rheometer could be implemented in an external circulation loop, measuring the rheological properties of *Aspergillus niger* fermentation broth in a shear rate range of 5-55s^{-1}. [17] Though this system was able to characterize the rheological properties of the broth, the complexity of the setup introduces a number of contamination risks and possible equipment failures. Björkman [18] also used an external loop, but measured the pressure drop in the tube to estimate the viscosity of a *Penicillum chrysogenum* broth. This somewhat simpler and more robust setup was able to measure at higher shear rates than that of Olsvik and Kristiansen [17] (up to 500s^{-1}), but the system was difficult to sterilise and pulsation from the circulation pump resulted in noisy data. [19]

Picque and Corrieu [20] used a vibrating rod sensor mounted inside the fermenter during a *Xanthomonas campestris* fermentation. This system is based on a vibrating rod which is excited at a constant frequency, and the viscosity is determined by measuring the damping of the rod. Because the shear rate of the sensor can not be precisely defined, it is necessary to calibrate the system with fluids with known rheological properties. The viscometer was reported to be easy to install and sterilize, and though it

was not possible to get a precise rheological characterization of the culture medium, Picque and Corrieu [20] were able to follow the changes in the viscosity in-line during a fermentation. In contrast to other in-line probes, the signal was reported to be independent of agitation and aeration intensity.

Due to the difficulties of determining the rheological properties of broths during fermentations, especially those containing fungal mycelium, several studies have proposed correlations between rheology and physical parameters of the fungi, such as biomass concentration and the mycelial size. [11, 21] These correlations are often only applicable to similar system setups, and on- or at-line sampling is still necessary to get an accurate rheological characterization of the broth.

2.3 Materials and Methods

2.3.1 Rheometers and set up

Five different types of rheometers and a viscometer were tested.

1. Cone-Plate: A Carrimed CSL 100 rheometer (TA Instruments, New Castle, United States) with temperature control, equipped with a 60mm in diameter acrylic cone with a 2° angle on a plate, with a 57µm truncation. Equipment control and initial data handling was performed using TA Instruments Rheology Solutions software version V123u. The shear stress was measured in the shear rate interval of $\acute{y}$=0-250s^{-1}.

2. Parallel-Plate: The Carrimed CSL 100 rheometer equipped with a 60mm in diameter acrylic Parallel-Plate setup with a 2mm gap. The shear stress was measured in the shear rate interval of $\acute{y}_r$=0-250s^{-1}.

3. Cone-Plate with Gap: Identical to the Cone-Plate setup but with a gap of h=2.000mm (h_0=1.943mm) as described by Pedersen [15]. The shear stress was measured in the shear rate interval of $\acute{y}_r$ =0-250s^{-1}.

4. Wide Gap Rheometer: A Haake Viscotester VT500 (Gebr. HAAKE Gmbh, Karlsruhe, Germany) was used with a MV-DIN sensor in a MV cup (L/D 58.08mm/38.72mm, r_I/r_O=0.92) placed in a temperature controlled vessel connected to a DC3-K20 circulating refrigerated bath. Control and initial data analysis were conducted using the RheoWin 2.97 software package. The torque was measured in the rotational velocity interval of 0-1.55RPS.

5. Impeller Rheometer: Two different impeller rheometers were tested.

5.a The previous mentioned Haake Viscotester VT500 with a FL10 vane spindle (L/D 60mm/40mm). A setup similar to that described by Cooke *et al*., 1988 was used. The sample container was 0.135m in diameter with a sample volume of 1.4L. No temperature control was connected to the setup, however, non-biological samples were stored in a temperature controlled room prior to measurement, and the viscosity

measurements of fermentation samples were initiated within 1 minute after the sample had been taken from the fermenter. Due to the large volume and a short measuring time, the temperature did not change during the measurement. The viscosity was determined as described in the following: The torque was first measured while the rotational velocity was increased linearly from 0RPS to 2.4RPS in 60s. The shear rate sweep was followed by a pause of 30s where the rotational velocity was kept constant (2.4RPS). Finally, the rotational velocity was linearly decreased to 0 in 60s. To avoid errors from inertial forces, the measured values were compared manually and the shear stress was calculated using an average of the torque from the two shear rate sweeps.

5.b A Brookfield LVDV-II+Pro (Brookfield Engineering Laboratories, Harlow, Essex, United Kingdom) with two different vane spindles V-73 (L/D 25.0mm/12.5mm) and V-74 (L/D 11.0mm/5.5mm) was examined. Different sample containers were used for each vane spindle, all of which had a diameter at least three times that of the vane in use. The sample depth was sufficient to provide a bottom clearance minimum equal to the vane spindle diameter. The sample container was placed in a water-bath to ensure constant temperature during the measurement. The torque was measured in the rotational velocity interval of 0-1.7RPS.

6. Online Sensor: A vibrating rod sensor, Marimex VA-300 with a ViscoScope control console (Marimex Industries Corp, Canada), was used as described by Picque and Corrieu [20]. The sensor was placed in a recirculation loop, connected to a 300L fermenter with a working volume of 225L, and data was recorded continuously. The diameter of the loop at the sensor was 97.60mm. During the calibration of the system, the probe was removed from the loop and placed in 1.5L samples without agitation. Throughout the fermentations the data was recorded online with a constant recirculation rate of approximately 1.8kg s^{-1} through the external loop holding the probe. The shear rate at the probe was estimate as the wall shear rate of the pipe, using equation 2.25, to $\dot{\gamma}=20s^{-1}$.

$$\dot{\gamma}_a = \frac{4Q}{\pi\left(\frac{D}{2}\right)^3} \qquad \textbf{Eq. 2.25}$$

2.3.2 Samples for comparing rheology measurements

Xanthan solutions (0.25-1.50% wt/wt, Rhodopol 23, Rhodia, France) were used as a model medium for all rheometers. All measurements were made in triplicate or more, and used to compare the performance of the six different rheometers and the online sensor. K and n values were determined by fitting the data to the power-law (Eq. 2.4).

For calibration of the Haake Viscotester VT500 with Wide Gap and the FL10 vane spindle, two Newtonian fluids were used. Glycerol (anhydrous, lot 1324145 32607165, Fluka, Sigma-Aldrich, Inc, United States) and Synperonic PE/L61 (Lot 43292888, Brenntag, Germany). The performance of both setups was tested using fermentation broth samples from *Aspergillus oryzae (*A1560) fermentations (see chapter 3 for further information on the fermentations). The Wide Gap Concentric Cylinder setup was further evaluated using bacterial fermentation broth from *Xanthomonas campestris* (ATCC 13951, DSMZ, Germany), see chapter 6 for further information on the fermentations.

To evaluate the performance of the Cone-Plate, Parallel-Plate and Brookfield Impeller Rheometer, the rheological properties of several samples from various fungal fermentations were measured. The samples consisted of fermentation broth from industrial *Aspergillus niger*, *Aspergillus oryzae* and *Trichoderma reesei* fermentations and were provided by Novozymes A/S.

The Marimex online sensor was evaluated using fermentation broth from a *Xanthomonas campestris* (ATCC 13951, DSMZ, Germany) batch fermentation (see chapter 6 for more details on the fermentation), and fungal fermentation broth from a fed-batch fermentation (*Aspergillus oryzae* (1560A), see chapter 3 for further information).

2.4 Results and Discussion

The broad aim of the study is to find a simple and accurate method for viscosity measurements for fungal fermentation broths. The evaluation and comparison of the rheometers are divided in two subsections. First, the rheometers are compared using xanthan solutions of different concentrations. In the second section, the rheometers are tested with fungal fermentation broths.

Xanthan was chosen for the first comparison due to its shear thinning rheological properties, which thus resemble a fungal fermentation broth, but without the interference of large particles, particle settling, and formation of low viscous film layers. When measuring the rheology, simplifications of the equations used to calculate the viscosity may be desirable to reduce the complexity of the calculations. When using automated systems, the software controlling the rheometers does, in some cases, assume Newtonian flow behaviour thereby eliminating the effect of shear thinning. The effects of such simplifications are evaluated using simple xanthan solutions for the rheometers under test.

2.4.1 Comparison of Rheometer Setups using Standardized Xanthan Solutions

The Cone-Plate geometry is mathematically well defined, and the shear stress and rate can be calculated based on the diameter and angle of the cone combined with the torque at a given rotation speed. In contrast to many of the other rheometers, the measured viscosity of the Cone-Plate geometry is independent of the power law constant which makes the rheometer easy to use with shear thinning samples. The Cone-Plate is unfortunately not suitable for viscosity measurements in fungal fermentation broths, as the mycelia pellets and other particulates get lodged between the cone and the plate resulting in incorrect measurements. However the geometry is ideal to be used as a reference for comparing the performance of the other rheometers, by calculating the flow behaviour index ‘n’ and consistency index ‘K’ for a range of different model broths consisting of solutions with different xanthan concentrations.

1. Cone-Plate: Shear rate sweeps (0-200s^{-1}) were conducted using the Carrimed CSL 100 rheometer with a Cone-Plate geometry, on xanthan solutions with concentrations between 0.25% and 1.50% with 0.25% increments. The constants of the power-law equation 2.4 were determined by plotting the Ln(τ) against Ln(ý) resulting in a straight line. The flow behaviour index and consistency index was then calculated from the slope and intersection of the line. An example of five shear rate sweeps of a 1.50% xanthan solution and corresponding shear stress is plotted in figure 2.2, and show excellent reproducibility. For each shear rate sweep the flow behaviour index and consistency index were then calculated (n=0.199±0.002, K=10.21±0.33). The solid line in figure 2.2 was calculated based on the average flow behaviour index and consistency index. As can be seen, an excellent fit to the data can be obtained using the simple equation 2.4. The fit of the data did not significantly improve by using equation 2.6 with more variables, and equation 2.4 was therefore used to minimise the complexity of the data processing. The n and K values were calculated for each xanthan solution and plotted in figures 2.3 and 2.4 and designated 'REF: CP'. The calculated values had a low variation for each sample as can be seen by the low standard deviation (below 0.005 and 0.33 respectively) of the data (figures 2.2 and 2.3). These values were used as the benchmark for comparison with the other rheometers. The results show that the values for n were all less than 1, as is to be expected for a pseudoplastic fluid, and declined as the xanthan gum concentration increased to 0.75% and then rose with further increases in concentration (figure 2.3). The values for the consistency index K rose as the xanthan concentration was increased (figure 2.4).

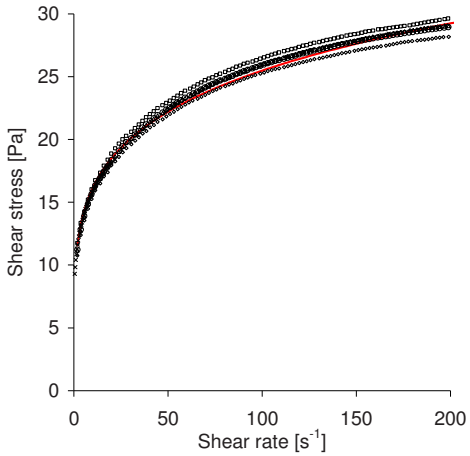

Figure 2.2: Shear stress recorded during five shear rate sweeps from 0 to 200s^{-1} of 1.50% xanthan (x, ◊, □, Δ, o) measured with a Cone-Plate rheometer. For each shear rate sweep, a new sample was loaded to the rheometer. For each sample, the consistency and flow behaviour indexes were calculated. The solid line represents the values for the resulting average values.

2. Parallel-Plate: This rheometer was found to give 'n' and 'K' values essentially the same as the reference Cone-Plate rheometer when measuring correctly loaded samples of xanthan solution ranging from 0.25% to 1.50% (data not shown). However, the rheometer had a small rim on the bottom plate to prevent low viscosity samples from flowing out from between the plates. Due to the rim, air-bubbles were prone to become trapped when lowering the ram with the top plate, resulting in large deviations in the measured viscosity. Due to these practical issues, no further evaluation of the system was performed.

3. Cone-Plate with Gap: In light of the issues of gas bubble entrapment with the Parallel-Plate rheometer, the Cone-Plate with Gap setup was used. It was also expected that the gap would allow better measurements of broths containing particles, such as mycelial pellets, or from coarse complex growth media. Viscosity measurements with xanthan

gum gave good results, and the shear rate and shear stress were calculated using equation 2.15 and 2.16. When fitting the data to the power-law (equation 2.4), both flow behaviour and consistency indexes equivalent to those found with the true Cone-Plate setup could be determined (figure 2.3 and 2.4, 'CP with gap'); the average numerical error was <0.01 for the flow behaviour indexes, and <0.2 for the consistency indexes. The accuracy of this method is well within the limits of what can be accepted for practical use in the laboratory by skilled personnel. However, the method for shear stress calculation is somewhat cumbersome and is not suited for non-specialist users, for example plant operators. To reduce the complexity of the shear stress calculations, different simplifications and assumptions were tested.

3.a Simplification of the Cone-Plate with Gap by assuming Parallel-Plate behaviour : If the angle of the cone is small or the gap is large ($h >> \tan\theta\, r \Rightarrow h \approx h_0$), the shear stress calculation for the Parallel-Plate setup (equation 2.14) can be used as an estimate of the shear stress of the Cone-Plate with Gap. This assumption will lead to a slight overestimation of the shear stress and thereby a higher consistency index, but as can be seen in figure 2.3 and 2.4 ('CP with gap- PP'), the error is insignificant compared to the overall deviations. This simplification does not affect the shear rate calculation, and thus does not affect the flow behaviour index. Hence this simplification of the calculation method can be applied without affecting the overall result. Unfortunately, the simplification of the shear stress calculation is somewhat limited as the flow behaviour index still needs to be determined before the shear stress can be calculated. If the complexity of the overall method is to be significantly reduced, the flow behaviour index must be removed as a variable from the shear rate and stress calculations.

3.b Simplification of the Cone-Plate with Gap by assuming Cone-Plate behaviour: If the effect of the fluid below the cone is neglected, the shear stress can be calculated using equation 2.8 (n=0), i.e. by using the method for the conventional Cone-Plate rheometer. The error associated with this simplification is little at low viscosities and at low values of 'n' where the effect of the fluid at the plate on the fluid at the measuring cone is minimal. The calculated consistency indexes (figure 2.4, 'CP with gap- CP') are therefore very similar to those found with the true Cone-Plate setup at low xanthan gum

concentrations with a numerical error< 0.07. As the xanthan concentrations were increased, the agreement between using the simplified Cone-Plate with gap calculation procedure and the reference Cone-Plate was not as good. For a xanthan concentration of 1.5%, the deviation of the calculated consistency indexes increased up to 0.84 Ns^nm^{-2}. This is due to deformation of the fluid below the cone in the wide gap setup, which dampens the stress resulting in lower measured torque and thus a lower consistency index. It is thus concluded that this viscosity measurement method is most suitable for low to medium viscosity fermentations.

3.c Simplification of the Cone-Plate with Gap using TA instruments software: The Cone-Plate with gap rheometer was controlled using TA Instruments Rheology Solutions software version V123u. The software could not be set for a Cone-Plate with Gap setup, thus the shear rate and stress were estimated using the settings for a Parallel-Plate rheometer, given the apparent suitability of making this assumption, which was found above. The software calculates the shear stress for a Parallel-Plate rheometer using equation 2.13 (figure 2.3, "CP with gap- TA Instruments') and the shear stress with equation 2.26 (figure 2.4, CP with gap- TA Instruments).

$$\tau = \frac{2M}{\pi r^3} \qquad \textbf{Eq. 2.26}$$

Good agreement with the reference rheometer setup was seen for the values of 'n'. However, Equation 2.26 is only valid for Newtonian fluids (n=1). Hence the shear thinning properties are neglected by the software. This method therefore resulted in shear stress and consistency index values that were on average 29% higher than the reference setup. Due to the large error, this approach cannot be recommended for viscosity measurements in xanthan gum or fungal fermentations, even though it is the only method which can be executed without extensive post-measurement data analyses.

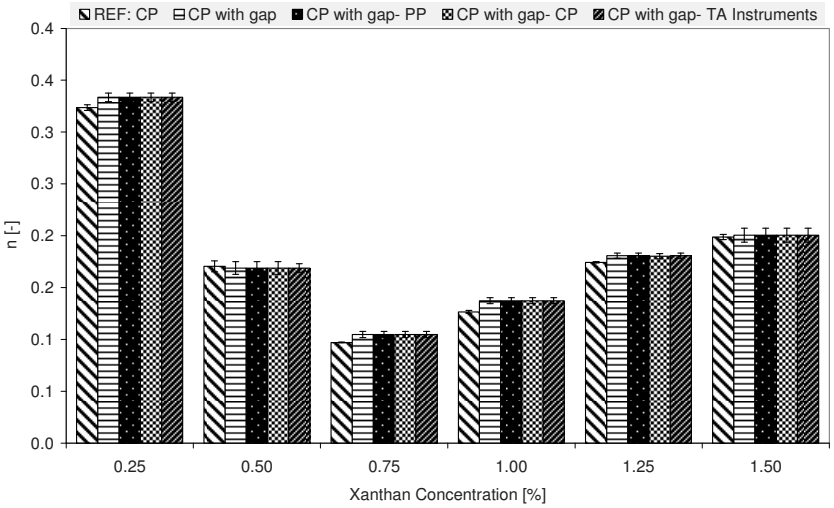

Figure 2.3: Flow behaviour index (n) for six Xanthan solutions measured on Carrimed CSL 100 rheometer with Cone-Plate (REF: CP) and Cone-Plate with Gap (CP with gap), plotted with standard deviation. Determination of 'n' for the Cone-Plate with Gap was subsequently simplified by assuming Parallel-Plate behaviour (CP with gap- PP) and Cone-Plate behaviour (CP with gap- CP), and finally determined using the software supplied with the equipment (CP with gap- TA instruments).

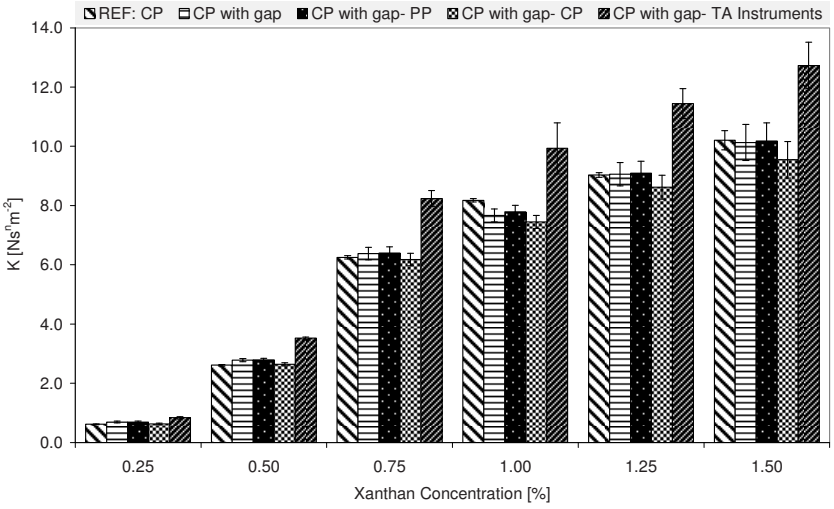

Figure 2.4: Consistency index (K) for six xanthan solutions measured on Carrimed CSL 100 rheometer with different setups plotted with standard deviation. See figure 2.3 for legend explanation.

4. Wide Gap Rheometer: The wide gap setup can be expected to be more suitable for fungal type fermentations than the other types examined above due to the 5mm gap available to accommodate particulates and pellets. The shear rate and shear stress of model xanthan solutions was calculated using equation 2.11 and 2.12, and the resulting data was fitting to the power-law (equation 2.4). The calculated flow behaviour and consistency indexes were plotted in figure 2.5 'n' and 'K' respectively (MV-DIN Wide gap). When compared to the reference Cone Plate setup, it can be seen that in general the Wide Gap Rheometer resulted in poor estimations of the rheological properties of the different xanthan solutions. The relatively large deviation could be caused be the bottom cone which is neglected in the calculations. The RheoWin data Manager program, which is used for setup and control of the Haake Viscotester VT500, uses a narrow gap estimation for shear rate and stress calculation (equation 2.9 and 2.10), even though this assumption is only acceptable for pseudoplastic fluids if the ratio of the radius for the inner to outer wall is $r_I/r_O<0.97$. In the present case, where $r_I/r_O=0.92$, using the software uncritically introduces a significant error. Thus, for a fluid with a flow behaviour index of 0.2, an angular velocity of $\Omega=10 rads^{-1}$ will give a result of $180s^{-1}$ using the wide gap method compared to $128s^{-1}$ using the narrow gap. This approximation leads to a lower calculated shear stress compared to using equation 2.12. The simplification of the governing equations by the software assuming narrow gap thereby results in consistency indexes which are closer to those determined with the Cone-Plate rheometer and better estimations of the viscosity (see figure 2.5 'K' and 'Viscosity', MV-DIN Narrow Gap). No significant difference is seen with respect to the flow behaviour index values (figure 2.5 'n').

5. Impeller Rheometer: This type of rheometer setup may be expected to be the most successful offline viscosity measurement method for fungal fermentations given that it does not rely on plates, cones or cylinders sliding past each other, but employs an impeller rotating in a large volume of liquid. Two different impeller rheometers were tested in model xanthan solutions; the Haake Viscotester VT500 and the Brookfield LVDV-II+Pro.

5.a Haake Viscotester VT500 with FL10 vane spindle: Before the shear rate and stress could be determined for the Viscotester VT500 with a FL10 vane spindle, the constant 'c'

was calculated using equation 2.21 and measured data from two Newtonian fluids with known viscosity Glycerol, μ(Gly)=0.934Pas and μ Synperonic PE/L61, μ(PE/L61)=0.348Pas (c = 314). The constant k was determined to be 13.4 for the spindle using equation 2.24 and a 1.25% xanthan solution with known flow behaviour value (n=0.174) and consistency index (K=9.03).

The flow behaviour and consistency indexes for the six different xanthan solutions measured with the FL10 sensor were similar to those found with the Cone-Plate reference system as illustrated in figures 2.5. Although some deviation (20-23% lower) of the calculated flow behaviour indexes could be observed at xanthan concentrations below 0.75%. For the remaining xanthan solutions, the average difference between the Cone-Plate and FL10 was less then the standard deviation (≈3.6%). The consistency indexes were determined with satisfactory precision with an average numerical deviation of 0.27 Ns^nm^{-2}.

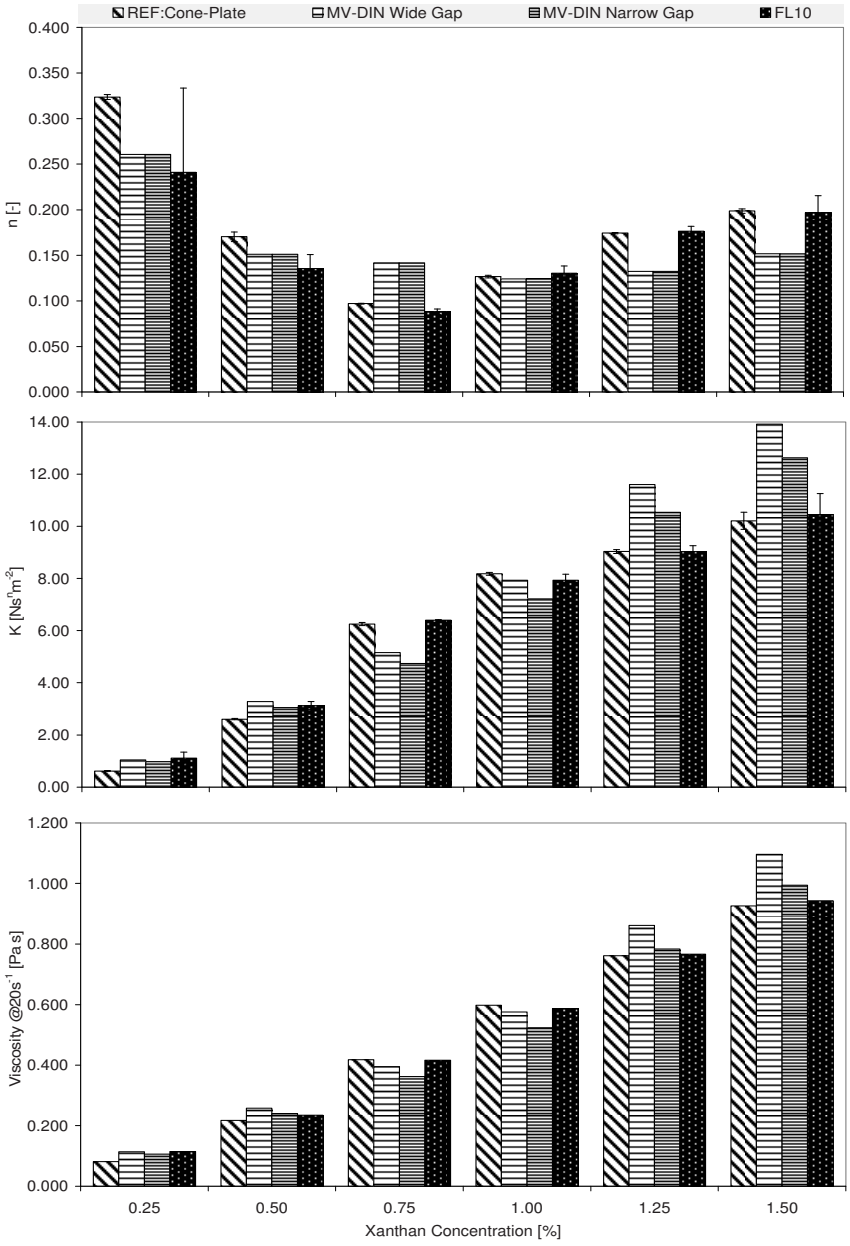

Figure 2.5: **Flow behaviour index (n), consistency index (K), and viscosity at a shear rate of $20s^{-1}$ for six different xanthan solutions measured on a Haake 500 rheometer equipped with a MV-DIN and a FL10 sensor, plotted with the corresponding values determined with a Cone-Plate rheometer. The values for MV-DIN Wide Gap are calculated using equation 2.11 and 2.12, whereas equation 2.9 and 2.10 are used for MV-DIN Narrow Gap.**

Even though the flow behaviour and in particular the consistency indexes determined with the Haake VT500 FL10 do deviate from those found with the Cone-Plate setup at low viscosities, the errors are of minor practical importance. In the bottom diagram of figure 2.5, the viscosities at $20s^{-1}$ have been calculated for each setup by inserting the determined n and K values in equation 2.1 and 2.4. From the figure, it is evident that the viscosities determined with the Haake VT500 with the FL10 impeller are essentially the same as those from the reference Cone-Plate setup, indicating that this simple setup is able to determine the flow behaviour and consistency index accurately.

5.b Brookfield LVDV-II+Pro with V-73 and V-74 vane spindles: The FL10 vane requires a sample volume of approximately 1.4L to ensure the measurement is not affected by the sample container walls. Such a large sample volume limits the use of the setup for laboratory fermentations and also represents a large sample volume at pilot scale. The Brookfield LVDV-II+Pro with smaller spindles was therefore tested in a attempt to minimize the sample volume. Initial tests with the V-73 spindle (L/D 25.0mm/12.5mm) showed that the maximum torque of the Brookfield LVDV-II+Pro severely limited the rotation speed when testing with xanthan solutions above 0.75%. Hence no further investigation was performed with this spindle. The V-74 (L/D 11.0mm/5.5mm) was able to measure the flow behaviour indexes for xanthan solutions. However, it was difficult to obtain consistent results (data not shown). The maximum torque measured with the V-74 was well within the acceptable range, and the small size of the spindle facilitated sample volumes as low as a few centilitres.

6. Online Sensor: When taking a sample to perform a rheological characterization, there is a risk of contaminating the fermenter. Furthermore, some rheometers, such as the vane spindle, require a relatively large sample volume. For some applications, it may therefore be desirable to use a non-destructive in-line probe, especially if the viscosity changes rapidly during the fermentation. The Marimex VA-300 vibrating rod sensor was therefore tested for in-line measurement of viscosity. The sensor was calibrated by submerging the rod in a 1.50% xanthan solution. A constant scale factor between the Marimex sensor and a reference value was then found by dividing the viscosity determined with the Carrimed CSL 100 Cone-Plate rheometer at $\acute{y}_a=20s^{-1}$ with the average of 20 measurements from the probe signal. This scale factor was then used to

determine the viscosity of the six xanthan solutions (0.00-1.50%). The viscosities found with the Marimex can be seen in figure 2.6 plotted with the corresponding viscosities calculated from the Carrimed CSL 100 Cone-Plate and Haake VT500 FL10 rheometers. The measured viscosities covered the range previously reported in fungal fermentations (at the same shear rate).[22] The results show that using this simple calibration method, the Marimex VA-300 vibrating rod sensor gives a very good estimation of the viscosity of the xanthan solutions (R^2=0.998).

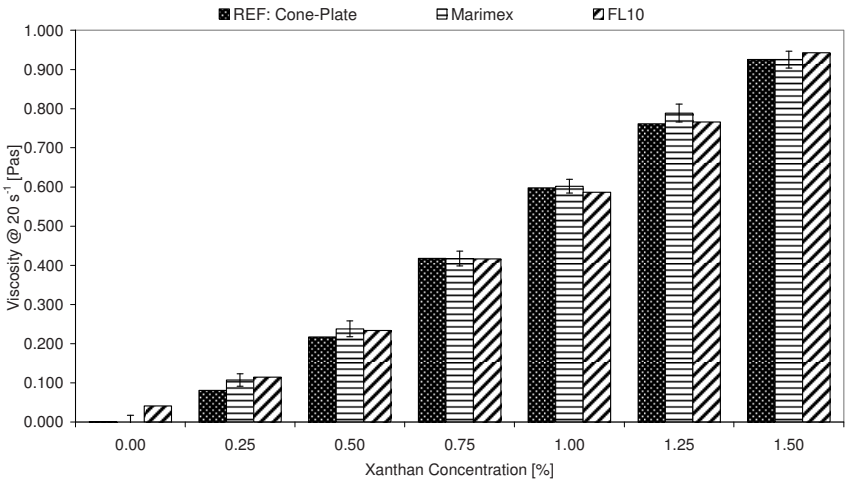

Figure 2.6: Viscosity determined at $\dot{\gamma}_a$=20s^{-1} using the Carrimed CSL 100 Cone-Plate, MariMex VA-300 and Haake VT500 FL10. The viscosity from the Marimex probe is based on an average of 20 measurements and plotted with the sample standard deviation.

2.4.2 Comparison of Rheometers for Viscosity Measurements in Fermentation Broths

The data above was collected using model xanthan gum solutions and indicated that all of the setups could give comparable results and were suitable for viscosity measurements. However the broad goal of the current work is to find a measurement method applicable to fungal fermentation broths. The successful rheometer setups were therefore tested with different fermentation broths.

1. Cone-Plate: Even though the Cone-Plate rheometer was able to give an efficient and precise rheological characterisation of the xanthan solutions, the setup could not be used for fungal fermentation broth due to pellets and other particles in the broth. The use of Cone-Plate type rheometers for fermentation broth characterisation is therefore limited to cultivations with single cells such as bacteria and yeasts.

2. Parallel-Plate: As previously discussed, the rheometer was found to function adequately when measuring solutions of xanthan loaded correctly onto the plate. However, the Parallel-Plate was found to be unsuitable for samples from fungal fermentations as it was difficult to avoid air-bubbles from being trapped between the plates. Due to these problems, the setup was neither easily applicable nor robust and was not examined any further.

3. Cone-Plate with Gap: This rheometer was found to give a precise rheological decription of *Trichoderma reesei* fermentation broth (Figure 2.7). For example, at room temperature, a viscosity of ~0.032 Pa s at 95 s^{-1} was measured in a complex cellulose containing fermentation broth. Further tests showed that the viscosity of industrial fermentation samples of *Aspergillus niger* and *Aspergillus oryzae* could also be tested for broths with pellets less then 1mm in diameter. Despite what could be expected, no evidence of the formation of a low viscous hydration layer could be detected in any of the samples measured. This may be an effect of the cone being made of plastic, with a slightly rough surface (compared to polished steel). Furthermore, no signs of significant sample degradation/break up could be observed during the shear rate sweeps. This was continuously tested by comparing the shear stress of the up and down sweep. Due to the angle of the cone, the risk of air-bubbles getting trapped was smaller compared to the Parallel-Plate setup. In contrast to the vane spindle rheometers, the Cone-Plate with Gap was equipped with precise temperature control. The rheometer was therefore used in the reference for comparison with the other rheometers and also to examine the effect of changing the temperature of the broth.

Effect of temperature on the viscosity of fungal broth. The Carrimed CSL 100 rheometer with Cone-Plate with Gap setup was used to measure a *Trichoderma reesei* fermentation broth sample. The viscosity was measured at different temperatures and

the results are shown in figure 2.7. No difficulties were observed when measuring the viscosity with this setup. The results in figure 2.7 indicate that temperature has a large impact on the viscosity of this fermentation broth, which fell by 38% over the temperature range studied. It is therefore important to perform the viscosity measurement at the correct fermentation temperature to get a precise result.

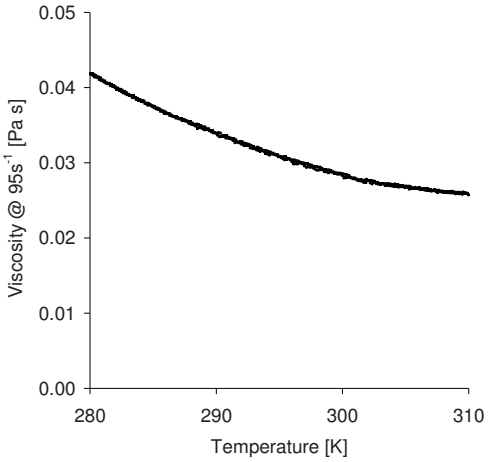

Figure 2.7: Viscosity of *Trichoderma reesei* fermentation broth at $95s^{-1}$ measured in the temperature interval 280-310K.

4. Wide Gap Rheometer:

Attempting to measure the rheology of fungal fermentation broths using the Haake MV-Din Wide Gap Concentric Cylinder rheometer did not result in reproducible results. As previously reported by Bongenaar *et al.* [14], a hydration layer was formed resulting in a seemingly thixotropic behaviour[1]. When lowering the cylinder into the broth there was to some extent a sieve effect even though the annulus was larger then the fungal pellets. Due to these problems, the Wide Gap Rheometer cannot be not used with fungal broths. The setup performed significantly better when testing *Xanthomonas campestris* fermentation broth, which resembled the xanthan solutions. The shear stress was measured in a shear rate interval of approximately $0\text{-}200s^{-1}$, and based on the

[1] **The sample was pseudoplastic and seemed to become less viscous over time when measured by the rheometer.**

calculated 'n' and 'K' values, the viscosity at higher shear rates could be estimated. In figure 2.8, the viscosity calculated at a shear rate of $1250s^{-1}$ during two *Xanthomonas campestris* fermentations is plotted against the in-line viscosity measured using the Marimex probe (see chapter 6 for further information on the fermentation).

5. Impeller Rheometer: As previously stated, this type of rheometer was considered likely to be the best choice for fungal fermentation broths, as the viscosity can be measured directly in the sample container, and the rheometer is compatible with mycelium as well as pelleted growth. Sample handling is therefore relatively simple, whereas the data processing is relatively complicated compared to the other rheometers tested as the flow behaviour index is needed when calculating the viscosity.

5.a Haake Viscotester VT500 with FL10 vane spindle: This rheometer gave results almost identical to the much more advanced Carrimed CSL 100 rheometer with a Cone-Plate geometry, in xanthan solutions with viscosity similar to that of fungal fermentations (0.5-1.5%, figure 2.5). After the initial calibration of the setup, the rheological measurements of fungal fermentation broths (*Aspergillus oryzae* and *Trichoderma reesei*) was uncomplicated. The spindle was able to keep insoluble particles in suspension in non-viscous broths, thus ensuring that the composition of the sample was constant during the measurement. Due to the large volume of the sample (1.4 L), no temperature control was needed. Furthermore, for cultures with highly differentiated morphology, the large volume ensured that the sample was a good representative of the 'average' conditions in the fermenter. In figure 2.9, the viscosity calculated at a shear rate of $1250s^{-1}$ during an *Aspergillus oryzae* fermentation is plotted against the in-line viscosity measured using the Marimex probe (see chapter 3 for further information on the fermentation). The large sample volume was, however, also the main drawback and the performance of smaller vanes were therefore tested.

5.b Brookfield LVDV-II+Pro with V-73 and V-74 vane spindles: The torque restrictions of the Brookfield LVDV-II+Pro made the V-73 unsuited for use with the fungal fermentation samples. The V-64 spindle was further tested with fermentation broth samples, but both failed to produce consistent results. When testing the V-74 spindle on industrial *Aspergillus niger*, *Aspergillus oryzae* and *Trichoderma reesei* broths, the torque available did not restrict the shear rate sweeps. However, the spindle was not able to agitate the sample sufficiently during the measurements resulting in sedimentation. Furthermore,

the radius of the spindle (2.75mm) was not significantly larger then the diameter of the largest pellets in the broth (up to 1.5mm). During the measurements, the pellets were forced out of the areas between the spindle blades resulting in a mycelium free cavity around the spindle rendering a precise characterisation of the broths impossible. Hence, it was concluded that neither the V-73 nor the V-74 were suitable for use with the LVDV-II+Pro for rheological characterisation of fungal broths.

6. Online Sensor: To evaluate the performance of the Marimex in-line sensor during fermentation, the probe was placed in a recirculation loop and data was measured during two *Xanthomonas campestris* batch fermentations. The online data was compared with data measured using the Haake MV-DIN Wide-gap rheometer, but correlated poorly when using the scale factor determined with the Carrimed CSL 100 Cone-Plate rheometer at $\acute{\gamma}_{app}=20s^{-1}$ (data not shown). The fit could be significantly improved by recalibrating the system to a shear rate of $1250s^{-1}$ (estimate maximum shear rate in the, 97.60mm in diameter, external loop section of the RJH system). During the initial calibration, the probe had been submerged in samples without any stirring or flow, whereas the flow during the fermentation was ~$1.8kgs^{-1}$ at the probe. In contrast to what was reported by Picque and Corrieu [20], the probe signal does therefore seem to be affected by the agitation/flow. Using the new scale factor, the signal from the in-line sensor was observed to give measurements similar to those determined at-line with the Haake MV-DIN (see figure 2.8).

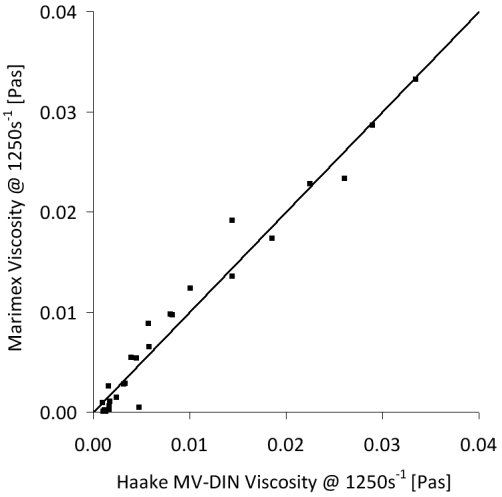

Figure 2.8: Viscosity determined at $\dot{\gamma}_{app}$=1250s^{-1} during two *Xanthomonas campestris* batch fermentations. Based on data from the Haake MV-DIN at-line rheometer plotted against values determined with the Marimex VA-300 in-line sensor.

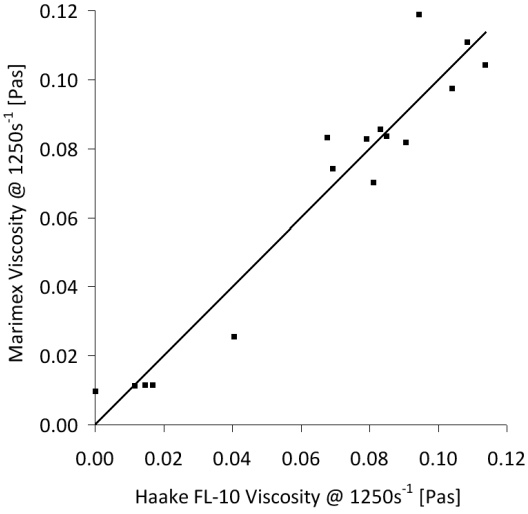

Figure 2.9: Viscosity determined at $\dot{\gamma}_{app}$=1250s^{-1} during an *Aspergillus oryzae* fed-batch fermentation. Based on data from the Haake FL-10 at-line rheometer plotted against values determined with the Marimex VA-300 in-line sensor.

An equally good fit was found when testing the probe with fungal fermentation broths and using the scale factor at $1250s^{-1}$, see figure 2.9 where the in-line measured viscosity from the marimex sensor is plotted against data from the Haake Viscotester VT500 with a FL10 vane spindle.

2.5 Conclusion

In this chapter, five different types of rheometers and a viscometer were tested. The Cone-Plate, Wide Gap Concentric Cylinder, Parallel-Plate and the small vane spindle rheometers all failed to give a precise rheological description of the fungal fermentation broths examined. In contrast, the Carrimed CSL 100 Cone-Plate with Gap could be used for both model broth and real fungal fermentations and was found to give highly reproducible and precise results. The data handling was complex, but could be simplified if the flow behaviour of the fluid was known, enabling the use of a constant flow behaviour index. The main drawback of the method was the great precision required when the samples were loaded to avoid air bubbles from being trapped. Furthermore, the results were affected by the small sample volume, which makes the rheometer difficult to use for non-specialist users.

Measurements with the Haake FL10 vane spindle rheometer were found to be easier than the Cone Plate with Gap setup and to give results with an acceptable accuracy and reproducibility, but the initial calibration and in particular the following data analysis were more complex. Nevertheless, the measurements can easily be performed by non-specialist users and are thus suitable for an industrial setting. The main drawback of the method is the large sample volume needed.

The Marimex VA-300 was found to be an excellent way to eliminate the need for sample taking and to provide frequent online measurements. The probe can provide valuable information in fermentations where rapid changes in viscosity takes place. It is, however, necessary to calibrate the probe against an at-line rheometer (such as the Haake FL10 vane spindle.

Combining the on-line data from the Marimex VA-300 sensor with the at-line data from the Haake FL10 vane spindle results in a precise and robust method for determination of the rheological properties in a pilot or industrial scale fungal fermentation.

2.6 References

1. Metz, B., N.W.F. Kossen, and J.C.V. Suijdam, *The rheology of mould suspensions.* Advances in Biochemical Engineering/Biotechnology. Vol. 11/1979. 1979: Springer Berlin / Heidelberg. 103–155.
2. Cooke, M., J.C. Middleton, and J. Bush, *Mixing and mass transfer in filamentous fermentations.* King R (ed) 2nd Int. Conf. on Bioreactor Fluid Dynamics, 1988: p. 37–64.
3. Jüsten, P., et al., *Dependence of mycelial morphology on impeller type and agitation intensity.* Biotechnology and Bioengineering, 1996. **52**(6): p. 672-684.
4. Walters, K., *Rheometry*. 1975, London: Chapman and Hall. 278.
5. Barnes, H.A., J.F. Hutton, and K. Walters, *An Introduction to Rheology*, ed. K. Walters. Vol. 3. 1989: Elsevier Science Publisher B. V. 210.
6. Olsvik, E. and B. Kristiansen, *Rheology of filamentous fermentations.* Biotechnology Advances, 1994. **12**(1): p. 1.
7. Mohseni, M., H. Kautola, and D.G. Allen, *The viscoelastic nature of filamentous fermentation broths and its influence on the directly measured yield stress.* Journal of Fermentation and Bioengineering, 1997. **83**(3): p. 281.
8. Marten, M.R., K.S. Wenger, and S.A. Khan. *Rheology, mixing time, and regime analysis for a production-scale Aspergillus oryzae fermentation*. in *4th International Conference on Bioreactor & Bioprocess Fluid Dynamics*. 1997. Edinburg UK: BHR Group.
9. Allen, D.G. and C.W. Robinson, *Measurement of rheological properties of filamentous fermentation broths.* Chemical Engineering Science, 1990. **45**(1): p. 37.
10. Reuss, M., D. Debus, and G. Zoll, *RHEOLOGICAL PROPERTIES OF FERMENTATION FLUIDS.* Chemical Engineer, 1982(381): p. 233-238.
11. Riley, G.L., et al., *Effect of biomass concentration and mycelial morphology on fermentation broth rheology.* Biotechnology and Bioengineering, 2000. **68**(2): p. 160-172.
12. Jackson, R. and A. Kaye, *The measurement of the normal stress differences in a liquid undergoing simple shear flow using a cone-and-plate total thrust apparatus only.* British Journal of Applied Physics, 1966(10): p. 1355.
13. Ponche, A. and D. Dupuis, *On instabilities and migration phenomena in cone and plate geometry.* Journal of Non-Newtonian Fluid Mechanics, 2005. **127**(2-3): p. 123.
14. Bongenaar, J.J.T.M., et al., *A method for characterizing the rheological properties of viscous fermentation broths.* Biotechnology and Bioengineering, 1973. **15**(1): p. 201-206.
15. Pedersen, A.G. *kla characterization of industrial fermentors*. in *4th International Conference on Bioreactor & Bioprocess Fluid Dynamics*. 1997. Edinburg UK: BHR Group.
16. Nielsen, J., J. Villadsen, and G. Lidén, *Bioreaction Engineering Principles*, ed. 2. 2003, New York: Kluwer Acedemic/Plenum Publishers. 528.
17. Olsvik, E.S. and B. Kristiansen, *On-line rheological measurements and control in fungal fermentations.* Biotechnology and Bioengineering, 1992. **40**(3): p. 375-387.
18. Björkman, U., *Properties and principles of mycelial flow: A tube rheometer system for fermentation fluids.* Biotechnology and Bioengineering, 1987. **29**(1): p. 101-113.
19. Björkman, U., *Properties and principles of mycelial flow: Experiments with a tube rheometer.* Biotechnology and Bioengineering, 1987. **29**(1): p. 114-129.
20. Picque, D. and G. Corrieu, *New instrument for on-line viscosity measurement of fermentation media.* Biotechnology and Bioengineering, 1988. **31**(1): p. 19-23.
21. Roels, J.A., J.V.D. Berg, and R.M. Voncken, *The rheology of mycelial broths.* Biotechnology and Bioengineering, 1974. **16**(2): p. 181-208.
22. Bhargava, S., K.S. Wenger, and M.R. Marten, *Pulsed addition of limiting-carbon during Aspergillus oryzae fermentation leads to improved productivity of a recombinant enzyme.* Biotechnology and Bioengineering, 2003. **82**(1): p. 111-117.

Chapter 3

Mass Transfer Optimization in Fed-batch *Aspergillus oryzae* Fermentations - using a Rotating Jet Head Mixing System

Chapter 3

Mass Transfer Optimization in Fed-batch *Aspergillus oryzae* Fermentations - using a Rotating Jet Head Mixing System

3.0 Abstract

At high biomass concentrations, mixing in traditional bioreactors becomes increasingly difficult due to the viscous nature of most fermentation broths. Cooling aggregates may further hinder mixing in the periphery of the tank. In poorly mixed areas, very limited mass and heat transfer takes place reducing the overall efficiency of the fermenter. The Rotary Jet Head (RJH) mixing system is a novel method with possible applications for efficient mixing and air sparging in highly viscous fermentations. In this chapter, a RJH of the type IM15 with 7mm nozzles and isolated gear was used for pilot scale fed-batch *Aspergillus oryzae* (A1560) fermentations. The tank volume was 310l with a working volume of 225l. For the first time, the performance of the RJH system was evaluated by conducting fermentations. The data was compared to fermentations conducted in a baffled 300l fermenter with a working volume of 195L equipped with an Intermig impeller set. Mass transfer and the effect of shear stress on the filamentous fungus were examined using a complex soy based medium and a defined medium. The complex soy based medium resulted in similar morphology and rheological properties for the two fermenter systems, however, the volumetric oxygen transfer rate of the RJH system was twice that of the Intermig, in spite of a lower energy consumption. In fermentation with defined medium, the RJH system did not affect the growth rate, but caused a significantly increased fragmentation rate compared to the Intermig fermenter, leading to a reduction of broth viscosity and improved volumetric gas transfer rates, without any apparent detrimental effects on the fermentation. The RJH system yielded a very open non-pelleted growth, and given the advantages with respect to mixing and mass transfer appears to be a very promising system for both fungal fermentation and other viscous oxygen demanding processes.

3.1 Introduction

Filamentous fungi are frequently used in industrial biotechnology due to their ability to produce and excrete large amounts of protein, as well as primary and secondary metabolites. During many fermentations, the oxygen transfer rate (OTR) is a key limiting parameter, and decreases in the dissolved oxygen tension (DOT) can result in significantly reduced yields or increased production time. [1] In fungal fermentations mycelium interactions may lead to increased viscosity resulting in a lower OTR and less mixing as described in equation 2.19. [1, 2] The morphology and growth of the fungal mycelium are therefore an important parameter when it comes to the rheological properties of a fermentation broth.[1] Numerous studies have been conducted to elucidate the relationship between fungal morphology and broth rheology [3-6], and there are several reviews on the topic, e.g. Metz et al. [7].

The effect of hyphal fragmentation on productivity and broth viscosity has been found to be highly strain and product specific. For lovastin production in *Aspergillus terreus* [8] as well as penicillin production in *Penicillium chrysogenum* [9], pelleted growth and low fragmentation give rise to high production rates, whereas high final titres of citric acid have been reached using *Aspergillus niger* growing in dispersed mycelium. [6] Amanullah *et al.* [10] and Bhargava *et al.* [1] demonstrated how hyphal fragmentation by highly intense mixing can reduce the viscosity of fungal fermentation broth without decreasing protein production. Mycelium fragmentation may therefore be used as a tool to reduce the viscosity and subsequently to increase the OTR during a fermentation. Hyphal fragmentation occurs when the shear force exceeds the tensile strength of the hypha.[11] The strength of the cell wall can be affected by several different physiological factors such as growth rate, mycelium age and medium components, but also physical parameters such as the specific energy dissipation rate in the mixing region of a fermenter and the frequency with which the fungi is subjected to high shear stresses. [3, 9, 12]

Amanullah *et al.* [13] and Li *et al.* [3] were both able to obtain a good fit between mycelium fragmentation of *Aspergillus oryzae* and the so-called energy dissipation/circulation function (EDCF). [3, 13]

For a classical impeller mixed system, the EDCF is defined as the following [3, 12, 14]:

$$EDCF = \frac{P}{kD_i^3 t_c} \qquad \textbf{Eq. 3.1}$$

Where P is the power input under gassed conditions, D_i is the impeller diameter, t_c is the circulation time and k is an impeller specific constant defined as:

$$k = \frac{\pi}{4}\frac{W}{D_i} \qquad \textbf{Eq. 3.2}$$

Where W is the height of the impeller. Combining equation 3.1 and 3.2 one gets:

$$EDCF = \frac{P}{V_i}\frac{1}{t_c} \qquad \textbf{Eq. 3.3}$$

Where V_i is the volume swept by the impeller. The hyphal fragmentation rate is therefore dependent on the power input, the volume in which the power of the impeller is applied, and how often the fungi are exposed to the high shear/power intensity conditions.

The circulation time is calculated using equation 3.4.

$$t_c = \frac{V_L}{Q_i} \qquad \textbf{Eq. 3.4}$$

Where V_L is the liquid volume in the fermenter and Q_i is the impeller liquid pumping rate. Q_i can be estimated using the gas flow number $N_{Fl,g}$ of the impeller as the following:

$$Q_i = N_{Fl,g} N D_i^3 \qquad \textbf{Eq. 3.5}$$

Where N is the impeller speed and $N_{Fl,g}$ can be calculated based on the flow number at ungassed conditions (N_{Fl}) and the ratio between the gassed (Po_g) and ungassed (Po) power numbers.

$$N_{Fl,g} = N_{Fl}\frac{Po_g}{Po} \qquad \textbf{Eq. 3.6}$$

When comparing different impeller systems, the power consumption of a given system can be estimated using equation 3.7.

$$P = Po\rho_L N^3 D_i^5 \qquad \textbf{Eq. 3.7}$$

When calculating the power consumption for gassed conditions Po_g is used.

3.2 Materials and Methods

3.2.1 Growth medium

Two different media were used. 1) A complex soy-based undefined medium provided by Chr. Hansen A/S, Denmark containing salts, soy flour, 0.05gl^{-1} streptomycin sulphate, and 20gl^{-1} glucose as carbon source. 2) The chemically defined minimal medium from Carlsen *et al.*[15]. The chemically defined minimal medium consisted of (per liter): 10.0g glucose (monohydrate), 5.0g $(NH_4)_2SO_4$, 1.5g KH_2PO_4, 1.0g $MgSO_4 \cdot 7H_2O$, 1.0g NaCl, 0.1g $CaCl_2 \cdot 2H_2O$, 0.05g streptomycin sulphate, and 0.5ml trace metal solution. The trace metal solution contained: 14.3g $ZnSO_4 \cdot 7H_2O$, 2.5g $CuSO_4 \cdot 5H_2O$, 0.5g $NiCl_2 \cdot 6H_2O$, 13.8g $FeSO_4 \cdot 7H_2O$, and 3.0g citric acid.(19) The streptomycin did not affect the growth rate of the fungi, but ensured the batches were not contaminated by bacteria growth. All fermentations were conducted as fed-batch and 50% (w/w) glucose was added with a constant rate of 4$gl^{-1}h^{-1}$ based on the start volume of the tank. The feed phase was initiated at the end of the batch growth phase, based on a drop in the volumetric CO_2 production rate '$q(CO_2)$'.

3.2.2 Fermenter setup and cultivation conditions

Two fermenter setups were used. 1) The RJH fermenter described in chapter 1 with a start volume of 200l when using the complex soy-based medium, and 225l for the chemically defined medium. The system was operated with a constant pump speed of 200RPM. 2) A baffled 300l fermenter with a working volume of 195L equipped with an Intermig impeller set. During the fermentation the stirrer speed was maintained at 300RPM.

Inoculum: 1.8ml of a spore stock ($6.6 \cdot 10^7$ spores/ml) in glycerol was used to inoculate three 2l shake flasks, each of which contained 0.67l of chemically defined minimal medium. After two days of shaking at 100 RPM at 30°C, the mycelium was used to inoculate the fermenter resulting in an inoculation percent of 0.9% and 1.0% for the RJH and Intermig system respectively.

Fermentation Conditions: Fermentations were conducted at 30°C with a volumetric airflow rate of 1VVM. The pH was maintained at 6.0 by automatic HCl and NH_4OH addition.

Determination of Power Input: The power input of the Intermig system (P_{IM}) was determined by measuring the power drawn from the motor (P_{tot}) under gassed conditions at a specific impeller speed and subtracting the corresponding power consumption for the system without liquid in the tank (P_{empty}). The power input from the air was calculated using equation 3.8.

$$P_{IM} = P_{tot} - P_{empty} + P_g \qquad \text{Eq. 3.8}$$

During the fermentations the impeller speed was maintained at 300 RPM while measuring the power drawn by the motor.

The power input of the RJH was estimated as the sum of the power from the air and the pump in the circulation loop.

$$P_{RJH} = P_g + P_{pump} \qquad \text{Eq. 3.9}$$

The power input from the gas (P_g) was calculated using equation 1.6. The power input from the pump was estimated as the difference in pressure in the circulation loop and the fermenter (equation 3.10).

$$P_{Pump} = Q_L \rho_L \Delta p \qquad \text{Eq. 3.10}$$

Where Q_L is the liquid flow, ρ_L is the density of the liquid and Δp is the pressure difference. The recirculation pump, which had a liquid displacement per revolution of $V_{dis}=0.54 \cdot 10^{-3} m^3$, was set at 200RPM equivalent to an average liquid flow rate in the loop of $1.8 kgs^{-1}$, which resulted in a recirculation time t_c=125s (using a liquid density of $1000 kgm^{-3}$).

Analysis: The rheological properties of the broth were measured on-line using a vibrating rod sensor, VA-300 with a ViscoScope control console (Marimex), and at-line using a Haake VT500 FL10 rheometer as described in chapter 2.

The volume weighted size distribution and average projected area of the mycelium was measured using a Mastersizer 2000 (Malvern instruments Ltd) with a Hydro SM manual small volume sample dispersion unit.

A BX-40 Microscope (Olympus) equipped with a RS Photometrics camera (CoolSNAP) was used to take pictures for subsequent manual evaluation of the morphology during the fermentations.

The OTR was calculated using a 5853 S Mass Flow Controller (Brooks Instruments) and a gas monitor model 1308 (Büel & Kjær).

The biomass concentration (g biomass pr. kg broth) in the fermentations with defined medium was determined by filtering a known volume (corresponding to approximately 3g) of sample from the fermenter using pre-weighed filter paper (45µm cut-off). The filter was subsequently washed using 0.9% NaCl and dried in a microwave oven to constant weight. After a minimum of 24h in a desicator, the filters were weighed and the cell dry weight calculated by difference.

To determine the concentration of glucose, ethanol, glycerol and organic acids, samples were centrifuged (10 minutes at 3500g) then filtered (0.20µm) and analysed with a Summit high-pressure liquid chromatograph (Dionex) as described in [16].

3.3 Results and Discussion

3.3.1 Energy dissipation/circulation function (EDCF)

Comparison of the EDCF for the fermenter containing the rotating jet head system with other conventional fermenter types may provide information on the type of fungal morphology and viscosity to be expected during a cultivation. To calculate the EDCF for the RJH system the following assumptions were made; $Q_i=Q_L$ and instead of V_i the volume displaced by the pump per revolution (V_{dis}) was used. Using these assumptions, the EDCF for the RJH system can be calculated, see table 3.1. As no value for N_{fl} for the Intermig impeller could be found in literature nor from the producers, the EDCF for two alternative systems were calculated based on values from experiments with a six blade Rushton turbine and a pitched blade impeller. The impeller systems were chosen as they are extreme cases of radial and axial flow impellers respectively; hence the EDCF of the mixed flow Intermig impeller is likely to be between these to extremes.

Table **3.1** EDCF for RJH, Rushton turbine and pitched blade impeller. Calculated values based on power consumption in water at 1VVM. Data for the power consumption of the impellers in the 300l fermenter were provided by Chr. Hansen A/S.

		RJH	Intermig Impeller	Rushton Turbine	Pitched Blade
Flow type		Jet	Counter	Radial	Axial
Working volume	[m^3]	0.225	0.200	0.200	0.200
Po			0.74	5.20	0.60
h_i/D_i		-	0.2	0.2	0.08
P/V	[kW m^{-3}]	1.6	2.6	2.8	1.8
$N_{Fl,g}$			-	0.48	0.55
V_i	m^3	$0.54 \cdot 10^{-3}$	-	$2.9 \cdot 10^{-3}$	$2.8 \cdot 10^{-3}$
Q_i	m^3 s^{-1}	0.0018	-	0.04	0.12
t_c	[s]	125	-	4.51	1.64
EDCF	[kW m^{-3} s^{-1}]	5.3	-	255	56

In spite of the small displaced volume per revolution of the RJH, the results in table 3.1 show that the EDCF value for the RJH system (5.3kW$m^{-3}s^{-1}$) is between 10 and 50 times lower than traditional impellers, mainly due to the large difference in circulation time 't_c'. These theoretical calculations could suggest that cell fragmentation would be less pronounced in the RJH system compared to traditional impeller type systems. The

morphology of the fungus fermented in the RJH system could thus be expected to contain longer hyphal elements. The EDCF calculation for the RJH does, however, not take the shear forces acting on the cells during their ejection through the jets nor at the interface between the jet streams and bulk liquid into account. These high shear areas may contribute significantly to cell fragmentation.

3.3.2 Fermentation with complex soy medium

In order to evaluate the RJH systems true effect on cell fragmentation, viscosity and cell morphology, fermentations were conducted in the RJH system using a complex industry inspired soy based medium, and compared with a fermenter mixed by an Intermig impeller. The complex medium was chosen since the broth was likely to become highly viscous, and enable a high growth rate. The high growth rate and readily available nutrients were anticipated to result in a high oxygen demand, thereby pushing the fermentation system's gas transfer capabilities.

The RJH system was observed to function without problems during the fermentation and coped easily with the complex particulate containing medium. No stagnant zones could be observed during the fermentation for neither of the fermenter systems. Due to the particulates present, it was not possible to determine cell dry weight for neither the RJH nor the Intermig fermentation. However, the volumetric production rate of CO2 'q(CO2)' increases exponentially up to $0.029 mol l^{-1} h^{-1}$ after 17.6h with a rate of 0.32 for the Intermig and $0.032 mol l^{-1} h^{-1}$ at 19.6h with a rate of 0.34 for the RJH system, see figure 3.1 top. The Inoculum was grown in a shake flask with a low agitation rate, which resulted in loose pelleted growth of the mycelium. When added to the fermenters, the pellets were broken up into smaller segments. The shorter initial lag phase of the Intermig system could indicate that the stress on the cells during the brake-up is larger in the RHJ system. However, the similar rate of increase of q(CO2) could indicate that the growth rate of the fungus is not affected by the fermenter during the following batch phase.

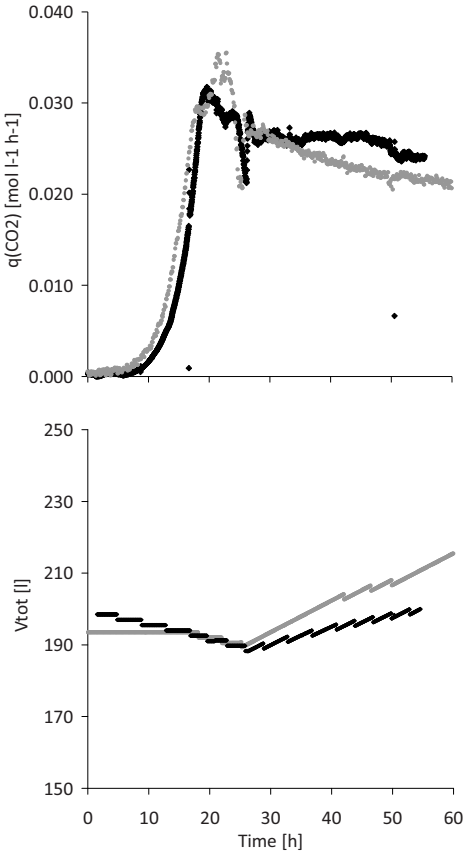

Figure 3.1: Top: Volumetric production rate of CO_2 measured during two fermentations with complex soy based medium.
Bottom: Total volume in the fermenters estimated based on initial volume, sample volumes of 1.5l, and a feed flow rate of $4gl^{-1}h^{-1}$. RJH: Black diamonds (♦), Intermig impeller set: gray circles (●).

After 23.4h and 24.6h for the Intermig and RJH system respectively, a drop in $q(CO_2)$ could be seen (figure 3.1, top), indicating the $20gl^{-1}$ glucose initially added to the medium was consumed. The fed-batch phase was thus initiated after 25.4h and 26.2h for the Intermig and RJH systems, respectively. The start volume in the two fermenters was 195l and 200l, but as the volume was reduced by 1.5l for each sample, total volumes were reduced to $V_{min,Intermig}$=189l and $V_{min,RJH}$=188l at the beginning of the fed-

batch phase. During the feed phase, the volume increased to a final value of $V_{max,Intermig}$=216l and $V_{max,RJH}$=200l, see figure 3.1 bottom. After the glucose feed had been started, the $q(CO_2)$ of the RJH system was constant (0.25-0.27mol$l^{-1}h^{-1}$) until 50h of fermentation where a small drop to 0.24 mol$l^{-1}h^{-1}$ was seen. For the Intermig system the $q(CO_2)$ decreased from 0.27 mol$l^{-1}h^{-1}$ to 0.21mol$l^{-1}h^{-1}$ during the fed-batch phase. As the glucose flow into the fermenter was constant, the drop in $q(CO_2)$ for the intermig system was an effect of the increasing volume. Due to more frequent sampling of the RJH, the effect was less pronounced.

The volume weighted size distribution, and viscosity, increased rapidly during the initial batch-phase (0-20h) for both fermentation systems, see figure 3.2. The majority of the mycelium was found growing on and around insoluble medium components, e.g. soy particles. During the feed phase, mycelium fragmentation could be observed in both fermentations, resulting in a decreasing volume weighted size distribution and viscosity, see figure 3.2. After 20h of fermentation, the soy particles started to break up into smaller units. As the mycelium "scaffold" disintegrated, the volume weighted size distribution and broth viscosity were reduced and continued to fall to a level of 0.45mm/2.2Pas for the Intermig fermenter and 0.28mm/1.7Pas for the RJH. The soy particles seemed to protect the mycelium from the shear stress in the systems, which could explain why no significant difference could be seen between the two systems during the batch phase. Apart from reduced support from the soy particle size after 20h, a reduction in mycelial tensile strength due to aging may also have affected the mycelium length.

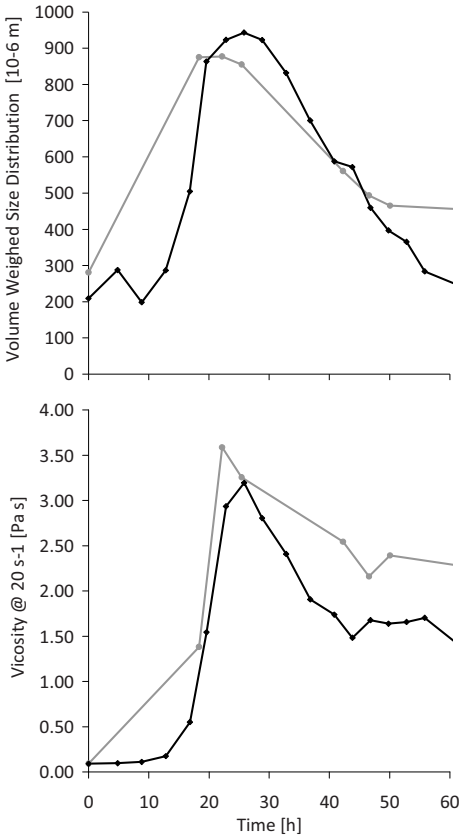

Figure 3.2: Top: Volume weighted size distribution of mycelium during fermentations with complex soy based medium.
Bottom: Fermentation broth viscosity measured at-line at a shear rate of 20 s^{-1}.
RJH: Black diamonds (♦), Intermig impeller set: gray circles (●).

Based on the calculated EDCF for the systems, the RJH was predicted to result in less mycelium fragmentation. The results from the actual fermentations indicates no significant difference between the two systems as the volume weighted size distribution of the RJH was similar to that of the impeller mixed system.

At the maximum viscosity (after 26h in the RJH system, n=0.21 and K=34.0), the minimum Reynolds number in the RJH was calculated (using equation 1.8, 2.1 and 2.4) to approximately 4250 in the jet nozzles (D=7mm). The flow was thus not fully turbulent. However, as no permanently stagnant zones could be seen, the signals from the DOT

probes were assumed to be representative for the conditions for the majority of the fermenter volume.

Through out the fermentation with the Intermig mixed system, the rotation speed was maintained at 300RPM and the air flow was 195lmin^{-1}. The volumetric power input for the Intermig system started at approximately at 2.6kW m^{-3} and slowly decreased to 2.2kWm^{-3} as the volume was increased, see figure 3.3 top. The increasing viscosity was anticipated to result in higher power input demands to maintain a rotation speed of 300RPM, but as the gas holdup increase is an effect of the viscosity, thereby reducing the broth density, the power input was constant throughout the fermentation. The increase of biomass resulted in a pressure increase in the recirculation loop of the RJH system from 1.6bar overpressure to 1.9bar at the end of the fermentation. However, the effect of the increased pressure on the volumetric power input was neutralised by the increasing volume during the fed-batch phase. Hence the volumetric power input of the RJH increased from 1.6-2.0kWm^{-3} during the first 36h of fermentation, where a drop to 1.8kWm^{-3} was seen due to the continually increasing volume.

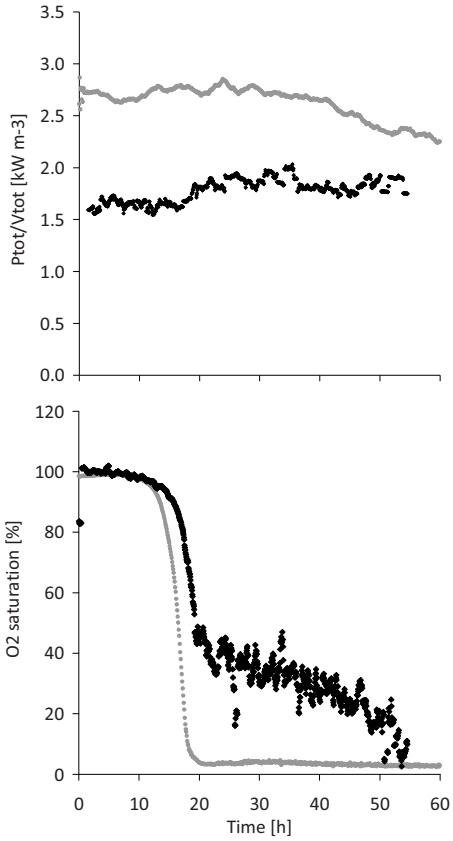

3.3: Top: Power input during fermentations with complex soy based medium.
Bottom: Oxygen saturation during fermentations with complex soy based medium. RJH: Black diamonds (♦), Intermig impeller set: gray circles (∘).

Though the volumetric power input of the RJH system was 18-40% less then that of the impeller mixed system and the rheological properties of the systems were similar, the oxygen saturation differed significantly, see figure 3.3 bottom. After 20h the Intermig system was depleted of oxygen, whereas the RJH was able to sustain an oxygen saturation above 20% for the first 50h of fermentation. The oxygen saturation in the RJH did drop with the same rate as the Intermig impeller from 100% to 45% after 20h, but during the fed-batch phase, the DOT saturation decreased with a lower rate thereby avoiding that the system became depleted of oxygen. The superior oxygen transfer of

the RJH system results in an approximately two fold increase of the k_La compared to the Intermig system during the fed-batch phase as illustrated in figure 3.4.

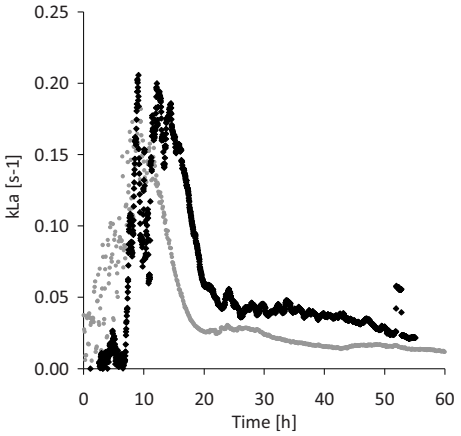

Figure 3.4: k_La during fermentations with complex soy based medium. RJH: Black diamonds (♦), Intermig impeller set: gray circles (●).

If the energy efficiency of the motors of the pump and impeller are similar, the RJH system is able to produce a k_La per kW used which is 2.2-2.6 times higher than the Intermig system during the fed-batch phase. A k_La increase of that magnitude may prove difficult to obtain purely by increasing the power input or airflow of a traditional system, which will be discussed further in chapter 5.

Carlsen *et al.* [15] reported that *Aspergillus oryzae* were able to produce up to $1gl^{-1}$ ethanol when growing in pellets. They assumed the ethanol production was a result of oxygen limitation inside the pellets. During the fermentations conducted in the current work, up to $3.4gl^{-1}$ ethanol was measured in the Intermig fermenter and $1.8gl^{-1}$ in the RJH fermenter, see figure 3.5. The formation of ethanol in the RJH system is initiated after approximately 50h, which coincides with the drop in DOT below 20%. For the Intermig system, the ethanol production also starts as the DOT drops below 20%, however, in the case of the Intermig system this occurs after 20h. These results indicate that although more efficient than the Intermig impeller, the fungi still becomes oxygen limited at the end of the fermentation in the RJH system. In figure 3.5, the glucose concentration is plotted with the ethanol concentration. For the Intermig system, the

glucose concentration drops to close to zero after 25h, but slowly increases during the following 35h (up to 1.2 gl^{-1}). For the RJH, the effect of the oxygen limitation seems to be more abrupt at 50h as both glucose and ethanol suddenly increases. This may be caused by the more homogeneous conditions throughout the fermenter compared to the impeller mixed system. In contrast to the dense clumps in the Intermig system, the dispersed mycelium in the RJH are suddenly all being exposed to oxygen limited conditions, which results in a large response.

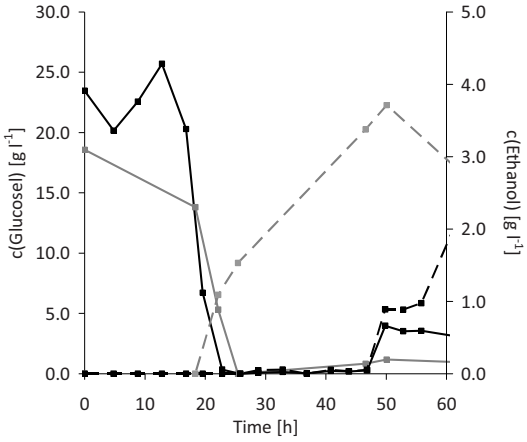

Figure 3.5: Glucose (solid lines) and ethanol (dashed lines) concentrations during fermentations with complex soy based medium. RJH: Black lines, Intermig impeller set: gray lines.

3.3.3 Fermentation with defined minimal medium

All fermentations with defined minimal medium both in the RJH and Intermig fermenter yielded similar biomass concentrations and growth rates as can be seen in figure 3.6 top.

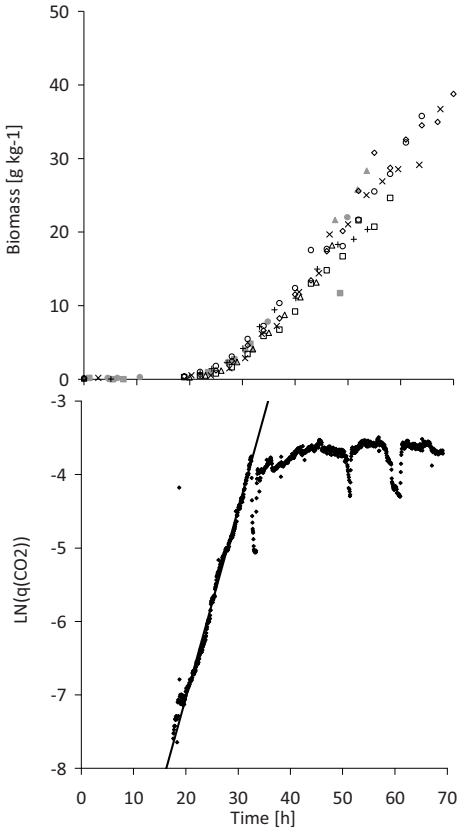

Figure 3.6: **Top:** Biomass concentration during six fermentations in the RJH system (□ ◊ Δ o + x) and three in the Intermig fermenter (■ ● ▲). **Bottom:** LN plot of the volumetric CO_2 production rate during a fermentation in the RJH fermentor. The rate increases exponentially with a rate of $0.26h^{-1}$ during the initial 32h. After 33.2h the fed-batch phase was initiated resulting in a constant $q(CO_2)$.

All fermentations had a batch phase with exponential growth phase which lasted until 31±1h after inoculation. The maximum specific growth rate in all fermentations in defined medium (Figure 3.6 top) was determined based on biomass concentration and $q(CO_2)$ during the exponential phase to be $0.26\pm0.2h^{-1}$, which is analogous to the maximum specific growth rate of $0.27h^{-1}$determined by Carlsen *et al.* [15] using the same medium. Figure 3.6 bottom is an example of LN plot of the $q(CO_2)$, and it can be

seen that the $q(CO_2)$ increased exponentially until 32h had elapsed. The solid line indicates the calculated maximum growth rate. After the exponential phase, a drop in the $q(CO_2)$ can be seen since the glucose is depleted. After the feed is established, the $q(CO_2)$ is constant throughout the fermentation with the exception of two drops (at 51h and 58h) due to pump failures. Based on the $q(CO_2)$, the fermentation seems to be carbon limited rather then oxygen limited. During fermentation in the Intermig and RJH fermenter with the defined minimal medium, the measured dissolved oxygen tension did not drop below 20% for either of the systems, see figure 3.7. In figure 3.7 the sudden increases in DOT for the RJH system is an effect of the glucose depletions (at 32h, 51h and 58h) mentioned earlier.

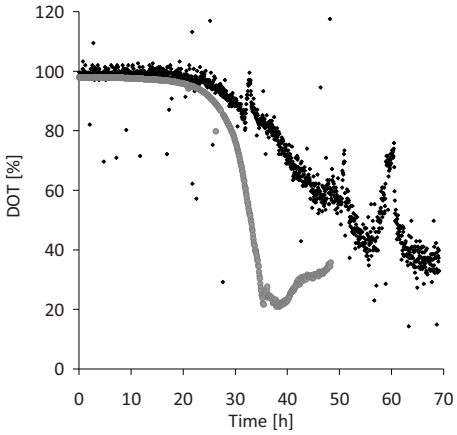

Figure 3.7: Dissolved oxygen tension during fed-batch fermentations with; RJH mixing system: black diamonds (♦) and Intermig impeller set: gray circles (•).

As previously mentioned *Aspergillus oryzae* have been shown to produce ethanol when oxygen limited.[15] During all fermentations, carbon balances were calculated, as illustrated in figure 3.8, to cross-validate the off-line measurements and to assure that all major carbon containing products could be accounted for.

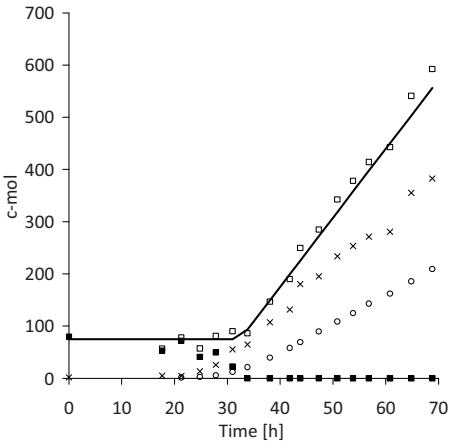

Figure 3.8: Carbon balances during fermentations with defenined minimal medium. c-mol added (—), c-mol accounted for (□), Glucose (■), Biomass (x) and CO2 (o).

For all fermentations on defined medium a simple carbon balance containing; biomass, CO_2, and glucose were generally able to account for more the 95% of the total carbon in the system (Figure 3.8). The Y_{SX} (c-mol biomass per c-mol consumed substrate) was determined to be between 0.6 and 0.8 for both fermenter systems. As no ethanol was produced in either of the fermentation systems, it is unlikely the cells are severely oxygen limited.

The power consumption of the Intermig system during the fermentations in defined medium were similar to that of the fermentations with the soy based medium (power drop of approximately 0.4kW m^{-3}) (see figure 3.9). During the initial 40h of fermentation, the power input of the RJH system was similar to the previous fermentation (approximately 1.6kW m^{-3}), but as the gas holdup and volume increased, the mass flow in the circulation loop decreased resulting in a drop in the volumetric power input (to 50% of the initial level).

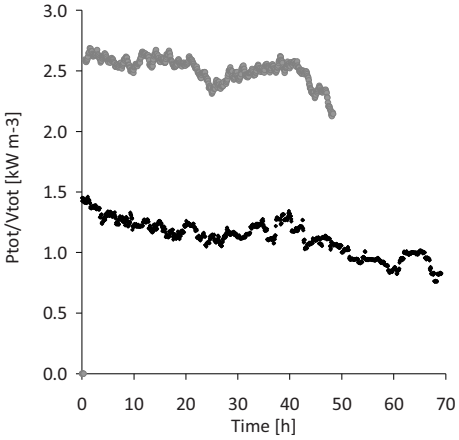

Figure 3.9: Power input during during fermentations with defined minimal medium. RJH: Black diamonds (♦), Intermig impeller set: gray circles (•).

The different power per volume did, as previously mentioned, not affect the formation of biomass, which is in accordance with other work with filamentous fungi. [3, 10]

Though the growth rate was not affected by the different P/V, the morphology differed significantly between the two fermentation systems. Fermentations with the RJH resulted in free mycelium and loosely associated mycelium clumps, whereas pellets/dense clumps could be observed in the Intermig mixed system, see figure 3.10.

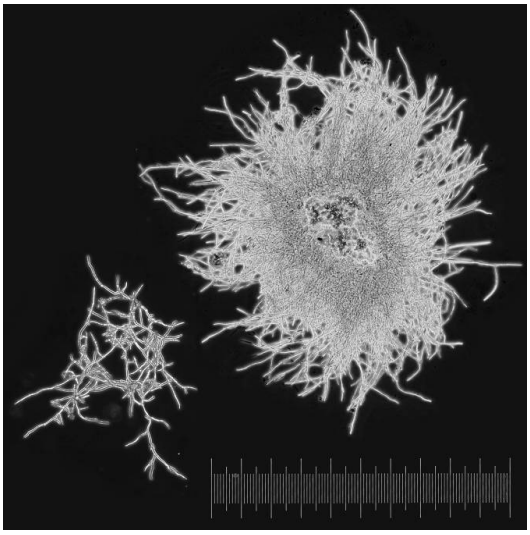

Figure 3.10: Typical fungal morphology at 18h: Left RJH and Right Intermig. Bar= 1mm.

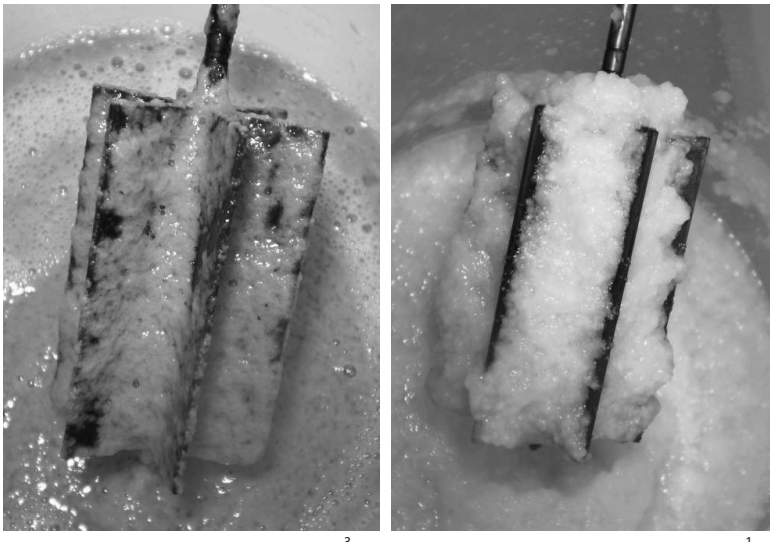

Figure 3.11: Left: RJH 1.6kW m^{-3} at 57h, biomass concentration= 28.6g kg^{-1}. Right: Intermig 2.6kW m^{-3} at 45h, biomass concentration= 22.0g kg^{-1}. Note the difference in rheological properties and colour.

The difference in rheology and morphology was also evident by visual inspection, as illustrated in figure 3.11. The broth from the fermentations in the impeller mixed system had a porridge-like rough structure with visible pellets and a pale yellow/cream colour,

whereas the broth from the RJH system was green-yellowish with a smoother texture. For the fermentations from the RJH system the average volume weighted size distribution was between 200 and 400µm throughout the fermentation, whereas the size distribution in the Intermig system resembled the results from the complex soy based medium with a maximum average volume weighted size distribution of 1085µm at 27h. In the case of the defined minimal media, the local high power dissipation zones in the nozzles of RJH system therefore seem to cause hyphal damage, thereby promoting mycelium fragmentation, in contradiction to predictions by the ECDF. Though the circulation time, and thereby the high stress frequency, of the Intermig impeller system is likely to be much higher then the RJH system (based on the values from the six blade Rushton turbine and a pitched blade impeller), the more homogeneous dissipation of the introduced energy results in less mycelium fragmentation. This result is in direct contradiction to the calculated EDCF values.

Fragmentation occurs when the shear force is larger than the tensile strength of a given hypha. [11, 12] During the fermentations with minimal medium in the RJH, an equilibrium between mycelium length and tensile strength seems to have been reached. The higher degree of fragmentation in the RJH system with defined minimal medium compared to the experiment with a complex soy based medium could be due to lower tensile strength, caused by a limiting substrate. Li *et al.* [3] argued that fragmentation in fungal fermentations could be caused by low levels of an important nutrient, and previous studies had shown that fungi lacking an important nutrient exhibit a significant increase in sensitivity to impeller-induced shear stress. [3] Other studies by Bhargava, Wenger and Marten (2003) have demonstrated how limiting the carbon source can decrease the mycelia size, lower broth viscosity, and thereby improve oxygen mass transfer. [1]

The fragmentation prediction by the EDCF may be caused by a secondary intense shear region in the pump. Small volumes of the mycelia may continuously become ground by the pump, resulting in a maximum size determined by the annulus of the pump. This “chopping” effect is, however, not seen in the fermentation with soy based medium, which could indicate that the solid particles in the medium, to some degree, protect the mycelium from the stress by the pump. If fragmentation is desirable in a fermentation with minimal medium, the high power dissipation zones in the RHJ system may be used

to promote fragmentation, thereby reducing the need to stress the fungi further in terms of limiting nutrients to get lower tensile strength.

The lower average volume weighted size resulted in a significantly lower viscosity in the RJH system, as can been seen in figure 3.12. This is somewhat surprising as pelleted growth previously has been reported to reduce the broth viscosity.

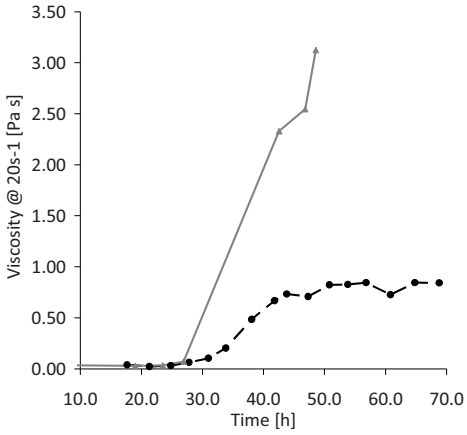

Figure 3.12: Viscosity measured at a shear rate at $20s^{-1}$ during fermentations with defined minimal medium. RJH: Black diamonds (♦), Intermig impeller set: gray circles (●).

The oxygen transfer is, as previously discussed in chapter 2, strongly affected by changes in viscosity, and increasing viscosity severely decreases the k_La. During the fermentation in the RJH system, the low viscosity is likely to be a significant contributor to the higher oxygen saturation compared to the Intermig system, as illustrated in figure 3.7.

3.4 Conclusion

This study has indicated that the RJH mixing system can be utilized as an efficient alternative to an Intermig impeller for mixing and air sparging during fungal fermentations. When using a complex soy based medium, no significant change in morphology or rheological properties could be observed between the two systems, but the volumetric oxygen transfer rate of the RJH system was, in spite of a approximately 50% lower energy consumption, twice that of the Intermig. In fermentation with a defined medium, a significant change in morphology was seen, from pelleted growth to mycelium in loosely associated clumps. The change in morphology led to a reduction of broth viscosity and improved volumetric gas transfer rates.

The growth rate was not affected by the mixing system, but the increased fragmentation in the RJH could cause the fungi to become stressed. One method to get a better understanding of the effect of the RJH system could be to look at the physiological state of the cells based on mRNA levels.

3.5 References

1. Bhargava, S., K.S. Wenger, and M.R. Marten, *Pulsed addition of limiting-carbon during Aspergillus oryzae fermentation leads to improved productivity of a recombinant enzyme.* Biotechnology and Bioengineering, 2003. **82**(1): p. 111-117.
2. Roels, J.A., J.V.D. Berg, and R.M. Voncken, *The rheology of mycelial broths.* Biotechnology and Bioengineering, 1974. **16**(2): p. 181-208.
3. Li, Z.J., et al., *Fungal morphology and fragmentation behavior in a fed-batch Aspergillus oryzae fermentation at the production scale.* Biotechnology and Bioengineering, 2000. **70**(3): p. 300-312.
4. Spohr, A., et al., *Morphological characterization of recombinant strains of Aspergillus oryzae producing alpha-amylase during batch cultivations*, in *Biotechnology Letters*. 1997, Kluwer Academic Publishers. p. 257.
5. Olsvik, E. and B. Kristiansen, *Rheology of filamentous fermentations.* Biotechnology Advances, 1994. **12**(1): p. 1.
6. Paul, G.C., M.A. Priede, and C.R. Thomas, *Relationship between morphology and citric acid production in submerged Aspergillus niger fermentations.* Biochemical Engineering Journal, 1999. **3**(2): p. 121.
7. Metz, B. and N.W.F. Kossen, *The growth of molds in the form of pellets-a literature review.* Biotechnology and Bioengineering, 1977. **19**(6): p. 781-799.
8. Casas López, J.L., et al., *Pellet morphology, culture rheology and lovastatin production in cultures of Aspergillus terreus.* Journal of Biotechnology, 2005. **116**(1): p. 61.
9. Jüsten, P., et al., *Dependence of Penicillium chrysogenum growth, morphology, vacuolation, and productivity in fed-batch fermentations on impeller type and agitation intensity.* Biotechnology and Bioengineering, 1998. **59**(6): p. 762-775.
10. Amanullah, A., et al., *Dependence of morphology on agitation intensity in fed-batch cultures of Aspergillus oryzae and its implications for recombinant protein production.* Biotechnology and Bioengineering, 2002. **77**(7): p. 815-826.
11. Nielsen, J. and P. Krabben, *Hyphal growth and fragmentation of Penicillium chrysogenum in submerged cultures.* Biotechnology and Bioengineering, 1995. **46**(6): p. 588-598.
12. Jüsten, P., et al., *Dependence of mycelial morphology on impeller type and agitation intensity.* Biotechnology and Bioengineering, 1996. **52**(6): p. 672-684.
13. Amanullah, A., et al., *Agitation induced mycelial fragmentation of Aspergillus oryzae and Penicillium chrysogenum.* Biochemical Engineering Journal, 2000. **5**(2): p. 109.
14. Jüsten, P., et al., *Dependence of <I>Penicillium chrysogenum</I> growth, morphology, vacuolation, and productivity in fed-batch fermentations on impeller type and agitation intensity.* Biotechnology and Bioengineering, 1998. **59**(6): p. 762-775.
15. Carlsen, M., et al., *Morphology and physiology of an α-amylase producing strain of Aspergillus oryzae during batch cultivations*, in *Biotechnology and Bioengineering*. 1996. p. 266.
16. Wattanachaisaereekul, S., et al., *Production of the polyketide 6-MSA in yeast engineered for increased malonyl-CoA supply.* Metabolic Engineering, 2008. **10**(5): p. 246.

Chapter 4

Intracellular Shear Stress Response in *Aspergilli*

Chapter 4

Intracellular Shear Stress Response in *Aspergilli*

4.1 Abstract

The Rotary jet-head mixing system has been shown to work as an efficient alternative to traditional impeller mixed systems for mixing and air sparging during fungal fermentations (Chapter 3). The intense power dissipation zones of the RJH system do, however, increase mycelium fragmentation in *Aspergillus oryzae* fermentations. Though the fragmentation does not reduce the growth rate, the high shear stress may have an impact overall stress level of the organism.

In this chapter the intracellular state of the fungi is investigated by studying gene regulation. Samples of mRNA from two fermentations in the Rotary jet-head system were compared to similar fermentations performed in an impeller mixed system. A number of stress related genes which were significantly regulated were identified, but the majority of the up regulated genes were found in the impeller mixed fermentations. The short time span in which the cells experience the high shear forces is likely too short to change the intracellular metabolic state. As the efficient mass transfer in the RHJ system ensures high average dissolved oxygen tension, compare to the reference system, the mRNA profile of the surviving fungi are less stressed. When comparing the results with the response of increased impeller speed for *Aspergillus niger* the same clear tendency was found.

These results indicate that the high degree of fragmentation induced by the RJH does not give rise to any significant stress response of the surviving cells, compared to oxygen limitations. The mycelium fragmenting rotary jet head system could therefore be used as an alternative to traditional mixing systems, in fermentations where high oxygen transfer is crusial.

4.2 Introduction

Several studies have investigated the effect of induced mycelium fragmentation in fungi. (1-6) Mycelium fragmentation is thought mainly to take place in regions of the mycelium weakened by aging or other stress factors such as limiting nutrients.(7) These regions do not contribute directly to the growth of the fungi, and mycelium fragmentation therefore does not generally decrease the growth rate (as discussed in the previous chapter).

Fragmentation can however, reduce the product yield from some fermentations. Jüsten *et al.* (8) found that Penicillin production by *Penicillium chrysogenum* decreased as mycelium fragmentation increased, because the main production of penicillin took place in the mycelium distal to the growing tips. The morphology of *Aspergillus niger* have also been shown to change at different shear force level which affected the productivity of the fungi. (*9*) The industrial use of *Aspergillus oryzae* is mainly related to the production of enzymes excreted to the medium. Enzyme secretion is thought mainly to take place in the growing hyphal tips. (*10*) This is consistent with the results of Amanullah *et al.* (3) who investigated the morphology and production of recombinant protein (amyloglucosidase) in *Aspergillus oryzae*, and found the specific production rate was related to the number of extending tips.(3) As mycelium fragmentation changes the rheological properties of the broth, it is difficult to characterise the physiological response to fragmentation on the cell under production conditions. In this chapter the physiological response to increasing shear stress is investigated for two different *Aspergili* (*Aspergillus oryzae* and *Aspergillus niger*) based on gene transcriptome data. The samples are taken from late in the exponential phase, before substrate limitations or reduced growth rates set in. Though increased fragmentation does not reduce growth rate or production of enzymes, the cells may display different stress levels as an effect of the different cultivation conditions.

4.3 Materials and Methods

The mRNA sampling, extraction, purification, and the preparation of the Microarrays were performed as described by Andersen *et al.* (*11*) and outlined in brief below.

4.3.1 Sampling for mRNA

Samples were extracted late in the exponential phase (based on $q(CO_2)$) from the four fermentations described in chapter 3. Two with complex soy-based undefined medium and two with chemically defined minimal medium. Immediately after the sample had been taken from the fermenter the mycelium was filtered through sterile Mira-Cloth (Calbiochem) and washed with 50ml chilled PBS buffer containing (per liter): 8.0g NaCl, 1.44g Na_2HPO_4, 0.24g KH_2PO_4 and 0.20g KCl.

The mycelium was dried by squeezing the filter between two paper towels. The filter cake was then wrapped in tin foil and frozen in liquid nitrogen within 1min after the sample had been taken from the fermenter, and the mRNA in the cells are thus representative for a specific time point during the fermentations. After freezing, the samples were stored at -80°C until RNA extraction took place.

4.3.2 Extraction and Purification

Approximately 50mg of frozen mycelium and three steel balls were placed in a microcentrifuge tube pre-chilled in liquid nitrogen. The cell wall of the mycelium was crushed, disrupting cells walls and plasma membranes, by shaking the tube in a Retsch Mixer Mill at 5°C for 12-15 minutes. The RNA was extracted from the powdered mycelium using a Qiagen RNeasy Mini Kit, as described in the protocol for isolation of total RNA from plant and filamentous fungi. The quantity and quality of the extracted RNA was determined using a NanoDrop 1000 Spectrophotometer (260nm/280 ratio) and a BioAnalyzer 2100 (Agilent Technologies).

4.3.3 cRNA Preparation and Microarray Processing

5μg of the RNA purified in the previous step was used as template to make 15 μg of fragmented and biotin-labeled cRNA, which were hybridized to a AsprgDTUa520520F GeneChip (Affymetrix), as described in the Affymetrix GeneChip(TM) Expression Analysis Technical Manual (Revision two). The quantity and quality was measured as indicated

above, and a GeneChip Fluidics Station FS-400 (Affymetrix) and a GeneChip Scanner 3000 (Affymetrix) were used for hybridization and scanning.

4.3.4 Analysis of transcriptome data

The scanned probe array images were converted into .CEL files by using the GeneChip Operating Software (Affymetrix) and preprocessed using the statistical language and environment R (www.r-project.org) version 2.8.1 with BioConductor 2.3 (*12*). The probe intensities were normalized for background using the robust multiarray average (RMA) method (*13*) using only perfect match (PM) probes. Normalization was subsequently performed using the quantiles algorithm (*14*). Gene expression values were calculated from the PM probes with the medianpolish summary method (*13*). All statistical preprocessing methods were used by invoking them through the Affymetrix package (*15*).

Statistical analysis was applied to determine genes with significantly different expression indices. The limma package (*16*) was used to perform one-way ANOVA analysis between the experimental groups, and the p-value was used for the comparative studies.

Bidirectional gene analysis: The list of bidirectional best hits (presumed 1:1 orthologues) in *A. niger* vs. *A. oryzae* was obtained from the comparison of *Aspergillus* genomes in Andersen *et al.* (*11*).

Gene annotations: The predicted genes of *A. oryzae* RIB40 genome sequence were assigned functions based on BLASTP (*17*) comparison to all characterized fungal proteins in the protein database SwissProt (*18*), data downloaded on March 31st, 2009). For each gene, the information on the best hit (if any present) was extracted and used for a prediction of function.

Statistical analysis: Hypergeometric testing was done using the statistical software package R version 2.8.1. (www.r-project.org).

4.3.5 *Aspergillus niger* samples

In addition to the *A. oryzae* data, transcriptome data from two *A. niger* fermentations (data kindly donated by Chr. Hansen A/S, Denmark, experiments conducted by Hans van

den Brink) were used to investigate the effect of different shear rates across different *Aspergilli*. The fermentations were conducted in a fermenter fitted with an Intermig impeller set, using the complex soy based medium and two different impeller speeds, Low; 252 RPM and High; 400 RPM. Two samples were used from each fermentation, one from the late exponential phase (~45h) and a second from the end of the fermentation (~120h).

4.4 Results and Discussion

For the analyses of the effect of the RJH system on *A. oryzae* one sample from each of the fermentations described in chapter 3 were used. The fermentation parameter for each sample is noted in table 4.1.

Table 4.1: Fermentation parameters when sampling mRNA in the exponential growth phase.

Mixing system		Intermig	Intermig	RJH	RJH
Medium		Defined	Complex	Defined	Complex
Sample time	[h]	26.8	23.3	30.9	19.8
Volume	[L]	195	195	225	200
P/V	[kW m^{-3}]	2.6	2.6	1.6	1.6
Glucose conc.	[g L^{-1}]	3.62	1.77	3.09	6.72
DOT	[%]	87.7	3.5	90.8	51.6
Viscosity @95s^{-1}	[Pa s]	0.069	1.072	0.105	0.496
q(CO2)	[mol L^{-1} h^{-1}]	0.008	0.016	0.013	0.031
c(Biomass)	[g kg^{-1}]	4.04		6.19	
r(CO2)	h^{-1}	0.049		0.051	

The samples were taken late in the exponential phase before substrate limitations set in (see figure 3.1 and 3.6). The difference in the physiological state, and thereby the gene expression, of the cell should therefore be a result of the mixing system. It was expected that the cells in the RJH would exhibit signs of physiological stress due to the high degree of mycelium fragmentation compared to the Intermig system.

4.4.1 Initial statistical survey of effect of mixing system

A statistical comparison, using one-way ANOVA test, of cultivations performed in the RJH versus the cultivations from the intermig impeller mixed system yielded 796 genes with significant (<0.050) p-values. These genes were used as the significant group in the further analysis. The complete list can be seen in Appendix I.

4.4.2 Gene by gene-examinations

Since only relatively few genes from *A. oryzae* have been characterized (315 found in SwissProt 12/5 2009), and even fewer of these are known to be involved in shear or oxidative stress relevant in this comparison, the genes of *A. oryzae* were annotated

based on sequence similarity (see materials and methods). These annotations were used to examine the differentially expressed genes. From this manual examination of the individual genes, a number of interesting observations were made:

AO090023000444 (Best hit: *A. nidulans* conidial yellow pigment biosynthesis polyketide synthase (wA)) is 1.46 fold upregulated during the RJH-fermentations. This corresponds well with the formation of a yellow pigment seen in the RJH cultivations (see figure 3.11 in chapter 3). The yellow pigment is a secondary metabolite which could be a stress indicator in the RJH system. Domínguez-Espinosa and Webb (*19*) showed that increases in shear stress affected both cell morphology and pigment production in *Monascus purpureus* fermentations. By increasing the agitation speed the size of the pellets in the fermentation was reduced and the amount of loose mycelia increased leading to improved dissolved oxygen concentration, and higher yields of both red and yellow pigment. This finding could support the theory that the average dissolved oxygen concentration in the RJH is higher than in the Intermig sytem.

Studies by Fillinger *et al.* (*20*) showed that trehalose is a major stress metabolite in *A. nidulans* induced by nutrient starvation, conidiospore differentiation, heat stress or oxidative stress. Based on sequence similarity, three trehalose-phosphatase genes were found in *A. oryzae* (AO090026000820, AO090005001531 and AO090020000035). AO090026000820 is significantly down regulated (-1.32 fold) in the RJH system compared to the Intermig fermenter. The remaining two genes which are annotated as trehalose-phosphatase (AO090005001531 and AO090020000035) are also down regulated but the change is less significant (-0.82 and -0.07 fold). These results could indicate that the cells in the dense clumps or poorly mixed regions of the Intermig system are suffering from stress due to either low levels of oxygen or nutrients.

Sakamoto *et al.* (*21*) investigated the stress response of *A. oryzae*, and found 29 genes which were up regulated when the fungi were exposed to stress, e.g. heat-shock or oxidative stress. Of the 29 genes 5 were found to be changed significantly between the mixing systems (listed in table 4.2).

Table **4.2: Stress related genes determined by Sakamoto *et al.* (*21*), found to be regulated significantly different in the RJH system compared to the Intermig system.**

ORF No.	Deduced function	Reg.
AO090003000770	Glycosyltransferases group 1	-5.02
AO090003000661	Thiamine pyrophosphate enzyme, central domain	-6.12
AO090026000820	Trehalose-phosphatase	-1.32
AO090020000603	FGGY family of carbohydrate kinases, C-terminal domain	0.54
AO090003000594	Glycosyltransferase family 2	-0.67

Of the five stress related genes four were down regulated in the RJH system. These results could further indicate the fungi are relatively more stressed in the Intermig fermenter, in contradiction to what was originally assumed at the end of chapter 3. If it should later be shown that the deduced functions of the genes are incorrect, it should be noted that both the RJH and Intermig studies were performed using *A. oryzae*, and it is therefore valid to conclude that the stress indication is correct.

4.4.3 Comparative study

To study the nature of the stress effect across *Aspergillus* species, the transcriptome data was compared to that of a similar experiment conducted with *A. niger* by Hans van den Brink (Chr. Hansen A/S, Denmark). That work studied the effect of raising the rotary speed of a set of Intermig impellers from 252 RPM to 400 RPM thereby increasing the shear rate but also dissolved oxygen tension. As the RJH was assumed to have a higher shear rate than the Intermig impeller system it was deemed valid to compare the *A. niger* results with those for *A. oryzae* found here.

Of the *796 A. oryzae* genes with significantly changed expression indices, 504 had direct bidirectional best hits in *A. niger*. Of these, 19 genes were significantly changed in both the *A. niger* and the *A. oryzae* experiments, but only 4 in the same direction (see Appendix II, table A.II). This led to the hypothesis, that at least a part of the response of *A. oryzae* to a RJH system versus an Intermig impeller at 300RPM is opposite to the response of *A. niger* to increasing stirring speed.

Examining the 504 significantly changed *A. oryzae* genes with direct bidirectional best hits in *A. niger*, 325 were found to be responding in the opposite direction in the two systems. To test whether this was just an effect of random sampling, the total number of genes with bidirectional best hits (7038) were examined for inverse response

patterns. In the entire population, 2886 genes (41%) were found to have inverse response patterns. Using a hypergeometric test for overrepresentation, it is found that the probability of randomly obtaining 325 or more inversely responding genes in the population of the 504 significantly changed genes $P[X >= 325] = 8.78x10^{-29}$. This makes it highly significant that the response in *A. niger* is opposite to that of *A. oryzae* under the compared conditions. Even so, one should be cautious of concluding that a RJH is less of a stress factor than the Intermig stirring. A further analysis of these 325 genes is needed.

4.4.4 Pathway-level differences in the 325 genes

When examining the 325 genes (see Appendix III), it is clear that there is a strong representation of genes in glycolysis (see figure **4.1**) that have expression which is lowered on RJH vs. Intermig (*A. oryzae*) while higher on 400 RPM vs. 252 RPM (*A. niger*). Regulation of glycolysis is often a result of general changes in growth rate. However, since the effect seems be isolated to glycolysis, it is unlikely that this is the case. Alternatively, glycolysis can also be down-regulated as a result of more carbon passing through the pentose phosphate pathway, but no indication of this is seen in the transcriptome analysis. Furthermore, glycolysis generates cytosolic ATP, which may be a factor in the observed regulation. Even so, none of these explanations are directly tied with a stress response or the absence of one.

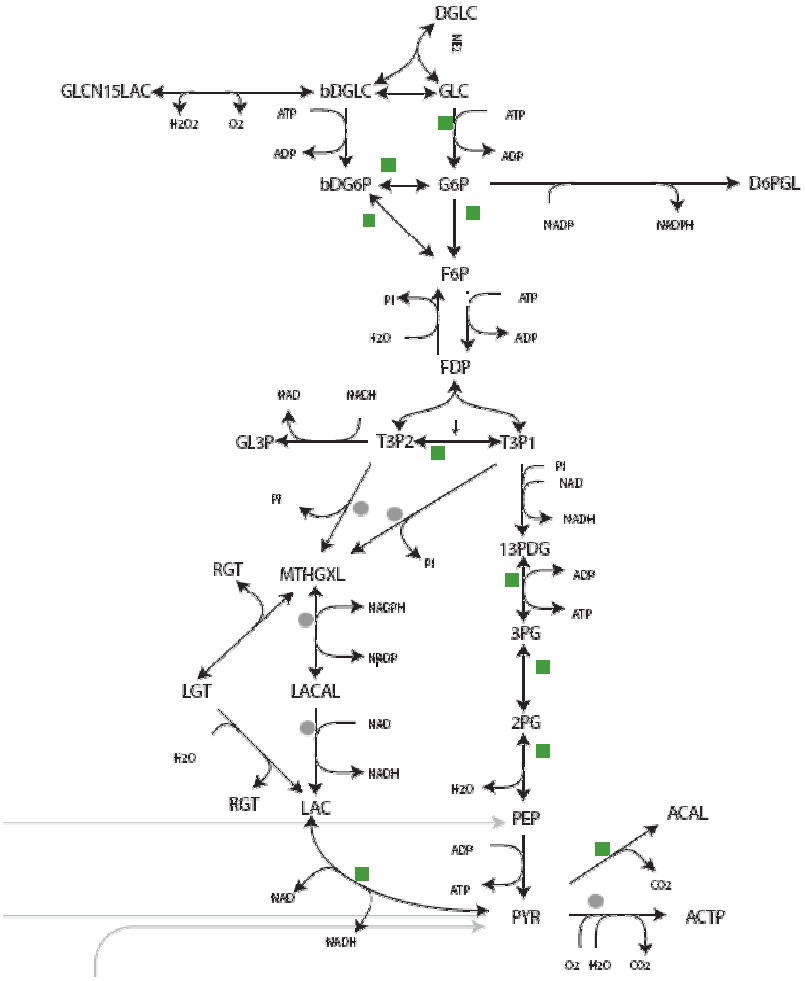

Figure 4.1: A subset of the genes that are lowered on RJH vs Intermig (*A. oryzae*) while higher on 400RPM vs. 252RPM (*A. niger*) marked with green squares.

Three steps of ergosterol biosynthesis from lanosterol are also affected. Ergosterol is interesting in the context of cell stress response, as it manipulates the properties of the cell membrane to be more flexible. However, the biosynthesis pathway is 21 steps, so this is not a tendency at pathway-level, as would be expected if the biosynthesis levels of ergosterols were to be affected.

4.4.5 Single gene examinations of the 325 genes

Of the 325 genes, 145 could be assigned a verified or putative function based on homology (see Appendix III). Of these, 83 are enzymes with an assigned EC number. Examining the non-enzymatic proteins, a number of interesting genes were found.

- Two genes AO090102000352 and AO090701000002, with homology to heat shock proteins from *A. nidulans* (Hsp30, Kusakabe *et al.* (*22*) and *N. crassa* (Hsp98, Vassilev *et al.* (*23*)), respectively. The proteins have nearly the same fold change in expression index, and are more highly expressed in the Intermig culture than in the RJH.

- Gene AO090701000709, with homology to DNA repair protein Rhp41p of *S. pombe* (Marti *et al.* (*24*)). This too is more highly expressed in the culture from the impeller mixed system compared to that of the RJH culture.

- AO090120000463 has homology with the *S. cerevisiae* gene YOR378W. This gene conveys resistance to DNA damaging agents (Schaus *et al.* (*25*)). AO090120000463 is found to be more highly expressed on the Intermig system.

As these stress and cell damage related genes are all upregulated in the intermig culture, it seems unlikely that the culture in the RJH fermenter is negatively affected by the system.

Interestingly, all 83 genes with assigned EC number are more highly expressed on *A. oryzae* grown in the Intermig and *A. niger* 400RPM, than for *A. oryzae* grown in the RJH system and *A. niger* 252RPM. In the enzymatic genes, the following genes of particular interest are found:

- Two genes with acetyl-coenzyme A synthetases as best hits (AO090023000577, AO090003000392) are found to be much higher (more than nine-fold for both genes) on *A. oryzae* grown in the Intermig as compared to the RJH. This effect is an extension of that shown in figure 4.1, as this processes the increased production of pyruvate generated in the glycolysis.

- Two genes are found with peroxiredoxins from *S. cerevisiae* as best hits; AO090005001449 (*PRX1*) and AO090005000630(HYR1). Prx1p is a mitochondrial protein which is overexpressed when the respiratory pathway is used, as well as under conditions of oxidative stress (Pedrajas *et al.* (*26*)). Hyr1p/Gpx3p is also involved in the oxidative stress response, and deletion mutations become hypersensitive to peroxide (Inoue *et al.* (*27*)). Both genes are approximately two-fold higher on *A. oryzae* Intermig than on RJH.

The higher level of enzyme expression could imply a higher metabolic turnover rate in the *A. oryzae* culture grown in the Intermig and the *A. niger* 400RPM.

4.5 Conclusion

It was unknown if highly intense power dissipation zones and mycelium fragmentation of the RJH system would lead to increased stress levels in the fungi, compared to the more homogeneous energy dissipation by the Intermig. By single gene examinations, combined with the comparative study with *A. niger,* stress related genes were identified to be significantly changed. Interestingly the vast majority of the stress related genes were up regulated in the Intermig impeller fermenter, compared to the RJH system. This result could indicate the time span in which the cells experience the high shear force is to short for the cells to react. A fraction of the cells are likely to get ripped apart during the circulation in the external loop but the majority of the cells are unaffected by the high shear. The mycelium which survives the frequent high shear can benefit from the higher dissolved oxygen tension in the RJH system, and does therefore show reduced stress levels compared to mycelium cultivated in the reference system.

Another explanation of the elevated stress levels in Intermig fermenter could be the difference in morphology at the sampling point. In the intermig fermenter a large fraction of the biomass was in the form of pellet or dense clumps compared to lose mycelium clumps in the RJH system. The samples were taken from the fermentations before oxygen and nutrient limitations reduced the growth rate, and any stress response was therefore assumed to be directly related to the mixing system. This assumption does not take diffusion limitations in the pellets into account. The concentrations of both oxygen and nutrient may be significant lower in the nucleus of the dense clumps compared to the surrounding media.(*28*) As the RNA samples used for the analysis are from a mixture of the fungal mycelium, the stress response in the Intermig fermenter may in fact be related to the difference between density of the mycelia clumps in the to systems, rather than different shear stress. This hypothesis however, does not account for the result with complex medium where the morphology was similar, nor the conserved response in *A. niger*.

4.6 References

1. P. Jüsten, G. C. Paul, A. W. Nienow, C. R. Thomas, *Biotechnology and Bioengineering* **52**, 672 (1996).
2. G. C. Paul, M. A. Priede, C. R. Thomas, *Biochemical Engineering Journal* **3**, 121 (1999).
3. A. Amanullah, L. H. Christensen, K. Hansen, A. W. Nienow, C. R. Thomas, *Biotechnology and Bioengineering* **77**, 815 (2002).
4. Z. J. Li *et al.*, *Biotechnology and Bioengineering* **70**, 300 (2000).
5. J. Nielsen, P. Krabben, *Biotechnology and Bioengineering* **46**, 588 (1995).
6. A. Amanullah *et al.*, *Biochemical Engineering Journal* **5**, 109 (2000).
7. S. Bhargava, K. S. Wenger, M. R. Marten, *Biotechnology and Bioengineering* **82**, 111 (2003).
8. P. Jüsten, G. C. Paul, A. W. Nienow, C. R. Thomas, *Biotechnology and Bioengineering* **59**, 762 (1998).
9. M. Papagianni, M. Mattey, B. Kristiansen, *Biochemical Engineering Journal* **2**, 197 (1998).
10. A. Spohr, M. Carlsen, J. Nielsen, J. Villadsen, in *Biotechnology Letters*. (Kluwer Academic Publishers, 1997), vol. 19, pp. 257.
11. M. R. Andersen *et al.*, *Proceedings of the National Academy of Sciences* **105**, 4387 (March 18, 2008, 2008).
12. R. Gentleman *et al.*, *Genome Biology* **5**, R80 (2004).
13. R. A. Irizarry *et al.*, in *Biostatistics*. (Oxford University Press, 2003), vol. 4, pp. 249.
14. B. M. Bolstad, R. A. Irizarry, M. Ã…strand, T. P. Speed, in *Bioinformatics*. (Oxford University Press, 2003), vol. 19, pp. 185.
15. L. Gautier, L. Cope, B. M. Bolstad, R. A. Irizarry, in *Bioinformatics*. (Oxford University Press, 2004), vol. 20, pp. 307.
16. G. K. Smyth, in *Statistical Applications in Genetics and Molecular Biology*. (Berkeley Electronic Press, 2004), vol. 3.
17. S. F. Altschul, W. Gish, W. Miller, E. W. Meyers, D. J. Lipman, in *Journal of Molecular Biology*. (1990), vol. 215, pp. 403.
18. E. Boutet, D. Lieberherr, M. Tognolli, M. Schneider, A. Bairoch, *Methods Mol Biol.* **406**, 89 (2007).
19. R. M. Domínguez-Espinosa, C. Webb, *World Journal of Microbiology and Biotechnology* **19**, 329 (2003).
20. S. Fillinger *et al.*, *Microbiology* **147**, 1851 (July 1, 2001, 2001).
21. K. Sakamoto *et al.*, *Fungal Genetics and Biology* **45**, 922 (2008).
22. T. Kusakabe, K. Koga, Y. Sugimoto, in *Biochimica et Biophysica Acta*. (1994), vol. 1219, pp. 555.
23. A. O. Vassilev, N. Plesofsky-Vig, R. Brambl, in *Biochimica et Biophysica Acta - General Subjects*. (1993), vol. 1156, pp. 1.
24. T. M. Marti, C. Kunz, O. Fleck, in *Genetics*. (Genetics Society of America, 2003), vol. 164, pp. 457.
25. S. E. Schaus, D. Cavalieri, A. G. Myers, in *Proceedings of the National Academy of Sciences of the United States of America*. (National Academy of Sciences, 2001), vol. 98, pp. 11075.
26. J. R. Pedrajas, A. Miranda-Vizuete, N. Javanmardy, J.-A. Gustafsson, G. Spyrou, in *Journal of Biological Chemistry*. (2000), vol. 275, pp. 16296.
27. Y. Inoue, T. Matsuda, K.-i. Sugiyama, S. Izawa, A. Kimura, in *Journal of Biological Chemistry*. (1999), vol. 274, pp. 27002.
28. B. Metz, N. W. F. Kossen, *Biotechnology and Bioengineering* **19**, 781 (1977).

Chapter 5

Effect of Viscosity on k_La during a Filamentous Fungus Fed-Batch Fermentation

Chapter 5

Effect of Viscosity on k_La during a Filamentous Fungus Fed-Batch Fermentation

David Kold[1], Karsten Hellmuth[2] and Timothy J. Hobley[1].

5.1 Introduction

Limited fossil fuel resources and increasing oil prices have led to an economic incentive to change from traditional petroleum-based chemical production to bio-based processes. Products to be produced can range from organic acids and chemical building blocks to bio-polymers, enzymes and cheap pharmaceuticals such as some antibiotics. Many of these processes are characterised by products produced in high volume but having a low value. For these low value added products expenses for mixing, mass and heat transfer become very important, and must be kept to a minimum. During fermentations with traditional impeller systems the oxygen transfer rate becomes severely reduced as the viscosity increases. Highly viscous fermentations commonly occur when filamentous fungi are used, but are also typical for microorganisms that produce extracellular polymers. To make such bio-based processes competitive more efficient fermenter systems must be applied. Previous studies using model solutions of carboxy methyl cellulose by Nordkvist *et al.* (*1*) showed that the Rotary Jet Head (RJH) mixing system can provide cost efficient mixing, mass and heat transfer in pilot scale fermentation tanks. However, investigations of the performance of the system during fungal fermentations have not been reported before. In this chapter, the effect of increased viscosity during fermentation on the volumetric oxygen mass transfer coefficient, in a RJH system is investigated for the first time.

5.1.1 Effect of viscosity on mass transfer in fermenters

The oxygen transfer rate (OTR) of a system can be expressed as a function of the volumetric oxygen mass transfer coefficient (k_La), the oxygen concentration (c) and the

[1] Center for Microbial Biotechnology, Institute of Systems Biology, Technical University of Denmark, Kgs. Lyngby, Denmark.
[2] Chr. Hansen A/S, Nienburg, Germany.

saturation concentration of oxygen (c*) at the specific temperature, pressure and medium conditions, as stated in equation 5.1 .(*2*)

$$OTR = k_L a(c^* - c) \qquad \textbf{Eq. 5.1}$$

Empirical correlations for the volumetric oxygen mass transfer coefficient often include the volumetric power input under gassed conditions (P_t/V) and the superficial gas velocity (u_s): (*2*)

$$k_L a = k u_s^{\alpha} \left(\frac{P_t}{V}\right)^{\beta} \qquad \textbf{Eq. 5.2}$$

Where α, β and k are equipment specific constants. P_t is the sum of the power from the mixer 'P' (equation 1.3) and the power provided by the gas 'P_g' (equation 1.4). Equation 5.2 does not take viscosity into account and is therefore only valid for fermentations with a viscosity below 50mPas. (*2*) Ryu and Humphrey (*3*) proposed a model including a viscosity term:

$$k_L a = k u_s^{\alpha} \left(\frac{P_t}{V}\right)^{\beta} (\eta_{app})^{\omega} \qquad \textbf{Eq. 5.3}$$

Were ω is an equipment specific constant. Ryu and Humphrey (*3*) calculated a ω=-0.86 to result in the best fit during *Penicillium chrysogenum* fermentations in a 550l vessel, but unfortunately with no information on the agitator type. Buckland *et al.* (*4*) was able to fit their data "reasonably well" to a ω value of -0.5 for a *Nocardia lactamdurans* fermentation. The same exponent value was determined by Tecante and Choplin (*5*) using different aqueous solutions of CMC, xanthan gum, and polyacrylamide in a fermenter equipped with a helical ribbon screw impeller. A more comprehensive study was performed by Cooke *et al.* (*6*) on fungal broth and paper pulp. In this study six different impellers were tested ranging from a Scabe axial flow impeller to a traditional six bladed disc turbine. Several tank setups were tested with an aspect ratio of 1:1 and 1:3, respectively, ranging from 20l to 4.3m^3. For the fermenter with an aspect ratio of 1:1 the data correlated within ±30% for α=0.3, β=0.56 and ω=-1 for all impellers. The fermenter with aspect ratio 1:3 resulted in similar values (α=0.3, β=0.5 and ω=-1).(*6*) The dimensions of the fermenter, within these aspect ratios, seem to be thus of minor importance when traditional impellers are used. In a more recent study by García-Ochoa and Gómez (*7*) a 20l tank was used with an aspect of ratio 1:1. They characterised different impellers using xanthan solutions with consistency index varying from 0.708 to 0.00492Pas^{-n} and flow behaviour index varying from 0.32 to 0.84. The superficial gas

velocity, volumetric power input and viscosity term of equation 5.3 were found to be of equal importance for the k_La (α=0.67, β=0.6 and ω=-0.67).(*7*) The consistency indexes and flow behaviour indexes for the fluids in that work are significantly lower then those of the solutions used in chapter 2 in the current work, which were found to resemble fungal fermentation broth (e.g. 1.25% xanthan, n= 0.174 and K=9.03Pas^n). One could speculate that the discrepancy in the calculated exponent factors was an effect of the large difference in viscosity and impellers. Tecante and Choplin (*5*) used a helical ribbon screw impeller whereas the exponent value of Cooke *et al.* (*6*) was determined using a Rushton disc turbine impeller. As the helical ribbon screw impeller is significantly more efficient for mixing viscous solutions compared to the Rushton disc turbine impeller, the difference in the ω exponent may indicate, whether a system is suited for mixing a given fluid. During a fermentation the superficial gas velocity and volumetric power input rarely change more then a factor 10, whereas a 1000 fold increase in the broth viscosity is not uncommon. Taking the relatively large ω exponent value into account, increasing viscosity can therefore cause a significant reduction in the oxygen transfer rate, which may be difficult to circumvent by increasing the power input and airflow due to either design constraints or economic considerations.

The aim of this chapter is, for the first time, to evaluate the oxygen mass-transfer and mixing performance of a 250 L pilot scale Rotary Jet-Head fermenter, during fermentations with *Aspegillus oryzae*. Sparging air directly into the high intensity mixing zone of the jet is hoped to ensure a high initial oxygen transfer rate, but the effect of high viscosity on the system is unknown. In this chapter of the thesis the focus is placed on examining the effect of increasing viscosity on the k_La value in the RJH fermenter. For reference, in Chapter 3 a detailed analysis of the effect of the RJH system on the fungus in terms of growth rate, cell morphology, etcetera, is conducted.

5.2 Materials and Methods

5.2.1 Fermenter setup

The fermentations were conducted in the Rotary Jet Head mixing system described in chapter 1. The k_La was calculated during the fermentations using the direct pseudosteady-state method as described by Nielsen *et al.* (*2*). The OTR was measured using a 5853 S Mass Flow Controller (Brooks Instruments, United States) and a gas monitor model 1308 (Büel & Kjær, Denmark). The c* was estimated using the average oxygen concentration in the air inlet and outlet of the tank.

5.2.2 Viscosity measurement

A vibrating rod sensor, Marimex VA-300 with a ViscoScope control console, was used as described in the chapter 2.3.1-6. The sensor was placed in the recirculation loop and the probe signal was recorded continuously. At-line measurements were made using a Haake VT500 FL10 rheometer from 1.4l samples, and power law constants were found as described in chapter 2.3.1-5.a.

5.2.3 Fermentation conditions

All fermentations were conducted using the fermentation conditions, strain, inoculation procedure and media described in chapter 3.3.2.

5.3 Results and Discussion

During the two fermentations described in chapter 3.4, which were conducted in the RJH fermenter system using a complex medium and a defined medium, the viscosity was measured in-line with the Marimex probe and at-line using the Haake VT500 FL10 rheometer. In the first fermentation in defined minimal medium a fermentation broth with medium viscosity resulted (figure 5.1, top). The results show that viscosity increased greatly after 20h had elapsed, which coincided with the onset of the exponential growth phase (for further details concerning biomass concentration, growth rate etcetera see chapter 3.4.2 for fermentations with complex medium and chapter 3.4.3 for fermentations with defined minimal medium). Viscosity rose to ca. 0.06 Pa s after ca. 50 h, at which point the mycelium network started to brake-up leading to a small drop in viscosity to 0.05Pas (mycelium size distribution and morphology is discussed in detail in chapter 4). The probe signal was measured in-line and gave a good indication of the true viscosity measured at-line, though there seemed to be a ~4h shift of the in-line measured values compared to those at line (figure 5.1).

The second fermentation was conducted using a complex soy based medium which gave rise to a fermentation broth approximately twice as viscous as the minimal medium. The maximum viscosity (0.10Pas) was reached after 30h, after which the mycelium was seen to break up into smaller segments thereby leading to a fall in viscosity to 0.06 during the following 10h. As the biomass concentration increased so did the viscosity, though the average mycelium size continued to decrease. The development in viscosity measured in-line and at-line can be seen in figure 5.1 (bottom).

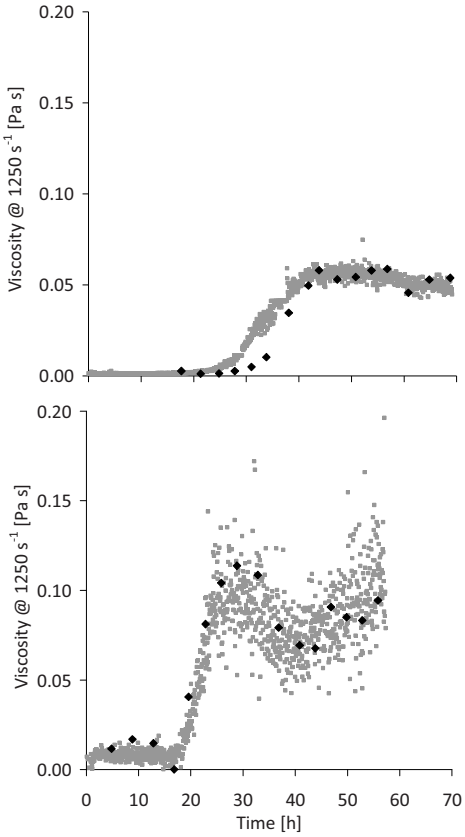

Figure 5.1: **<u>Top</u>: *Aspergillus oryzae* fermentation using a defined minimal medium. <u>Bottom</u>: *Aspergillus oryzae* fermentation using a complex soy based medium. The viscosity is calculated at $\gamma_{av}=1250s^{-1}$ for both fermentation. Marimex VA-300 sensor - gray squares ■, and Haake FL10 rheometer - black diamonds ♦.**

As shown above, the trend of the Marimex probe signal was similar to the true broth viscosity measurements at-line with the Haake VT500 FL10 rheometer. Some noise could be seen in the online-data, especially at high viscosities. The noise was mainly caused by air bubbles which became entrained in the liquid passing through the recirculation loop. This problem could possibly be minimized by degassing the fluid in the recirculation loop. This could be done as proposed by Nordkvist *et al.* (*1*) simply by inserting a degasser in the recirculation loop. Nevertheless the average viscosity of the fungal broth measured on-line did not seem to be reduced by the air bubbles in the

broth, though a significant increase in the gas holdup could be observed during the time course of the fermentation resulting in a 20-25% increase of the broth volume. During the fermentations, sudden increases in online viscosity could be seen and were found to be due to mycelium sticking to the on line probe. This problem was eliminated by periodically changing the flow direction for a few seconds every 4-5h, thereby dislodging the mycelium.

Of particular interest for a fermentation is to understand how viscosity affects k_La so that the best way of supplying sufficient oxygen to the cells can be found. During the two fermentations conducted above, the gas flow rate and power input (i.e. through the lobe pump in the recirculation loop) were kept constant in the period 20-55h for the fermentation with complex medium and 15-40h for the defined medium, as illustrated in figure 3.3 top and 3.9. By plotting the k_La from the two fermentations in these time periods against the on-line viscosity, the exponent factor ω from equation 5.3 could be determined by calculating the slope of the line in the LN-LN plot, see figure 5.2.

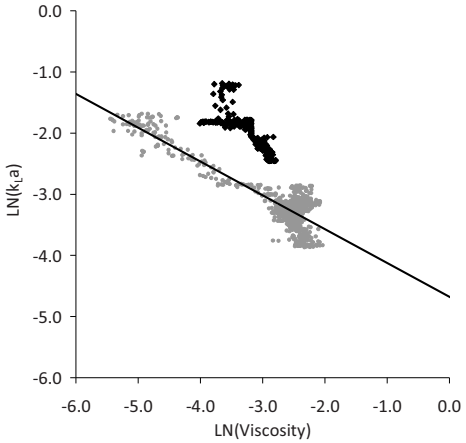

Figure 5.2: **The ln(viscosity) plotted against the ln(k_La) for the fermentation of moderate viscosity conducted with defined medium (Black diamonds ♦) and the highly viscous fermentation conducted with complex medium (gray circles ●), both measured using the Marimex probe on-line. The line indicates the best fit for the data from the fermentation on complex medium, slope= ω= -0.6 (R^2=0.796).**

Though the viscosity profiles during the two fermentations differed significantly the effect of the viscosity on the k_La was identical, as the exponent factor ω=-0.6 was determined for both fermentations. In previous studies, ω values ranging from -1 to -0.50, have been determined. (*3-7*) The exponent factor for the RJH fermenter is thus in the lower end of the previously determined values, which could indicate that the k_La in the RHJ system is less susceptible to increases in viscosity, compared to most traditional fermenter types. Specialized impellers for viscous fermentations, such as the helical ribbon screw impeller, have shown even lower ω exponents. However, this impeller type is less suitable for non-viscous fermentations. The RJH system is, on the other hand, able to provide efficient mixing both under viscous and non-viscous conditions. The relative low effect of viscosity on the RJH system could be due to the way in which the air is added. The air inlet is in the loop where the fluid velocity is highest, furthermore the fluid jets exiting into the bulk liquid cause high shear forces. For shear thinning fluids this

is a clear advantage. Additionally, the high local power input of the jet streams from the RJH results in the formation of small bubbles which are rapidly distributed in the fermenter.

The calculated exponent value (ω=-0.6) was determined based on the data from the fermentations with constant power input. By using the exponent values (α and β) from García-Ochoa and Gómez (*7*) an estimation of the k_La during the entire fermentation could be made. For both fermentations the calculated k_La is plotted against the measured k_La in figure 5.3.

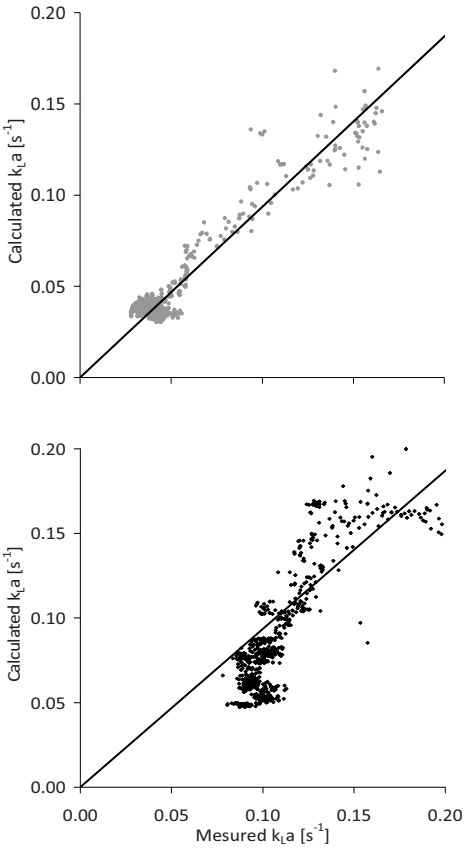

Figure 5.3: **The measured k_La plotted against the calculated (k_La). Complex medium (top) gray circles ●. Defined medium (bottom) black diamonds ♦. α=0.67, β=0.6, ω=-0.55 and k=1.2·10^{-4}. Slope of line=1**

The calculated k_La values correlate well to the measured data for the fermentation with complex medium, as illustrated in figure 5.3 top. For the fermentation with the defined medium (figure 5.3 bottom) the data did not fit as well which could indicate that one or both of the remaining exponent values are incorrect. Further studies, with varying airflow and power input are performed in chapter 6 to determine these values. If the constants from equation 5.3 are known, an in-line viscosity measurement enables an online estimation of the k_La without the use of a gas analyser or performing dynamic k_La tests. In-line viscosity measurement thereby enables an on-line control of the k_La value, and the OTR control can be performed based on the properties of the fluid instead of the increased viscosities effect on e.g. the dissolved oxygen concentration, resulting in a shorter response time.

5.4 Conclusion

The oxygen mass transfer rate of the Rotary Jet-head system was found to be less susceptible to increases in broth viscosity than for most traditional impeller mixed fermenters at similar scale, indicating that the new fermenter type may have advantages for viscous fermentations. The reduced effect of viscosity on k_la may be due to that the air is sparged directly into the high intensity mixing zones ensuring a high oxygen transfer rate. It was furthermore demonstrated how viscosity data can be use to estimate the k_La of a mixing system, without the use of a gas analyser or probe for measuring the dissolved oxygen tension, thereby facilitating reduced response time of the air flow control.

5.5 References

1. M. Nordkvist, T. Grotkjær, J. S. Hummer, J. Villadsen, *Chemical Engineering Science* **58**, 3877 (2003).
2. J. Nielsen, J. Villadsen, G. Lidén, *Bioreaction Engineering Principles*. 2, Ed. (Kluwer Acedemic/Plenum Publishers, New York, 2003), pp. 528.
3. D. Y. Ryu, A. E. Humphrey, *Journal of Fermentation Technology* **50**, 424 (1972).
4. B. C. Buckland *et al.*, *Biotechnology and Bioengineering* **31**, 737 (1988).
5. A. Tecante, L. Choplin, *Canadian Journal of Chemical Engineering* **71**, 859 (1993).
6. M. Cooke, J. C. Middleton, J. Bush, *King R (ed) 2nd Int. Conf. on Bioreactor Fluid Dynamics*, 37–64 (1988).
7. F. García-Ochoa, E. Gómez, *Biochemical Engineering Journal* **1**, 1 (1998).

Chapter 6

Characterization of Mass Transfer in a Rotary Jet Head Fermenter during *Xanthomonas campestris* fermentations

Chapter 6

Characterization of Mass Transfer in a Rotary Jet Head Fermenter during *Xanthomonas campestris* Fermentations

6.1 Abstract

A 300L Rotary Jet-Head (RJH) fermenter was used for the first time in viscous aerated cultivations of the xanthan gum producing bacterium *Xanthomonas campestris* . The RJH was found to have very promising performance. The maximum growth rate of the cells was as expected ($0.13h^{-1}$) and a good k_La value of $0.15s^{-1}$ at low power input ($1.1kW\ m^{-3}$) and air flow (0.1VVM) was achieved. The following correlation for the k_La with the superficial gas velocity (u_s), power input (P_t), volume of the tank (V), viscosity (η_{app}) and a constant (k) was found :

$$k_L a = k u_s^{0.4} \left(\frac{P_t}{V} \right)^{0.122} (\eta_{app})^{-0.8}$$

The implications of this equation are that for a fermenter with a single jet head , the effect on k_la of increasing the power input or superficial gas velocity is limited. Therefore for scale-up, a fermenter tank setup with several jet heads would thus be a better solution for supplying oxygen to the cells, compared to simply increasing the power input or gas flow rate.

6.2 Introduction

Due to increasing raw material prices and growing environmental awareness, some industries which traditionally used petrochemical based non-degradable polymers are shifting to more environmentally sustainable alternatives such as biopolymers. [1] Several biopolymers are commercially available, such as; alginate, dextran, gellan, pullulan and xanthan, where xanthan is the most widely used. [2]

6.2.1 Xanthan producing bacteria

Xanthan gum was discovered in the late 1950s as a biopolymer being excreted by the gram negative phytopathogenic bacteria *Xanthomonas campestris*.[1] In liquid media *X. campestris* is mainly found as single cells or in pairs; however chains or filaments can also be observed. [2, 3] The cells are oblong rod shaped (0.2-0.7 by 0.7-2.9µm) with a single polar flagellum. [2, 4] On solid medium *X. campestrisi* grows in smooth yellow colonies surrounded by a protective mucoid xanthan layer. The polymer layer is thought to provide the cells with some protection from the surrounding environment thereby increasing the colonies resistance towards e.g. dessication. Stress factors such as detergents and antibiotics have been shown to induce the biosynthesis of xanthan. [2]

6.2.2 Composition and properties

The xanthan polymer consists of repeating pentassaccharide subunits of D-glucose, D-mannose and D-glucoronate in a molar ratio of 2:2:1. The D-glucose units are β-[1-4]-linked and form the polymer backbone with α-[3-1] linked trisaccharide side-chains on every other glucose unit. [1, 2] The side-chains consist of a D-glucoronosyl unit between two D-mannosyl units. Approximately half of the terminal D-mannose units are linked to a pyruvic acid residue, via a keto group on the 4 and 6 positions. The D-mannose unit linked to the main chain often contains an acetyl group at position O-6. Variations in substituent groups and chain length may significantly alter the polymer properties. [2, 4, 5] The repeating pentamer structure can be seen in figure 6.1.

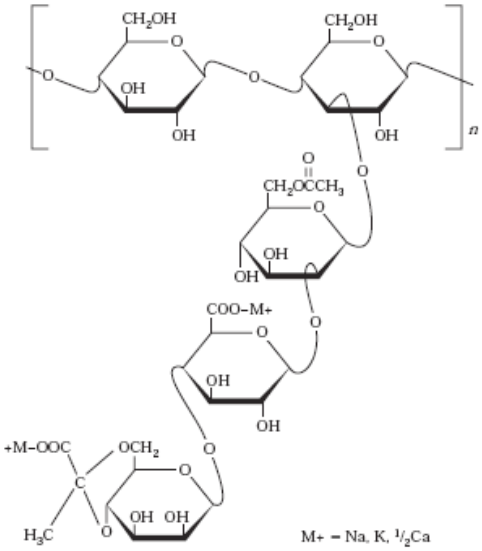

Figure 6.1: Chemical structure of xanthan gum. [2]

Xanthan is pseudoplastic and highly shear thinning and the power law (see chapter 2, equation 2.4) can therefore be used to describe the rheological properties. In contrast to many other biopolymers xanthan gum is stable and retains its viscous properties in aqueous solutions, at a wide variety of pH values (from 3–9), temperatures (up to 80℃) and salt concentrations (up to 150g/l NaCl). [2, 4] Due to the excellent properties of xanthan gum, it has been used in a very wide range of applications.

6.2.3 Applications for xanthan gum

In 1969 xanthan was approved by the United States Food and Drug Administration (FDA) to be used in food products, and it was the first biopolymer to be produced commercially. In Europe xanthan was approved for use as a food emulsifier and stabilizer in 1980 as item E-415. Today xanthan is used for a wide variety of industrial applications with a world wide production of 40,000 ton per annum (2002 values).[6] The majority of the produced xanthan is however, still being used in food products, and the main food applications are listed in table 6.1. [2, 4]

Table 6.1: Main applications of xanthan gum in the food industry. Adapted from Flickinger and Drew [2]

Function	Application
Adhesive	Icings and glazes
Binding agent	Pet foods
Coating	Confectionery
Emulsifying agent	No-oil, low-oil and regular salad dressing
Encapsulation	Powdered flavours
Film formation	Protective coatings sausage casings
Foam stabilizer	Beer
Gluten substitution and dough processing	Baked goods, pasta
Stabilizer	Ice cream, salad dressings, juice drinks, margarine
Swelling agent	Processed meat products
Syneresis inhibitor, freeze–thaw stability	Cheese, frozen foods
Thickening agent	Jams, sauces, syrups, and pie fillings
Pumping and filling improvement	Processing of canned products

In later years xanthan gum has been extensively used in low-fat products to achieve the right mouth-feel, but the pseudo plastic flow behaviour of xanthan is also utilized in other industries including: Agriculture to improve the flow and cling ability of pesticides; in cosmetics as an emulsifier, and in creams and lotions for a good “skin-feel”. In the pharmaceutical industry xanthan may be used in controlled-release applications and is already being used for a variety of applications to stabilise emulsions. In inkjet printers xanthan improves the ink flow, prevents leaking from the ink cartridge, smudging and improves cling. [1] In the petroleum industry xanthan has been proven to be an effective additive to drilling fluids. At high shear rates e.g. at the drill head, the viscosity is low, and the xanthan solution is used to lubricate the moving parts. In low shear regions the xanthan helps suspend cuttings in the annulus and to stabilise the well. [2]

6.2.4 Industrial xanthan production:

X. campestris is able to utilise a broad range of carbon sources, such as glucose, sucrose, citric acid, enzymatic hydrolysates of starch, as well as molasses or corn syrup.[7-9] Changing the carbon source and other limiting nutrients does not affect the polymer main chain, but rather leads to changes in the amount of pyruvic acid and acetyl incorporated, the molecular mass and the xanthan yield can also be altered. Due to the varying nutrient conditions during production, the xanthan purified from a batch fermentation is therefore a mixture of different polymers, which may have very different rheological properties. Continuous production is therefore a tempting alternative due to the constant production conditions and hence consistent product properties and quality, but due to contamination risks and the development of fast growing mutants not producing xanthan, batch fermentations are still the preferred operational mode for industrial production of xanthan. [2, 7]

Media and feed optimization have resulted in significant improvements in xanthan yield during batch fermentations, but mass and heat transfer at high product concentration still presents a major challenge. Oxygen limitation has been shown to reduce the xanthan production rate, which decreases linearly with decreases in the specific oxygen uptake rate.[1, 2] Jana and Ghosh [8] demonstrated that limitations in oxygen transfer and mixing behaviour can reduce both the final xanthan concentration and yield of xanthan.

Several reactor designs have been tested in the literature in order to improve mixing, mass and heat transfer during *Xanthomonas* fermentations. By changing the impellers in a traditional stirred tank reactor (STR), significant improvements have been achieved. Shifting from Rushton turbines to an Intermig impeller set has been reported to give a four fold increase in k_La at the same power input during *X. campestris* batch fermentations. [10] Finding the optimal impeller configuration has proven difficult as the choice of impeller is often a compromise between efficient sparging at low viscosities and sufficient mixing at high viscosities. In an attempt to overcome the problems associated with the highly viscous fermentation broths other designs have also been investigated (airlift reactor, centrifugal fibrous-bed bioreactor, stirred tank reactor (STR)

with draft tube, bubble column and a plunging jet). [2, 10, 11] The plunging jet reactor showed significantly higher efficiency with respect to oxygen transfer compared to the STR with Rushton turbines, STR with Intermig impellers, airlift reactor, STR with draft tube and bubble column. The specific growth and production rates were not affected by the shear forces in the pump, but problems with stagnant zones in the reactor at high product concentrations was observed [10], indicating that improved bioreactors were needed.

In earlier chapters the RJH fermenter system was introduced and it was shown to have significant advantages over fermenters mixed with intermig impellers in highly viscous fermentation broths with respect to oxygen mass transfer and mixing. The RJH system utilises the same mixing principles as the plunging jet reactor, but since the direction of the jet nozzles of the RJH system are continuously moving, the formation of stagnant unmixed zones is avoided. In this chapter a comprehensive examination of the RJH fermenter system for *X. campestris* fermentations is conducted, by varying the superficial gas velocity, power input and broth viscosity.

6.3 Materials and Methods

6.3.1 Microorganism, medium and cultivation procedures

Freeze-dried *Xanthomonas campestris* (ATCC 13951) from Deutsche Sammlung von Mikro-organismen und Zellkulturen (DSMZ, Germany) was used to make cell stocks in glycerol, a new tube of which was used to inoculate the initial cell propagation (pre-inoculum) for each fermentation. The pre-inoculum consisted of six 500ml Erlenmeyer flasks containing 100ml complex medium composed of (per litre): 10.0g sucrose, 5.0g peptone, 3.0g yeast extract, 3.0g malt extract. The medium was adjusted to pH 6.5 with H_2SO_4. Following inoculation, the flasks were left in a shaking incubator (ca. 100 RPM) at 30°C until an OD_{600} of 2.0 was reached (after approximately 32h). The chemically defined medium from Letisse *et al.* [9] was used for growth of the inoculum and for xanthan production in the RJH fermenter system. The medium consisted of (per litre): 1.94g NH_4Cl, 5.00g K_2HPO_4, 0.25g $MgSO_4 \cdot 7H_2O$, 2.00g citric acid, 0.20g antifoam, and the following trace metals (per litre): 0.012mg $ZnSO_4$, 0.018mg $CaCl_2 \cdot 2H_2O$, 0.0024mg $FeCl_3 \cdot 6H_2O$, 0.006mg H_3Bo_3. The pH was adjusted with 4M NaOH to 6.8±0.1 and a concentrated sucrose solution was prepared and autoclaved separately. The fermentations were carried out in the pilot scale RJH fermenter described in chapter 1. The inoculum was grown in three 5L bioreactors each with a working volume of 4L and containing growth medium with $10gl^{-1}$ sucrose. The inocula were allowed to grow for 32h until an OD_{600} of approximately 3.5-4 was reached and then transferred aseptically to the RJH fermenter system, containing 225l growth medium with $42gl^{-1}$ sucrose. Both the inoculum and the following fermentation were carried out at 28°C. The airflow rate was varied from 0.1-0.5VVM during the fermentation in the RJH to maintain a dissolved oxygen tension (DOT) above 20%. The pH was maintained at 6.8±0.1 by automatic HCl and NaOH addition. The speed of the circulation pump for the RJH was constant during the fermentations (200RPM) equivalent to a displacement of $1.8kgs^{-1}$.

6.3.2 Analysis

k_La calculation: The k_La was calculated during the fermentations using the direct pseudo-steady-state method as described by Nielsen *et al.* [12] The oxygen uptake rate (OTR) was measured using a 5853 S Mass Flow Controller (Brooks Instruments) and a gas monitor, model 1308 (Büel & Kjær, Denmark). The saturation concentration of oxygen

and at equilibrium (c*) was estimated using the average oxygen concentration in the inlet and outlet gasses of the fermenter.

Viscosity measurement: A vibrating rod sensor, VA-300 with a ViscoScope control console (Marimex) was used as described in Chapter 2. The sensor was placed in the recirculation loop on the pressure side of the pump and the probe signal was recorded continuously. At-line measurements were made using a Haake VT500 MV-DIN rheometer, and power law constants were found as described in chapter 2, based on shear rate scans (0-200s^{-1}).

Biomass and xanthan concentration: Due to the viscous nature of the fermentation broth, a special analysis method adapted from Lettise [9] was used. Samples for determination of biomass and xanthan concentration were chilled on ice and centrifuged at 12,500 g for 30 min at 5 °C. The cell pellet was suspended in 1% KCl and the OD measured at 600nm. The xanthan gum in the cell free supernatant was precipitated using iso-propanol, and filtered using a pre dried 45µm filter (Pall Life Sciences). The filter with xanthan was dried in a microwave oven at 150W for 15min to constant weight and after a minimum of 24 h in a desiccator, the filters were weighed and the xanthan dry weight calculated. All biomass and xanthan measurements were prepared in triplicate.

6.4 Results and Discussion

6.4.1 Suitability of the RJH system for *Xanthomonas campestris* growth

Determination of the maximum specific growth rate can give a good indication of whether fermentation conditions are suitable for a microorganism, and can be expected to be reduced if cells are stressed due to e.g. shear forces or gradients in concentration of substrates including oxygen. The maximum specific growth rate for *Xanthomonas campestris* in the RJH equipped pilot scale fermenter was therefore calculated based on the OD_{600} determined during the exponential growth phase of two identical fermentations. In figure 6.2 the growth rate is calculated as the slope of the natural logarithm of the OD_{600} from the cells during two identical fermentations (Fermentation 1: Gray diamonds, Fermentation 2: Black squares).

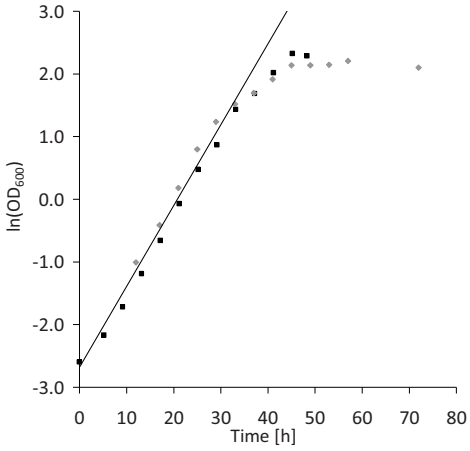

Figure 6.2: Growth of *X.campestris* during two duplicate fermentations with the RJH system. Maximum specific growth rate calculated during exponential growth, $\mu=0.13h^{-1}$ ($R^2=0.99$), (Fermentation 1: Gray diamonds, Fermentation 2: Black squares).

The calculated growth rate of $0.13h^{-1}$ is identical to that determined by Letisse *et al.* [9]. Furthermore, growth rate calculations based on $q(CO_2)$ values gave a similar result (0.14

h^{-1}). It was not possible to detect any changes in the morphology of the cells in the RJH system when compared to the inoculum culture of *X. campestris*. *X. campestis* cells have been reported to be adversely affected by intense mechanical agitation. [4] However no such effect could be seen in the RJH system in spite of the expected high shear forces in the pump and jet nozzles. It was thus concluded that there are no negative effects on the cells and their growth in the RJH fermenter.

6.4.2 Xanthan production

During the fermentations xanthan was excreted by the cells leading to increased broth viscosity. However, it was not possible to determine the xanthan concentration based on dry matter measurements, even though triplicate measurements were made. A more robust method for xanthan determination from fermentation broths is needed

6.4.3 Broth rheology

Though it was difficult to get a precise estimate of the xanthan concentration based on dry matter measurements the xanthan production could be determined indirectly as the secreted polymer caused the viscosity to increase. The increase in viscosity was monitored both at-line and on-line. The development in power-law and consistency indexes (see chapter 2 for a discussion of the meaning of these) during the two fermentations can be seen in figure 6.3, measured at-line with the Haake VT500 MV-DIN rheometer.

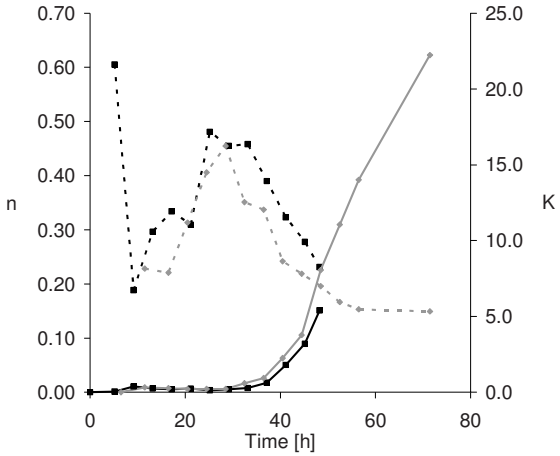

Figure 6.3: Development in n (dashed line) and K (solid line) during two *X. campestis* fermentations (Fermentation 1: Gray diamonds, Fermentation 2: Black squares).

During the initial 30h no significant change in broth rheology could be observed, but as the xanthan concentration increased so did the consistency index, from close to 0 to up to 22.2 at 74h. Based on the calculated power-law and consistency indexes the apparent viscosity at a shear rate of $1250s^{-1}$ could be calculated and plotted, see figure 6.4 (black diamonds).

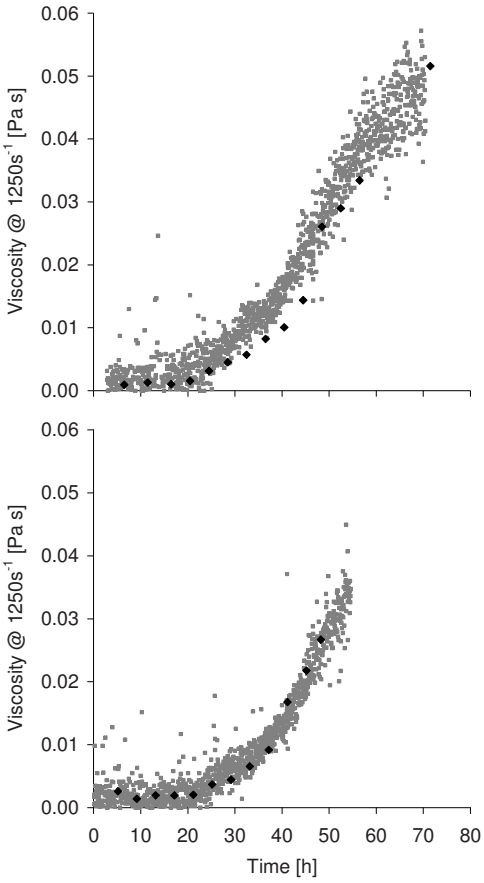

Figure 6.4: Viscosity measured at $\gamma_{app}=1250s^{-1}$ during two *Xanthomonas campestris* batch fermentations (Fermentation 1 top, Fermentation 2 bottom). The Haake MV-DIN rheometer (black diamonds ♦) and Marimex VA-300 sensor (gray squares ■) were used.

As expected, the viscosity measured at-line increased throughout the fermentation. Increased viscosity leads to higher gas holdup, and it was therefore anticipated that the in-line Marimex sensor would record a lower apparent viscosity at high xanthan concentrations, compared to the unaerated at-line measurement. This effect could, however, not be detected, as the broth viscosity measured by the Marimex sensor did not seem to be effected by the air bubbles in the recirculation loop, hence the in-line sensor was able to give a good estimation of the viscosity throughout both fermentations.

6.4.4 Suitability of the RJH system for aeration of *Xanthomonas campestris* fermentation broths

The results above indicate that the RJH system is suitable for production of xanthan gum with *X. campestris* fermentations at pilot scale. However to evaluate it's potential for large scale fermentations, it is necessary to determine oxygen mass transfer rates and to understand the factors influencing them from a fermentation and process perspective. The critical process bottleneck for industrial production of xanthan gum is to maintain sufficient dissolved oxygen tension throughout the fermentation. In figure 6.5 the development in dissolved oxygen tension (DOT) during the two batch fermentations are plotted as gray squares, and there is excellent reproducibility between them. The DOT started close to 100% but decreased as the biomass concentration increased. After 38h the DOT was reduced to 20% of the original value. In the first fermentation the DOT level starts to increase after 60h, which was not seen in the second fermentation since it was stopped after 54h.

During the whole fermentation the speed of the recirculation pump driving the RJH was kept constant. Whereas the airflow was varied to maintain a minimum dissolved oxygen tension above 20%. During the initial growth phase the airflow was kept constant at 22.5l min^{-1} (0.1VVM), but as the DOT decreased the airflow was incrementally increased up to 63l min^{-1} after 48h for the first fermentation, and 128l min^{-1} at 54h for the second, see figure 6.5, black diamonds. When the nitrogen source became depleted, after approximately 45h, the growth stagnated, see figure 6.2. This caused the oxygen consumption to decrease in the first fermentation, leading to an automatically controlled drop in the aeration rate, via a control loop from the dissolved oxygen probe. For the second fermentation, the air flow reached 115lh^{-1} at 45h followed by a short drop to 91lh^{-1} during the subsequent 2h, however this temporary drop was followed by a rapid increase where after the fermentation was terminated.

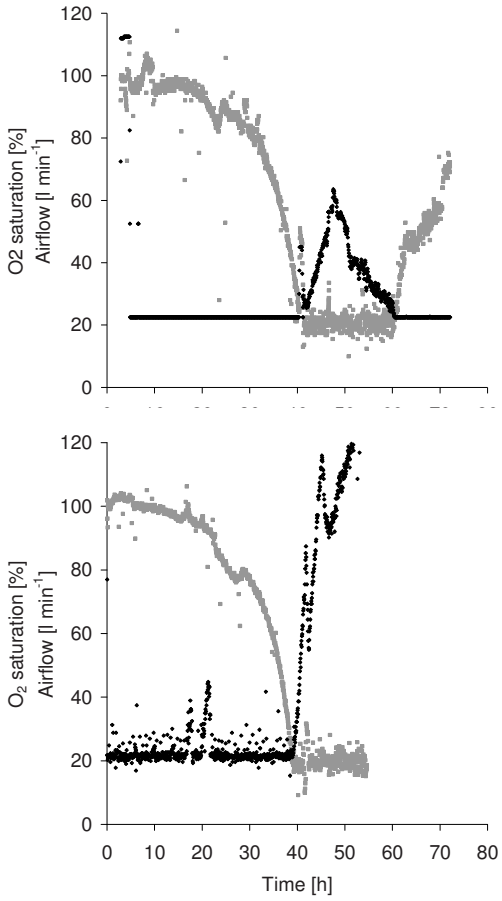

Figure 6.5: DOT in % and airflow during two *X. campestris* batch fermentations (Fermentation 1 top, Fermentation 2 bottom). DOT: Gray squares ■. Airflow : Black diamonds ♦.

The continuous airflow increase during the second fermentation could indicate a longer growth phase. The OD measurements (figure 6.2) however, indicate that the cell propagation stopped at 45h for both fermentations. To investigate whether the increased airflow was caused by an error in the DOT probe measurement, the volumetric CO_2 production rate (qCO_2) and O_2 consumption rate (qO_2) were plotted in figure 6.6. The qCO_2 and qO_2 initially increases during both fermentations but after approximately 40h the increase stops. Had there been a difference between the fermentations, as indicated by the DOT and airflow measurements, it should have been

evident in this plot. As this is not the case the difference in DOT response to increased airflow after 40h, is likely to be due to a malfunctioning DOT probe. One could speculate that the viscous broth may have hindered efficient oxygen transfer to the probe, thereby resulting in a reduced effect by increasing the airflow.

After 56h the carbon source was depleted resulting in a drop the both qCO_2 and qO_2 (figure 6.6).

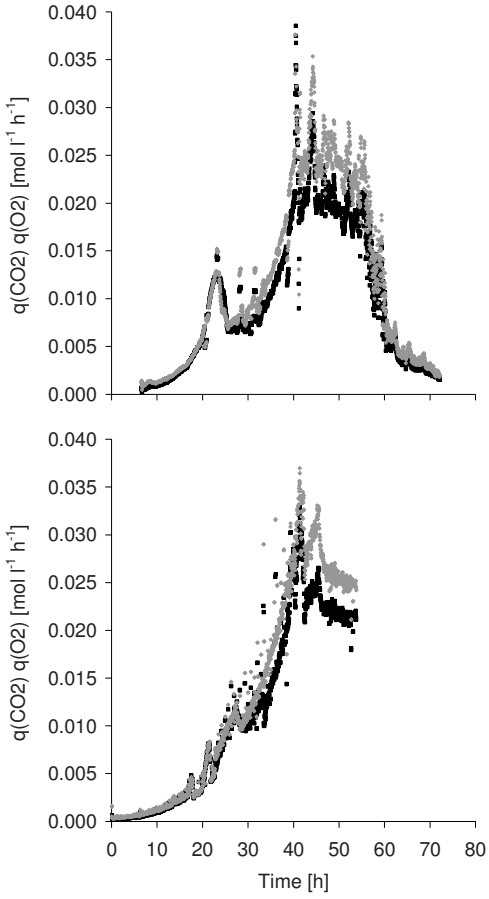

Figure 6.6: q(CO_2) and q(O_2) during two *X. campestris* batch fermentations (Fermentation 1 top, Fermentation 2 bottom). DOT: Gray squares ■. Airflow : Black diamonds ♦.

As discussed in chapter 5, the k_La at a given time during a fermentation is a function of the OTR and the dissolved oxygen concentration, see equation 5.1. In figure 6.7 the k_La

during the two fermentations are plotted. During the initial 20h, where the OTR is close to zero and the oxygen saturation is close to 100%, the calculated k_La values vary from 0 to $50s^{-1}$. In this period even a small variation in the measured oxygen concentration and saturation results in large errors. As the oxygen saturation decreases (see figure 6.5) more consistent data can be obtained and k_La of ~0.15 s^{-1} is found. During the exponential growth phase (30-40h) the viscosity increased (figure 6.4) while the power input (figure 6.8) and aeration rate (figure 6.5) was kept constant, causing the k_La to drop rapidly from a level of $0.12s^{-1}$ to $0.05s^{-1}$. After 41h the airflow was increased and the rapid drop in k_La stopped. During the following 20h the viscosity continued to increase and the k_La decreases asymptotically towards $0.04s^{-1}$. As the carbon source is depleted (after 56h) and the OTR dropped, the k_La was further reduced close to $0.01s^{-1}$, which it remained at throughout the rest of the fermentation.

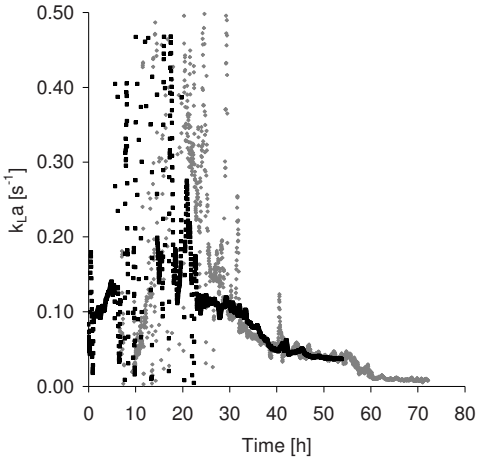

Figure 6.7: k_La during two *X. campestris* fermentations with the RJH system (Fermentation 1: Gray diamonds, Fermentation 2: Black squares).

As described in chapter 1, the power input of the RJH system is affected by changes of the pressure in the recirculation loop. During the two fermentations conducted in the current chapter, the rotation speed of the lobe-pump was kept constant, but as the airflow and mass flow varied so did the total power input, see figure 6.8. During the initial 40h of the fermentation the power input slowly increased from 1.1 to $1.3kwm^{-3}$ due to sample taking, which reduced the total broth volume. As the airflow was increased so did the pressure in the loop and thus the power input, up to 1.4-$1.6kwm^{-3}$.

The increase in power input however, was shortly thereafter followed by a significant drop to 0.2-0.4 kwm^{-3}. This dramatic drop was caused by recirculating air bubbles trapped in the increasingly viscous broth, which reduced the liquid density and thus the mass flow and thereby the efficiency of the pump in terms of mass displaced per revolution. As discussed previously, the air bubbles sparged into the tanks have a small diameter due to the shear effect at the jet nozzles. The small bubble diameter results in a large interface area and thus high k_La. The small bubble diameter does have the (in this case) undesired side effect, that the bubble rise velocity is low, which causes the fermentation broth to have a foam like consistency.

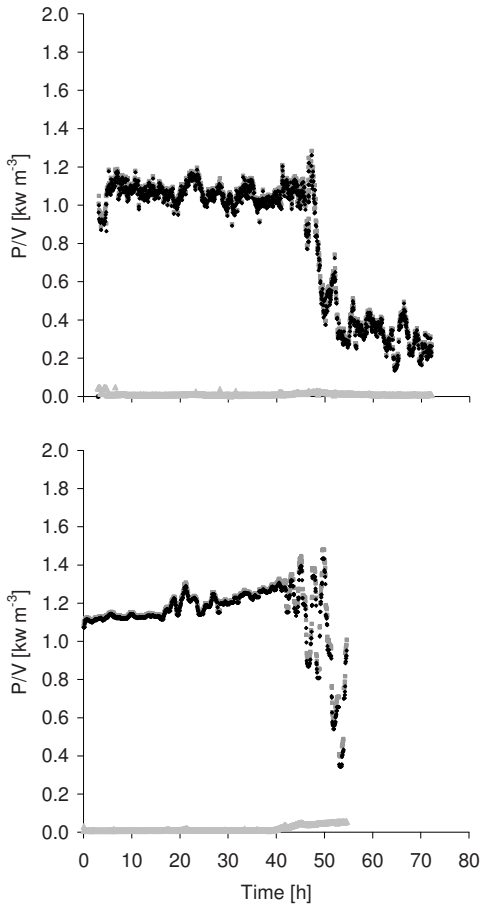

Figure 6.8: Volumetric power input during two *X. campestris* batch fermentations (Fermentation 1 top, Fermentation 2 bottom). P_{tot}: Gray squares ■. P_{Pump}: Black diamonds ♦. P_g: Light gray triangles ▲.

6.4.5 Effect of viscosity on k_La

The main factors contributing to the k_La during a fermentation are described in chapter 5 equation 5.4, and are the superficial gas velocity $(u_s)^{\alpha}$, the volumetric power input $(P/V)^{\beta}$ and the viscosity $(\mu)^{\omega}$. Examination of figure 6.5 shows that during the period of 30-40 h the air-flow was constant and in addition, power input to the recirculation pump was close to unaltered (figure 6.8), thus the decrease in k_La from $0.12s^{-1}$ to $0.05s^{-1}$ over the same period was due to the increasing viscosity. By plotting the natural logarithm of the viscosity against the natural logarithm of the k_La (as described in chapter 5) the

value for the equipment specific power constant ω (see equation 5.3) was found to be ω =-0.8, see figure 6.9.

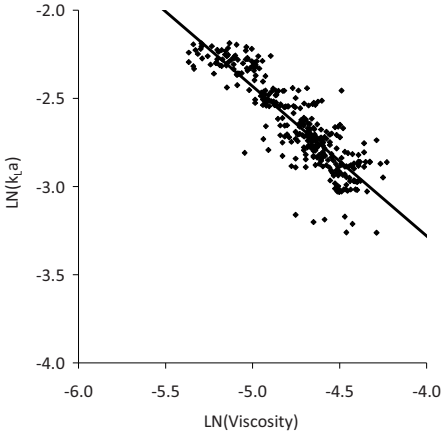

Figure 6.9: The ln(viscosity) plotted against the ln(k_La) for the two fermentations, where viscosity was measured using the in-line Marimex probe. The solid line indicates the best fit for the date, slope = ω = -0.8, R^2=0.78.

As can be seen from equation 5.3, the ω exponent is a direct measure of how sensitive the k_La of a given mixing system is to increased viscosity. Thus a low ω exponent (e.g. ω <-1) indicates the system handles increased viscosity poorly. The determined exponent value is lower for the *X. campestris* broth compared to that determined for fungal fermentation broth, $\omega_{(Fungal\ broth)}$ = -0.6 see chapter 5. The negative impact of increasing viscosity on the oxygen transfer in the RJH system is thus larger for this type of fermentation broth. Though the exponent value is lower than for fungal fermentation broth it is in the same range as traditional mixing systems, e.g. those determined by García-Ochoa and Gómez [13] and Cooke *et al.* [14] for different impellers gave, ω = -0.67 and ω = -1 respectively. The RJH system therefore does not seem to have a significant advantage compared to traditional mixing systems, when working with viscous fermentation broths containing xanthan.

6.4.6 Effect of power input on k_La

At 41h during the first fermentation the speed of the circulation pump powering the RJH was varied to determine the significance of altering the power input. The experiment was performed within 15minutes. Due to the short time period the volumetric oxygen consumption rate of the microorganism was assumed to be constant throughout the test. Five different pump speeds (160-320RPM) were tested and the pressure increase in the loop were recorded for each setting (see figure 6.10). In the pump speed interval which was tested the positive pressure in the loop (P) increased proportionally to the pump speed, according to the following: P=0.011(Pump Speed)-0.91 (R^2=0.994).

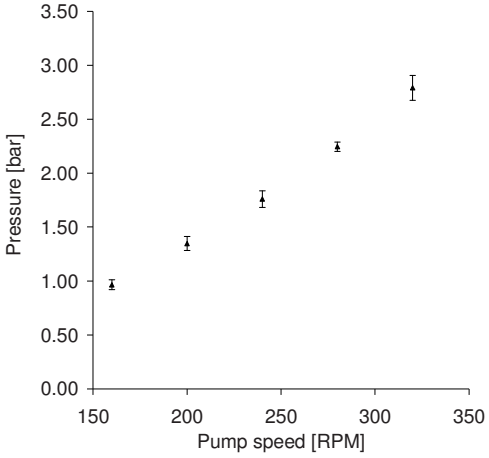

Figure 6.10: Pressure difference between recirculation loop and tank plotted as average of 12-16 measurements with standard deviation at different pump speeds.

For each pump speed the volumetric power input (P_{pump}/V) was calculated as described in chapter 1 using equation 1.3, and plotted with the recorded DOT level (see figure 6.11). From figure 6.11 it is evident that increasing the power input results in an increase in the DOT. The effect is however most distinct at low volumetric power inputs ($P/V<2kW\ m^{-3}$).

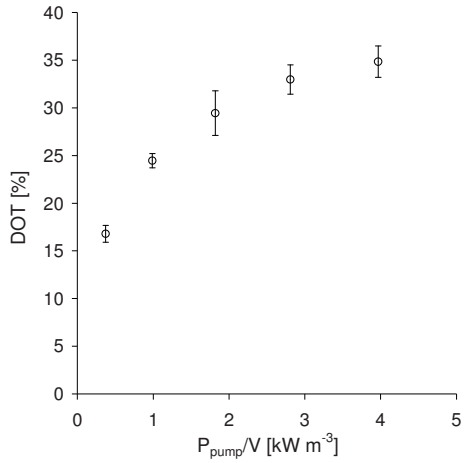

Figure 6.11: DOT at different volumetric power inputs plotted with standard deviation of the data.

To evaluate the effect of different power inputs the k_La at each pump speed was calculated as described in chapter 5. The calculated k_La can be used to determine the exponent value of β from equation 5.3. By taking the natural logarithm of the k_La and P/V, and plotting them against each other, the exponent value β can be determined as the slope of the line, see figure 6.12.

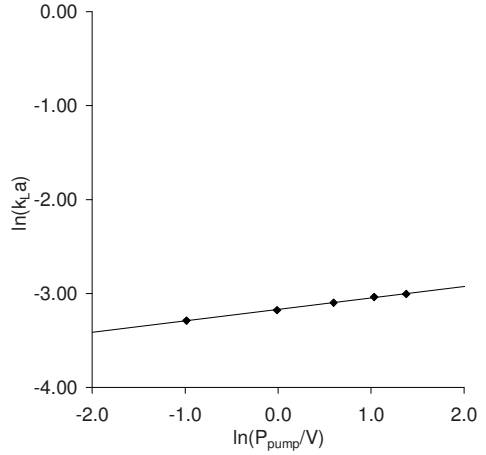

Figure 6.12:Effect of increased power input from the circulation pump on k_La.

An exponent value of β=0.122 was calculated (Figure 6.12, R^2=0.998). This value is significantly lower than values which have been reported for traditional impeller mixed systems e.g. 0.6 by García-Ochoa and Gómez [13]. Although increasing the pump speed did result in a proportional increase in power output (see figure 6.10) the beneficial effect on DOT and k_La is limited at high (>2kW m^{-3}) power inputs.

6.4.7 Effect of superficial gas velocity

Altering the gas flow rate in the RJH systems affects;

- The superficial gas velocity
- The pressure in the recirculation loop
- The average density of the jet
- The amount of gas being recirculated in the loop

Increasing the superficial gas velocity and pressure in the recirculation loop are both beneficial in terms of achieving a high k_La, whereas reductions in the density of the jets and recirculating gas are not. Increasing the gas flow in the RJH system is therefore not a failsafe method for achieving higher k_La values.

In a traditional fermenter, gas flooding may significantly reduce the performance of the impeller. A similar effect of high air flow rate can be seen in the RJH system. As the airflow increases, the density of the jet streams decreases. Though the average velocity of the liquid increased, the lower density decreases the jet steams mixing range, especially under viscous conditions. The air to liquid ratio may also affect the k_La. When the flow changes from a liquid with small air bubbles, to two largely unmixed phases, the area of the liquid gas interface is reduced.

Special care must be taken when working with viscous broths in the RJH. As the viscosity increases, the mass-flow in the loop, and thereby power input, decreased due to recirculation of gas bubbles, as illustrated in figure 6.8. The power input from the airflow is thereby lost due to reduced pump efficiency. This problem could possibly be reduced by inserting a degasser in the loop before the pump. In addition, placement of a deflector plate above the intake for the recirculation loop would hinder direct uptake of the air bubbles from the jet streams, which periodically pass over the hole in the bottom of the fermenter.

The negative effects of increasing the gas flow however, only affect the power input and not the superficial gas velocity. Using the calculated exponent value for viscosity and power input (ω =-0.8, β=0.122) the effect of the superficial gas velocity can be calculated based on the data with varying airflow (i.e. in the period after 40h (figure 6.5)). By rearranging equation 5.3 one gets:

$$\alpha \ln(u_s) = \ln\left(\frac{k_L a}{k}\right) - \beta \ln\left(\frac{P_t}{V}\right) - \omega \ln(\eta_{app}) \qquad \textbf{Eq. 6.1}$$

Using equation 6.1 the exponent value 'α' can be determined as the slope of an appropriate plot of the data, see figure 6.13. The plot indicates that there is some noise in the data for fermentation 2, but nevertheless a positive tendency from increasing the superficial gas velocity can be deduced, which is illustrated with the solid line of best fit through the data from fermentation 1 (figure 6.13).

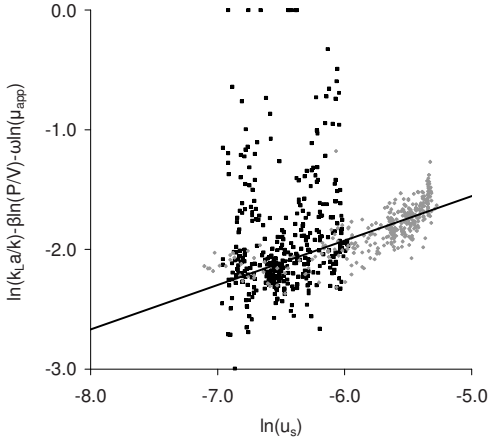

Figure 6.13: Effect of superficial gas velocity. The line indicates the best fit for the date, slope= α = 0.4. Fermentation 1: Gray diamonds, Fermentation 2: Black squares.

The calculated exponent value α =0.4 is comparable with values determined both for jet mixed and impeller mixed systems as listed in table 6.2.

Table 6.2: List of exponent 'α' values found for different mixing systems. For a more comprehensive list see García-Ochoa and Gómez [13]

Exponent value, α	System description	Reference
0.5	RJH system but with larger nozzles and a non-viscous model solution	Nordkvist *et al.* [15]
0.4	For non-viscous broth in a fermenter equipped with six-bladed Rushton turbines	Pedersen *et al.* [16]
0.3	Fungal fermentation both and model broth consisting of paper pulp in a range of impeller mixed fermenters.	Cooke *et al.* [14]
0.67	Xanthan solutions in impeller mixed fermenters.	García-Ochoa and Gómez [13]

Examination of table 6.2 suggests that increasing the airflow rate to get higher k_La values is thus as efficient for the RJH system as for impeller mixed fermenters, though the air sparging is performed in the loop in the RJH and not through a separate sparger in the bottom of the tank.

6.5 Conclusion

The experimental Rotary Jet Head fermenter system has no negative effects on the growth of the bacteria *Xanthomonas campestris*, and the cells were able to grow with the same rate as in reference fermentations from the literature. Furthermore the system was able to provide high (compared to impeller mixed systems) k_La values ($0.15s^{-1}$) at low power input ($1.1kW\ m^{-3}$) and air flow (0.1VVM), and during the fermentation no visible stagnant zone could be detected in the system. In the fermentations conducted here in which viscosity arose from the biopolymer product and not from the microbial cells morphology, the Rotary Jet Head system did not present any significant advantage with respect to k_La when compared to impeller mixed systems in term of coping with increasing viscosity. As the viscosity increased, so did the number and total volume of bubbles recirculated in the system, thereby severely reducing the efficiency of the pump. Furthermore the effect of increasing viscosity and airflow on the k_La were the same as for traditional mixed fermenter systems, and increasing the power input had only a small effect in the RJH system. Thus the RJH system can be used for fermentations with bacteria which increase the viscosity of the broth, but the beneficial effects caused by the change in morphology during the fungal fermentations are obviously not seen.

By varying the power input and gas flow rate the following exponent values of equation 5.3 (describing the correlation between the k_La with the superficial gas velocity, power input, volume of the tank and apparent viscosity) was determined:

$$k_L a = k u_s^{0.4} \left(\frac{P_t}{V}\right)^{0.122} (\eta_{app})^{-0.8} \qquad \textbf{Eq. 6.2}$$

6.6 References

1. Rosalam, S. and R. England, *Review of xanthan gum production from unmodified starches by Xanthomonas comprestris sp.* Enzyme and Microbial Technology, 2006. 39(2): p. 197.
2. Flickinger, M.C. and S.W. Drew, *Encyclopedia of Bioprocess Technology - Fermentation, Biocatalysis, and Bioseparation*. Vol. 5. 1999: John Wiley & Sons. 2695-2711.
3. García-Ochoa, F. and E.G. Castro, *Estimation of oxygen mass transfer coefficient in stirred tank reactors using artificial neural networks.* Enzyme and Microbial Technology, 2001. 28(6): p. 560.
4. García-Ochoa, F., et al., *Xanthan gum: production, recovery, and properties.* Biotechnology Advances, 2000. 18(7): p. 549.
5. Papagianni, M., et al., *Xanthan production by Xanthomonas campestris in batch cultures.* Process Biochemistry, 2001. 37(1): p. 73.
6. Bilanovic, D.D., S.H. Malloy, and P. Remeta, *Solid or semi-solid state fermentation of xanthan on potato or potato waste*. 2008, Bemidji State University Foundation (Bemidji, MN, US),State of Minnesota Environment and Natural Resources Trust Fund (St. Paul, MN, US): United States.
7. Becker, A., et al., *Xanthan gum biosynthesis and application: a biochemical/genetic perspective.* Applied Microbiology and Biotechnology, 1998. 50(2): p. 145.
8. Jana, A.K. and P. Ghosh, *Stimulation of xanthan production by Xanthomonas campestris using citric acid.* World Journal of Microbiology and Biotechnology, 1997. 13(3): p. 261.
9. Letisse, F., et al., *Kinetic analysis of growth and xanthan gum production with Xanthomonas campestris on sucrose, using sequentially consumed nitrogen sources.* Applied Microbiology and Biotechnology, 2001. 55(4): p. 417.
10. Zaidi, A., et al., *Xanthan production in a plunging jet reactor*, in *Applied Microbiology and Biotechnology*. 1991. p. 330.
11. Amanullah, A., et al., *Reproducibility of Pilot Scale Xanthan Fermentations.* Biotechnology Progress, 1996. 12(4): p. 466-473.
12. Nielsen, J., J. Villadsen, and G. Lidén, *Bioreaction Engineering Principles*, ed. 2. 2003, New York: Kluwer Acedemic/Plenum Publishers. 528.
13. García-Ochoa, F. and E. Gómez, *Mass transfer coefficient in stirred tank reactors for xanthan gum solutions.* Biochemical Engineering Journal, 1998. 1(1): p. 1.
14. Cooke, M., J.C. Middleton, and J. Bush, *Mixing and mass transfer in filamentous fermentations.* King R (ed) 2nd Int. Conf. on Bioreactor Fluid Dynamics, 1988: p. 37–64.
15. Nordkvist, M., et al., *Applying rotary jet heads for mixing and mass transfer in a forced recirculation tank reactor system.* Chemical Engineering Science, 2003. 58(17): p. 3877.
16. Pedersen, A.G., et al., *A novel technique based on 85Kr for quantification of gas--liquid mass transfer in bioreactors.* Chemical Engineering Science, 1994. 49(6): p. 803.

Chapter 7

Preliminary Results, Further Work and Conclusion

Chapter 7

Preliminary Results, Further Work and Conclusion

7.1 Preliminary Results

7.1.1 Feed strategy optimization during *Aspergillus oryzae* fed-batch fermentations

During the project the majority of the fed-batch *Aspergillus oryzae* fermentations were run with a constant feed rate of the dextrose. However, alternative feed strategies were also tested.

Pulse feeding, as described by Bhargave *et al.* [1], did not affect the growth rate. However, a pulse cycle of 15min with a pulse time of 30% of the cycle, resulted in an approximately 8-10h delay in the viscosity increase seen in other fermentations. Despite these promising results, the pulse feeding strategy was abandoned as it could not be applied in the reference pilot scale impeller mixed system.

In another set of trials, exponential feed rates were examined in the RJH system. As the main objective of using *A. oryzae* was to benchmark the mass transfer capabilities of the RJH system, feed profiles designed for maximising the growth rate were designed while keeping the DOT above 20%. During the fermentation the airflow rate was automatically varied from 0.2-1VVM to ensure a DOT above 20%.
During the batch phase of the fermentation no additional carbon source was added. When the initial $10gl^{-1}$ dextrose had been consumed by the cells, marked as a drop in the $q(CO_2)$, the feed pump was initiated. The feed rate was set to increase exponentially with a predetermined factor until the airflow reached 1VVM and the DOT dropped below 20%. At this point the increase in the feed rate would be stopped and controlled by DOT to ensure a minimum DOT of 20%. In figure 7.1 the three control stages can be seen; 1) batch phase with airflow control at minimum 0.2VVM. 2) Exponential feed phase with DOT controlled air flow and exponential increasing feed rate (in this case with a factor of $0.1h^{-1}$). 3) DOT controlled feed rate and a airflow of 1VVM.

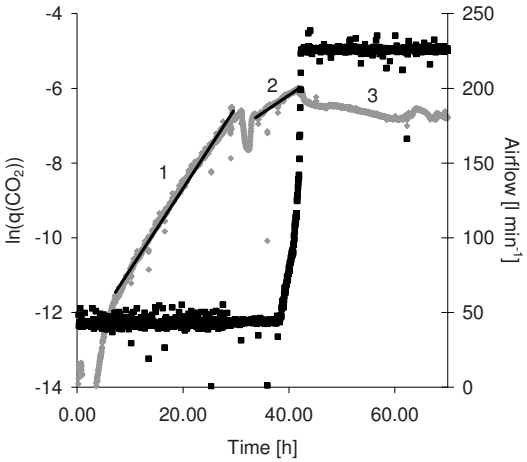

Figure 7.1: ln(q(CO_2)) ♦ and Airflow ■ during an optimised *A. oryzae* fed-batch fermentation. The straight black lines indicate the exponential increase in q(CO_2). Slope during batch phase (1)= 0.24h^{-1}. Slope during feed rate controlled growth (2)= 0.10h^{-1}.

Using this feed and airflow control strategy the fermentation time and air consumption could be significantly reduced. However, as these control features were not possible for the pilot scale reference system the strategy was not examined further.

7.1.2 Cellulase production with *Trichoderma reesei*

Trichoderma reesei is able to secrete a large amount of cellulolytic enzymes. In recent years these enzymes have become of great interest due to possible applications in second generation bio-ethanol production. To make bio-ethanol an economical alternative to traditional gasoline, the production cost at all levels of manufacturing must be kept at a minimum. This includes reducing the capital and production cost of the enzymes used for lignocellulosic biomass pretreatment and cellulose degradation. Thus it was interesting to examine whether the RJH system could be utilised for *T. reesei* fermentations.

Three aerobic *T. reesei* fermentations were conducted in corporation with PhD student Linda Lehman and project student Tilde Jordal. The *T. reesei* strain RutC30 was grown at 23℃, in the RJH fermenter described in chapter 1 with a working volume of 225l, on a

medium with 25gl^{-1} microcrystalline cellulose (Avicel) as the main carbon source and a pH of 4.5 (see Ph.D. thesis of Linda Lehmann for the growth medium composition which was the same as that used in 5L fermentations used to determine optimal enzyme production conditions). The air flow and power input were kept constant at 0.11VVM and a power input of approximately 1.1kWm^{-3}. The concentration of cellulolytic proteins was estimated based on enzymatic activity, measured as Filter Paper Units per gram (FPUg^{-1}) as described by Xiao et al. [2].

Unfortunately all three batches had to be stopped prematurely (after ca. 160h) due to equipment failures unrelated to the culture (uncontrolled automatic shut down of the cooling system leading to high temperatures in the fermenter). Thus only very limited useful data was generated on the production and secretion of cellulolytic proteins. However, the initial data looked very promising as the fungus grew as a freely dispersed short branched mycelium, resulting in a non-viscous broth. As the enzyme secretion in this fungus also mainly takes place from the hyphal tips (see chapter 4), this morphology may prove beneficial in relation to both broth rheology and enzyme secretion. Some cellulolytic activity was also detected in the medium, up to 4.4FPUg^{-1}, however this is only one third of that, measured in small scale reference systems (*i.e*. 5l stirred tank fermenters running for ca. 200h). It is firmly believed that the low enzymatic activity is a result of the fermentation being stopped before reaching its final titre, rather than being indicative of a lower enzyme production of the *T. reesei* in the RJH system. However, more fermentations must be conducted to fully elucidate the effect of the RJH on the production of cellulolytic proteins by *T. reesei.*

7.2 Further Work

7.2.1 Scale up of the Rotary Jet Head system

In this thesis the performance of a pilot scale fermenter equipped with a RJH model IM15 with 7mm nozzles has been evaluated. This model was found to have an adequate size for the 310l fermenter used. However, for larger fermenter systems it may prove necessary with a jet head with larger nozzles, as simply increasing the pressure in the recirculation loop may result in cell damage. Furthermore, the rotation speed of the RJH models presently offered for sale by ISO-MIX A/S is controlled by the flow speed in the loop. Recent studies by Nordkvist *et al.* [3] have shown that the rotation speed of the RJH has an effect on the mixing time. In some cases it would thus be desirable to have a separate motor to power the rotation of the distributor arms of the RJH. By having a separate motor driving the rotation, the susceptibility of the gearing system of the IM15, which can get blocked by large media components (such as grits in crude soy based media) could be eliminated. Though an optimized prototype version of the IM15 RJH with improved cleanability and isolated gear was designed for the project and manufactured by ISO-MIX A/S, it could be advantageous to remove the turbine and gearing system altogether. It would also be possible to optimise the rotation speed of the RJH for both mixing of a fermentation broth with a specific rheological property and subsequent cleaning of the fermenter. This could be achieved by adapting a Gunclean Toftejorg model SSt40A tank cleaning machine from Alfa Laval to be used for mixing. The tank cleaner is equipped with an external motor and up to 12mm nozzles. However, before being used for mixing of fermentation broth the machine must be optimised to run aseptically. If manufactured it is expected to represent a cost-competitive alternative for traditional impellers, which should be considered when building or renovating medium-scale to large-scale fermenter systems.

7.2.2 Computational Fluid Dynamics

In this thesis turbulent flow was assumed in the RJH system. However, during viscous fermentation, areas with transitional or even laminar flow might develop. Computational fluid dynamics (CFD) could be used to elucidate where these regions may arise and give valuable insight how to optimize the RJH fermenter design, e.g by multiple jet heads. The studies by Nordkvist *et al.* [3] demonstrated how altering the jet head

rotation speed affects the mixing. CFD could be used to model and optimise the rotation speed at different viscosities and broth densities. It is however still necessary with pilot or production scale tests to validate the CFD models, and it may prove challenging to produce sufficiently precise CFD models, which are able to describe the complex interaction between liquid and gas phase, recirculation bubbles, different flow regimes etc.

7.3 General Conclusions

This project has demonstrated how a RJH mixing system can be utilized as an efficient alternative to traditional stirred tank reactors. An optimized version of the IM15 RJH with improved cleanability and isolated gear was designed in cooperation with the company ISO-MIX A/S, enabling the system to be used for fermentations with filamentous microorganisms. The system was shown to be especially advantageous for use in fungal fermentations. The RJH system caused a beneficial change of the fungal mycelium, from pelleted growth to loosely associated mycelium, leading to reduced broth viscosity and improved volumetric gas transfer rates. The change of the mycelium morphology made the culture in the RJH system significantly more homogeneous compared to an impeller mixed system, which reduces the complexity and enables more efficient process optimization. Contrary to expectations, the RJH did not seem to have any negative effect on the fungi. Several stress related genes in *Aspergillus oryzae* were down-regulated in the RJH system, and the growth rate of the culture was identical to that found in impeller mixed reference systems.

To be able to accurately monitor the broth viscosity a combination of at- and in-line measurements with a Haake FL10 vane spindle rheometer and a Marimex VA-300 vibrating rod sensor were utilised. By combining the two datasets it was possible to continuously monitor the rheological properties in the fermenter, during both bacterial and fungal fermentations, which may prove highly valuable information for process control.

The RJH fermenter system was also demonstrated to be able to be used successfully for fermentations with the exopolysaccharide (EPS) producing bacteria *Xanthomonas campestris*. The following correlation between the k_La and the superficial gas velocity, power input, volume of the tank and apparent viscosity) was determined:

$$k_L a = k u_s^{0.4} \left(\frac{P_t}{V}\right)^{0.122} (\eta_{app})^{-0.8}$$

The viscous broth caused the power input from the pump to decrease due to recirculation of air bubbles in the external loop, which could make the RJH less suitable

for such fermentations, unless a degasser is placed in the recirculation loop. The tested system also shows great potential for viscous bacterial fermentations where air sparging is not necessary, but rapid mixing is desired e.g. during EPS forming anaerobic fed-batch bacteria fermentations. The high shear zones in the RJH fermenter were furthermore shown to shorten the average chain length of the bacteria, which could be advantageous in productions where the final product concentration or yield is based on colony forming units ($CFUg^{-1}$), e.g. lactic acid bacteria cultures to be used for dairy, human health and nutrition products. Generally, fermentations must be run under strictly aseptic conditions and the fermenter should be easy to clean and sterilize. This makes the RJH system highly desireable, as it is also able to be used as a CIP machine between batches and there is no need for 'difficult to clean' baffles inside the tank.

7.4 References

1. Bhargava, S., K.S. Wenger, and M.R. Marten, *Pulsed addition of limiting-carbon during Aspergillus oryzae fermentation leads to improved productivity of a recombinant enzyme.* Biotechnology and Bioengineering, 2003. 82(1): p. 111-117.
2. Xiao, Z., et al., *Effects of sugar inhibition on cellulases and β-glucosidase during enzymatic hydrolysis of softwood substrates.* Applied Biochemistry and Biotechnology, 2004. 115(1): p. 1115.
3. Nordkvist, M., et al., *Mixing by rotary jet heads: Indications of the benefits of head rotation under turbulent and transitional flow conditions.* Chemical Engineering Research and Design, 2008. 86(12): p. 1454.

Appendix I

LOCUS	Coef	F.p.value	PFAM_NAME	PFAM_DESCRIPTION	
AO090003000770	-5.0178	0.00001	Glycos_transf_1	Glycosyl transferases group 1	1
AO090102000482	-4.1403	0.00003	GST_N	Glutathione S-transferase, N-terminal domain	2
AO090103000165	-3.6399	0.00004	MFS_1	Major Facilitator Superfamily	3
AO090010000018	-4.371	0.00005	p450	Cytochrome P450	4
AO090020000500	-5.1678	0.00008	KR	KR domain	5
AO090020000501	-3.8496	0.00009	KR	KR domain	6
AO090103000167	-3.863	0.00011	PP-binding	Phosphopantetheine attachment site	7
AO090103000166	-2.6965	0.00012	ABC_membrane	ABC transporter transmembrane region	8
AO090012000174	-2.6367	0.00012	Patatin	Patatin-like phospholipase	9
AO090003000392	-3.3587	0.00014	UCH	Ubiquitin carboxyl-terminal hydrolase	10
AO090206000078	-2.3036	0.00015	DUF1774	Fungal protein of unknown function (DUF1774)	11
AO090009000634	-5.0503	0.00015	ADH_zinc_N	Zinc-binding dehydrogenase	12
AO090005000652	-2.8658	0.00015	AA_permease	Amino acid permease	13
AO090003001320	-3.7142	0.00017	CoaE	Dephospho-CoA kinase	14
AO090701000780	-2.2457	0.00017	FHA	FHA domain	15
AO090026000144	-2.9833	0.00018	MFS_1	Major Facilitator Superfamily	16
AO090120000176	-2.2334	0.00023	FAD_binding_8	FAD-binding domain	17
AO090102000480	-3.6024	0.00024	GST_N	Glutathione S-transferase, N-terminal domain	18
AO090001000203	-1.9901	0.00027	AMP-binding	AMP-binding enzyme	19
AO090011000202	-3.1367	0.00030	NAD_binding_1	Oxidoreductase NAD-binding domain	20
AO090001000189	-3.2998	0.00030	Fungal_lectin	Fungal fucose-specific lectin	21
AO090020000412	-2.6068	0.00030	RRM_1	RNA recognition motif. (a.k.a. RRM, RBD, or RNP domain)	22
AO090038000281	-3.4536	0.00030	F-box	F-box domain	23
AO090120000376	2.8907	0.00034	AMP-binding	AMP-binding enzyme	24
AO090010000443	-2.8983	0.00035	Zn_clus	Fungal Zn(2)-Cys(6) binuclear cluster domain	25
AO090023000513	-2.6358	0.00038	DnaJ	DnaJ domain	26
AO090005001318	2.362	0.00039	FMO-like	Flavin-binding monooxygenase-like	27
AO090120000175	-2.5484	0.00040	Ctr	Ctr copper transporter family	28
AO090120000106	-1.8891	0.00040	p450	Cytochrome P450	29
AO090009000496	-2.1146	0.00042	Cyclin	Cyclin	30
AO090010000243	-1.9892	0.00042	Zn_clus	Fungal Zn(2)-Cys(6) binuclear cluster domain	31
AO090010000444	-6.0805	0.00044	PFK	Phosphofructokinase	32
AO090005001622	-7.2937	0.00051	Nexin_C	Sorting nexin C terminal	33
AO090166000070	-4.0901	0.00051	p450	Cytochrome P450	34
AO090020000191	-1.8155	0.00052	MFS_1	Major Facilitator Superfamily	35
AO090701000877	2.1035	0.00053	Transferase	Transferase family	36
AO090020000685	-3.3617	0.00057	p450	Cytochrome P450	37
AO090010000015	-2.2193	0.00057	p450	Cytochrome P450	38
AO090011000885	-1.6716	0.00059	MFS_1	Major Facilitator Superfamily	39
AO090701000669	-2.0733	0.00061	RTC	RNA 3'-terminal phosphate cyclase	40
AO090020000652	2.1434	0.00063	BBE	Berberine and berberine like	41
AO090005001430	-1.5731	0.00066	Mito_carr	Mitochondrial carrier protein	42
AO090023000857	-1.7779	0.00072	OTCace	Aspartate/ornithine carbamoyltransferase, Asp/Orn binding domain	43
AO090113000063	-2.776	0.00072	Chitosanase	Fungal chitosanase	44
AO090011000725	-2.1464	0.00073	Ank	Ankyrin repeat	45
AO090023000382	1.7553	0.00073	Peptidase_S10	Serine carboxypeptidase	46
AO090010000469	-3.0017	0.00075	Ribosomal_S12	Ribosomal protein S12	47
AO090701000738	-4.1631	0.00079	Mannosyl_trans2	Mannosyltransferase (PIG-V))	48
AO090011000266	-1.6086	0.00080	Acetyltransf_2	N-acetyltransferase	49
AO090010000445	-5.2369	0.00086	DUF833	Protein of unknown function (DUF833)	50
AO090003000006	-1.4452	0.00106	Proteasome	Proteasome A-type and B-type	51
AO090005001107	-5.2323	0.00110	Sterol_desat	Sterol desaturase	52
AO090005000588	-4.2382	0.00111	AcetylCoA_hydro	Acetyl-CoA hydrolase/transferase N-terminal domain	53
AO090011000337	-2.3971	0.00114	NAD_binding_6	Ferric reductase NAD binding domain	54
AO090102000388	-4.7097	0.00117	MFS_1	Major Facilitator Superfamily	55
AO090113000062	-1.5935	0.00118	MFS_1	Major Facilitator Superfamily	56
AO090011000343	-1.2621	0.00120	Helicase_C	Helicase conserved C-terminal domain	57
AO090009000212	-1.9796	0.00120	G_glu_transpept	Gamma-glutamyltranspeptidase	58
AO090103000170	-1.5088	0.00124	DUF1749	Protein of unknown function (DUF1749)	59
AO090012001027	-2.1451	0.00132	SWIRM	SWIRM domain	60
AO090011000699	-1.6632	0.00137	PhyH	Phytanoyl-CoA dioxygenase (PhyH)	61
AO090120000214	-2.6266	0.00138	Ctr	Ctr copper transporter family	62
AO090012000673	-1.2451	0.00154	Pyr_redox	Pyridine nucleotide-disulphide oxidoreductase	63
AO090001000738	-1.953	0.00156	Yippee	Yippee putative zinc-binding protein	64
AO090120000179	-1.7834	0.00161	ICL	Isocitrate lyase family	65
AO090011000747	-1.8508	0.00163	MFS_1	Major Facilitator Superfamily	66
AO090102000479	-2.4377	0.00168	GST_N	Glutathione S-transferase, N-terminal domain	67
AO090003001008	-1.2902	0.00169	E3_binding	e3 binding domain	68
AO090005001117	-1.8999	0.00170	FA_hydroxylase	Fatty acid hydroxylase superfamily	69
AO090023000318	-1.6671	0.00171	C4dic_mal_tran	C4-dicarboxylate transporter/malic acid transport protein	70
AO090020000043	-1.5662	0.00172	Zn_clus	Fungal Zn(2)-Cys(6) binuclear cluster domain	71
AO090701000273	-1.2943	0.00176	GRAM	GRAM domain	72
AO090010000061	-1.2358	0.00178	Methyltransf_2	O-methyltransferase	73
AO090001000291	-2.6846	0.00179	Methyltransf_2	O-methyltransferase	74
AO090012000168	1.2855	0.00180	DUF590	Protein of unknown function, DUF590	75
AO090003001067	1.1255	0.00181	FGGY_C	FGGY family of carbohydrate kinases, C-terminal domain	76
AO090038000539	-1.2284	0.00185	Amidase	Amidase	77
AO090010000667	-4.8723	0.00193	Sterol_desat	Sterol desaturase	78
AO090102000297	-3.5725	0.00194	Thioredoxin	Thioredoxin	79
AO090026000357	-3.7372	0.00195	Cerato-platanin	Cerato-platanin	80
AO090023000949	-1.2377	0.00204	COesterase	Carboxylesterase	81
AO090103000367	-1.6766	0.00207	FAD_binding_8	FAD-binding domain	82
AO090011000926	-2.7726	0.00210	Pkinase	Protein kinase domain	83
AO090023000577	-3.2002	0.00217	2-Hacid_dh_C	D-isomer specific 2-hydroxyacid dehydrogenase, NAD binding domain	84
AO090011000149	-1.3112	0.00223	NAD_binding_1	Oxidoreductase NAD-binding domain	85
AO090023000687	-1.5366	0.00223	PLA2_B	Lysophospholipase catalytic domain	86
AO090003000141	-1.538	0.00233	Glyoxalase	Glyoxalase/Bleomycin resistance protein/Dioxygenase superfamily	87
AO090701000353	-1.7783	0.00233	Cupin_2	Cupin domain	88
AO090001000689	-1.4129	0.00236	RRM_1	RNA recognition motif. (a.k.a. RRM, RBD, or RNP domain)	89
AO090003001209	-1.0499	0.00243	Glyco_hydro_31	Glycosyl hydrolases family 31	90
AO090023000514	-2.3417	0.00243	DnaJ	DnaJ domain	91
AO090011000358	-1.0711	0.00243	Pyr_redox	Pyridine nucleotide-disulphide oxidoreductase	92
AO090009000095	-1.0601	0.00245	polyprenyl_synt	Polyprenyl synthetase	93
AO090102000525	-1.703	0.00253	HATPase_c	Histidine kinase-, DNA gyrase B-, and HSP90-like ATPase	94
AO090010000650	-1.1322	0.00256	Methyltransf_12	Methyltransferase domain	95
AO090005001239	-2.1096	0.00268	Sec63	Sec63 Brl domain	96
AO090005000739	-1.1845	0.00268	GSHPx	Glutathione peroxidase	97
AO090023000430	-4.9618	0.00300	NUDIX	NUDIX domain	98
AO090023000624	-3.5175	0.00301	Ubie_methyltran	ubiE/COQ5 methyltransferase family	99
AO090012000601	-4.5329	0.00302	Phosphorylase	Carbohydrate phosphorylase	100

LOCUS	Coef	F.p.value	PFAM_NAME	PFAM_DESCRIPTION	
AO090003000309	-1.1931	0.00304	GMC_oxred_C	GMC oxidoreductase	101
AO090026000463	1.6762	0.00317	NUC173	NUC173 domain	102
AO090003000331	1.0425	0.00320	Transferase	Transferase family	103
AO090010000501	-1.4612	0.00323	MFS_1	Major Facilitator Superfamily	104
AO090003000316	-0.96	0.00340	LSM	LSM domain	105
AO090003000624	-1.0527	0.00341	Acetate_kinase	Acetokinase family	106
AO090011000453	1.3303	0.00345	CTP_transf_2	Cytidylyltransferase	107
AO090010000628	-1.5827	0.00350	ABC_membrane	ABC transporter transmembrane region	108
AO090038000253	-1.4501	0.00351	Ank	Ankyrin repeat	109
AO090012000821	-2.5789	0.00356	Sds3	Sds3-like	110
AO090005000828	-2.6115	0.00356	TPR_2	Tetratricopeptide repeat	111
AO090023000349	-1.318	0.00369	Transketolase_C	Transketolase, C-terminal domain	112
AO090701000554	-1.3302	0.00380	HSP20	Hsp20/alpha crystallin family	113
AO090005000471	-2.1775	0.00385	MFS_1	Major Facilitator Superfamily	114
AO090009000493	-2.5345	0.00390	Cyclin	Cyclin	115
AO090005000583	-5.8382	0.00401	Sel1	Sel1 repeat	116
AO090120000471	1.9446	0.00407	PalH	PalH/RIM21	117
AO090003001519	-1.1893	0.00409	AA_permease	Amino acid permease	118
AO090026000396	-3.6706	0.00415	MFS_1	Major Facilitator Superfamily	119
AO090026000711	2.3163	0.00420	MHYT	Bacterial signalling protein N terminal repeat	120
AO090038000500	-1.3135	0.00420	RasGEF	RasGEF domain	121
AO090120000103	-0.9755	0.00423	FAD_binding_8	FAD-binding domain	122
AO090701000238	-1.6135	0.00427	Abhydrolase_1	alpha/beta hydrolase fold	123
AO090011000867	-1.4459	0.00433	Ank	Ankyrin repeat	124
AO090003000206	-1.3421	0.00434	p450	Cytochrome P450	125
AO090102000533	-2.2958	0.00442	EMP24_GP25L	emp24/gp25L/p24 family/GOLD	126
AO090701000343	-3.4696	0.00443	Dioxygenase_C	Dioxygenase	127
AO090010000221	-2.8067	0.00444	Bac_rhodopsin	Bacteriorhodopsin	128
AO090010000065	-2.3072	0.00456	UDPG_MGDP_dh	UDP-glucose/GDP-mannose dehydrogenase family, central domain	129
AO090026000248	-2.7055	0.00480	MFS_1	Major Facilitator Superfamily	130
AO090102000168	1.6445	0.00485	p450	Cytochrome P450	131
AO090023000431	-5.9574	0.00485	NUDIX	NUDIX domain	132
AO090103000273	0.9435	0.00486	MFS_1	Major Facilitator Superfamily	133
AO090020000493	-1.0647	0.00493	Acyl-CoA_dh_M	Acyl-CoA dehydrogenase, middle domain	134
AO090038000424	-2.2357	0.00515	UPF0261	Uncharacterised protein family (UPF0261)	135
AO090003000906	-1.1774	0.00518	Glyco_hydro_12	Glycosyl hydrolase family 12	136
AO090005001449	-0.9398	0.00527	Aldo_ket_red	Aldo/keto reductase family	137
AO090003000980	-0.8993	0.00533	SurE	Survival protein SurE	138
AO090001000555	-1.0955	0.00534	E1_dh	Dehydrogenase E1 component	139
AO090012000997	-1.1893	0.00539	MAP1_LC3	Microtubule associated protein 1A/1B, light chain 3	140
AO090012000521	-1.0173	0.00542	NAD_binding_4	Male sterility protein	141
AO090012000652	-1.1532	0.00545	KTI12	Chromatin associated protein KTI12	142
AO090005001249	1.1824	0.00546	Acyl-CoA_dh_1	Acyl-CoA dehydrogenase, C-terminal domain	143
AO090005000125	-1.0043	0.00547	ADH_zinc_N	Zinc-binding dehydrogenase	144
AO090001000692	-1.2357	0.00548	MFS_1	Major Facilitator Superfamily	145
AO090023000304	-0.8748	0.00555	F-actin_cap_A	F-actin capping protein alpha subunit	146
AO090103000026	-0.8365	0.00557	Peptidase_S10	Serine carboxypeptidase	147
AO090003000831	-4.4339	0.00559	FAD_binding_2	FAD binding domain	148
AO090012000646	-1.5142	0.00566	HEAT	HEAT repeat	149
AO090005000804	-1.5601	0.00573	Helicase_C	Helicase conserved C-terminal domain	150
AO090009000484	-1.0334	0.00575	Aminotran_1_2	Aminotransferase class I and II	151
AO090020000684	-2.6961	0.00578	p450	Cytochrome P450	152
AO090120000183	-3.0748	0.00584	Asn_synthase	Asparagine synthase	153
AO090005000161	1.1194	0.00596	Methyltransf_2	O-methyltransferase	154
AO090003000893	1.3479	0.00603	ADH_zinc_N	Zinc-binding dehydrogenase	155
AO090206000069	-1.7196	0.00613	MFS_1	Major Facilitator Superfamily	156
AO090009000228	-2.6348	0.00614	Asp	Eukaryotic aspartyl protease	157
AO090011000922	-0.9516	0.00616	Hydrolase	haloacid dehalogenase-like hydrolase	158
AO090038000395	-1.264	0.00617	PGK	Phosphoglycerate kinase	159
AO090206000052	-2.1163	0.00618	Actin	Actin	160
AO090009000516	-0.89	0.00621	zf-C2H2	Zinc finger, C2H2 type	161
AO090023000314	-1.0923	0.00628	3-HAO	3-hydroxyanthranilic acid dioxygenase	162
AO090011000875	-1.8286	0.00631	DnaJ_CXXCXGXG	DnaJ central domain (4 repeats)	163
AO090120000174	-2.5831	0.00647	Abhydrolase_2	Phospholipase/Carboxylesterase	164
AO090701000318	-2.5717	0.00649	Aldedh	Aldehyde dehydrogenase family	165
AO090023000528	-1.2113	0.00660	PP-binding	Phosphopantetheine attachment site	166
AO090701000639	-1.079	0.00662	Glyco_hydro_31	Glycosyl hydrolases family 31	167
AO090038000590	-1.1257	0.00671	LisH	LisH	168
AO090011000757	-2.0636	0.00672	Acetyltransf_1	Acetyltransferase (GNAT) family	169
AO090120000385	-1.2304	0.00675	GTP_EFTU_D2	Elongation factor Tu domain 2	170
AO090012000787	-0.794	0.00685	Band_7	SPFH domain / Band 7 family	171
AO090020000504	1.1444	0.00693	Thioredoxin	Thioredoxin	172
AO090026000696	-1.7182	0.00693	ADH_zinc_N	Zinc-binding dehydrogenase	173
AO090038000589	-1.1604	0.00699	LisH	LisH	174
AO090012000228	-0.8622	0.00704	Methyltransf_12	Methyltransferase domain	175
AO090012000708	-0.8327	0.00707	Peptidase_S10	Serine carboxypeptidase	176
AO090038000173	-1.9255	0.00710	NPD	2-nitropropane dioxygenase	177
AO090003000459	-1.5916	0.00714	UDG	Uracil DNA glycosylase superfamily	178
AO090001000012	-0.7805	0.00715	2OG-FeII_Oxy	2OG-Fe(II) oxygenase superfamily	179
AO090023000932	-0.9707	0.00719	RasGEF	RasGEF domain	180
AO090026000066	-1.7365	0.00725	DUF917	Protein of unknown function (DUF917)	181
AO090005000683	-0.7843	0.00727	3-HAO	3-hydroxyanthranilic acid dioxygenase	182
AO090005001147	-1.8767	0.00733	ADH_zinc_N	Zinc-binding dehydrogenase	183
AO090011000454	1.0459	0.00733	PMI_typeI	Phosphomannose isomerase type I	184
AO090012000287	-3.531	0.00739	KR	KR domain	185
AO090012000665	0.7841	0.00746	Peptidase_C14	Caspase domain	186
AO090023000147	-0.9858	0.00769	Cupin_2	Cupin domain	187
AO090020000239	-0.8545	0.00773	NmrA	NmrA-like family	188
AO090023000935	1.2352	0.00774	MutL_C	MutL C terminal dimerisation domain	189
AO090003000661	-6.1244	0.00777	TPP_enzyme_M	Thiamine pyrophosphate enzyme, central domain	190
AO090005000114	1.8991	0.00779	AA_permease	Amino acid permease	191
AO090009000542	1.4889	0.00781	Aldo_ket_red	Aldo/keto reductase family	192
AO090038000427	-1.5467	0.00786	KR	KR domain	193
AO090138000023	-1.4156	0.00795	adh_short	short chain dehydrogenase	194
AO090010000210	-2.1089	0.00822	RPEL	RPEL repeat	195
AO090011000884	-1.1819	0.00823	MFS_1	Major Facilitator Superfamily	196
AO090026000392	-1.6463	0.00827	HMGL-like	HMGL-like	197
AO090005001641	-0.7646	0.00837	WD40	WD domain, G-beta repeat	198
AO090001000273	-0.7781	0.00839	ADH_zinc_N	Zinc-binding dehydrogenase	199
AO090206000070	-1.204	0.00840	MFS_1	Major Facilitator Superfamily	200

LOCUS	Coef	F.p.value	PFAM_NAME	PFAM_DESCRIPTION	
AO090011000715	-2.3787	0.00875	CBM_1	Fungal cellulose binding domain	201
AO090701000734	-1.1388	0.00878	Autophagy_C	Autophagocytosis associated protein, C-terminal domain	202
AO090005001060	-0.8054	0.00879	Cyt-b5	Cytochrome b5-like Heme/Steroid binding domain	203
AO090023000256	-1.7246	0.00887	Amidohydro_1	Amidohydrolase family	204
AO090011000830	1.2476	0.00887	Endonuclease_NS	DNA/RNA non-specific endonuclease	205
AO090011000096	-0.8563	0.00892	HET	Heterokaryon incompatibility protein (HET)	206
AO090023000032	-1.5723	0.00894	Aegerolysin	Aegerolysin	207
AO090011000751	-0.9614	0.00899	MFS_1	Major Facilitator Superfamily	208
AO090038000404	-1.1468	0.00906	zf-C2H2	Zinc finger, C2H2 type	209
AO090005000264	-1.3936	0.00911	HhH-GPD	HhH-GPD superfamily base excision DNA repair protein	210
AO090038000421	-1.4226	0.00912	UPF0261	Uncharacterised protein family (UPF0261)	211
AO090103000438	-0.7205	0.00914	3Beta_HSD	3-beta hydroxysteroid dehydrogenase/isomerase family	212
AO090003000705	-0.7596	0.00915	GatB_Yqey	GatB domain	213
AO090103000406	-1.4359	0.00918	Thiolase_C	Thiolase, C-terminal domain	214
AO090011000122	0.8431	0.00922	Ribonuclease	ribonuclease	215
AO090001000508	-3.2939	0.00924	Ketoacyl-synt_C	Beta-ketoacyl synthase, C-terminal domain	216
AO090023000534	0.7754	0.00933	Glyco_hydro_71	Glycosyl hydrolase family 71	217
AO090026000278	-0.7549	0.00943	NmrA	NmrA-like family	218
AO090120000378	-0.8566	0.00945	Arrestin_N	Arrestin (or S-antigen), N-terminal domain	219
AO090010000442	-1.1388	0.00960	Zn_clus	Fungal Zn(2)-Cys(6) binuclear cluster domain	220
AO090701000537	0.7078	0.00961	ABC_tran	ABC transporter	221
AO090005001312	-0.9504	0.00963	CoA_transf_3	CoA-transferase family III	222
AO090005001558	-0.8583	0.00965	F-box	F-box domain	223
AO090020000119	-0.823	0.00966	SURF1	SURF1 family	224
AO090701000254	-2.1157	0.00979	DAO	FAD dependent oxidoreductase	225
AO090026000173	-1.3536	0.00989	NmrA	NmrA-like family	226
AO090103000023	-0.8966	0.00998	Amidohydro_1	Amidohydrolase family	227
AO090005000057	1.0205	0.01000	Aminotran_1_2	Aminotransferase class I and II	228
AO090005000882	-0.9386	0.01001	AAA_2	ATPase family associated with various cellular activities (AAA)	229
AO090701000109	-1.0798	0.01013	GIDA	Glucose inhibited division protein A	230
AO090003001538	-1.5739	0.01024	MFS_1	Major Facilitator Superfamily	231
AO090010000724	0.7116	0.01028	Glyco_hydro_76	Glycosyl hydrolase family 76	232
AO090701000534	0.745	0.01037	MFS_1	Major Facilitator Superfamily	233
AO090003001385	-0.7333	0.01042	ABC2_membrane	ABC-2 type transporter	234
AO090012000975	-0.8597	0.01045	FMN_dh	FMN-dependent dehydrogenase	235
AO090026000570	0.7819	0.01049	ApbA_C	Ketopantoate reductase PanE/ApbA C terminal	236
AO090003000207	-2.2211	0.01052	zf-CHY	CHY zinc finger	237
AO090005000775	-0.8318	0.01056	PQ-loop	PQ loop repeat	238
AO090038000067	-1.0951	0.01057	Ank	Ankyrin repeat	239
AO090003001184	-1.0652	0.01057	Transferase	Transferase family	240
AO090001000531	-2.4383	0.01061	Methyltransf_12	Methyltransferase domain	241
AO090005000315	0.7023	0.01069	Peptidase_M20	Peptidase family M20/M25/M40	242
AO090001000507	-2.8154	0.01084	Ketoacyl-synt_C	Beta-ketoacyl synthase, C-terminal domain	243
AO090020000355	0.8779	0.01084	MFS_1	Major Facilitator Superfamily	244
AO090012000054	1.6215	0.01095	Ank	Ankyrin repeat	245
AO090023000692	-1.1811	0.01105	Acid_phosphat_A	Histidine acid phosphatase	246
AO090005001111	-0.9375	0.01114	Syja_N	SacI homology domain	247
AO090003001124	0.7531	0.01118	MOZ_SAS	MOZ/SAS family	248
AO090011000195	0.7849	0.01123	MFS_1	Major Facilitator Superfamily	249
AO090005000160	0.7947	0.01127	ATP11	ATP11 protein	250
AO090003000593	-0.8933	0.01133	Glycos_transf_2	Glycosyl transferase family 2	251
AO090701000539	0.8794	0.01135	MFS_1	Major Facilitator Superfamily	252
AO090120000370	-0.8864	0.01138	Amidohydro_2	Amidohydrolase	253
AO090012000624	-0.829	0.01142	Pyr_redox	Pyridine nucleotide-disulphide oxidoreductase	254
AO090003000869	-0.7771	0.01144	tRNA-synt_2	tRNA synthetases class II (D, K and N)	255
AO090001000419	-1.0699	0.01155	KR	KR domain	256
AO090113000137	-1.1105	0.01160	Fungal_trans	Fungal specific transcription factor domain	257
AO090003001049	-1.2574	0.01163	Pro_isomerase	Cyclophilin type peptidyl-prolyl cis-trans isomerase/CLD	258
AO090023000125	-1.1049	0.01169	Lipase_3	Lipase (class 3)	259
AO090011000865	-1.2739	0.01173	Ank	Ankyrin repeat	260
AO090005001236	-1.0116	0.01183	ALO	D-arabinono-1,4-lactone oxidase	261
AO090012000130	-1.293	0.01187	Aldedh	Aldehyde dehydrogenase family	262
AO090102000589	-0.8694	0.01187	Cu-oxidase	Multicopper oxidase	263
AO090020000458	-1.906	0.01188	PHD	PHD-finger	264
AO090701000417	1.8198	0.01192	p450	Cytochrome P450	265
AO090023000370	0.7823	0.01200	Acyl_transf_3	Acyltransferase family	266
AO090003001376	0.808	0.01208	ADH_zinc_N	Zinc-binding dehydrogenase	267
AO090020000199	-0.6723	0.01216	Abhydrolase_3	alpha/beta hydrolase fold	268
AO090026000648	-1.151	0.01223	Myb_DNA-binding	Myb-like DNA-binding domain	269
AO090103000096	0.8288	0.01234	MFS_1	Major Facilitator Superfamily	270
AO090026000230	-0.9339	0.01240	UQ_con	Ubiquitin-conjugating enzyme	271
AO090138000045	-1.2698	0.01241	FMN_dh	FMN-dependent dehydrogenase	272
AO090005001199	-0.6721	0.01242	N2227	N2227-like protein	273
AO090003000979	-1.4648	0.01249	SurE	Survival protein SurE	274
AO090701000791	1.743	0.01251	Metallophos	Calcineurin-like phosphoesterase	275
AO090020000420	2.7123	0.01253	Lyase_1	Lyase	276
AO090003000497	-0.7626	0.01255	Glyco_hydro_1	Glycosyl hydrolase family 1	277
AO090120000256	-1.1848	0.01261	IATP	Mitochondrial ATPase inhibitor, IATP	278
AO090010000463	-1.0198	0.01265	RmlD_sub_bind	RmlD substrate binding domain	279
AO090003001302	2.7257	0.01279	EHN	Epoxide hydrolase N terminus	280
AO090038000463	-3.3672	0.01283	MFS_1	Major Facilitator Superfamily	281
AO090023000114	-1.5288	0.01288	IF-2B	Initiation factor 2 subunit family	282
AO090010000126	1.0566	0.01288	Sugar_tr	Sugar (and other) transporter	283
AO090701000579	1.8385	0.01297	Peptidase_S41	Peptidase family S41	284
AO090005000539	1.1651	0.01308	Pyridoxal_deC	Pyridoxal-dependent decarboxylase conserved domain	285
AO090012000998	-2.4705	0.01309	Coprogen_oxidas	Coproporphyrinogen III oxidase	286
AO090701000219	-1.2148	0.01314	DnaJ_C	DnaJ C terminal region	287
AO090026000168	1.568	0.01333	Acyltransferase	Acyltransferase	288
AO090012000429	0.7744	0.01339	ECH	Enoyl-CoA hydratase/isomerase family	289
AO090003001112	-0.844	0.01348	AMP-binding	AMP-binding enzyme	290
AO090701000487	1.8179	0.01359	SGL	SMP-30/Gluconolaconase/LRE-like region	291
AO090011000403	1.0119	0.01361	COesterase	Carboxylesterase	292
AO090026000514	-0.7824	0.01363	AMP-binding	AMP-binding enzyme	293
AO090011000588	-1.9969	0.01371	Uricase	Uricase	294
AO090001000592	-1.4787	0.01372	UQ_con	Ubiquitin-conjugating enzyme	295
AO090012000396	2.5861	0.01378	Abhydrolase_1	alpha/beta hydrolase fold	296
AO090701000147	-0.941	0.01379	MFS_1	Major Facilitator Superfamily	297
AO090023000883	-1.0157	0.01393	Abhydrolase_1	alpha/beta hydrolase fold	298
AO090102000063	-2.556	0.01407	Sulfatase	Sulfatase	299
AO090701000471	-1.0484	0.01411	p450	Cytochrome P450	300

LOCUS	Coef	F.p.value	PFAM_NAME	PFAM_DESCRIPTION	
AO090120000052	-1.7222	0.01413	Glyco_hydro_65C	Glycosyl hydrolase family 65, C-terminal domain	301
AO090001000587	-0.6534	0.01420	MFS_1	Major Facilitator Superfamily	302
AO090009000294	-0.8955	0.01422	FAD_binding_3	FAD binding domain	303
AO090023000893	-1.1169	0.01423	FA_desaturase	Fatty acid desaturase	304
AO090005000796	-1.2536	0.01428	MA3	MA3 domain	305
AO090113000010	-0.9786	0.01430	GMC_oxred_C	GMC oxidoreductase	306
AO090005001229	-1.0855	0.01450	adh_short	short chain dehydrogenase	307
AO090120000260	-0.9087	0.01451	37694	14-3-3 protein	308
AO090103000084	0.9436	0.01454	AA_permease	Amino acid permease	309
AO090005000630	-0.9472	0.01454	ERO1	Endoplasmic Reticulum Oxidoreductin 1 (ERO1)	310
AO090003000278	-0.8432	0.01458	KR	KR domain	311
AO090005000690	1.601	0.01466	KR	KR domain	312
AO090701000558	-0.6444	0.01467	Glyco_hydro_31	Glycosyl hydrolases family 31	313
AO090005001300	-0.8892	0.01501	Metalloenzyme	Metalloenzyme superfamily	314
AO090026000164	-0.9035	0.01504	Helicase_C	Helicase conserved C-terminal domain	315
AO090010000435	-1.3791	0.01517	RTA1	RTA1 like protein	316
AO090001000634	0.6549	0.01534	Na_Ca_ex	Sodium/calcium exchanger protein	317
AO090003001250	-1.5518	0.01540	YEATS	YEATS family	318
AO090012000132	-1.4043	0.01571	Hist_deacetyl	Histone deacetylase domain	319
AO090005001379	-0.7874	0.01572	NUDIX	NUDIX domain	320
AO090003000208	-0.9142	0.01581	Glyoxalase	Glyoxalase/Bleomycin resistance protein/Dioxygenase superfamily	321
AO090102000483	-0.805	0.01582	adh_short	short chain dehydrogenase	322
AO090005001429	-0.8137	0.01584	G6PD_C	Glucose-6-phosphate dehydrogenase, C-terminal domain	323
AO090120000334	-1.0366	0.01594	Glyco_transf_15	Glycolipid 2-alpha-mannosyltransferase	324
AO090012000417	-0.9382	0.01598	Tubulin_C	Tubulin/FtsZ family, C-terminal domain	325
AO090012000457	-4.0837	0.01604	Pyridoxal_deC	Pyridoxal-dependent decarboxylase conserved domain	326
AO090011000679	-1.386	0.01621	Aminotran_1_2	Aminotransferase class I and II	327
AO090001000481	-0.997	0.01624	PB1	PB1 domain	328
AO090026000508	-1.7855	0.01631	MFS_1	Major Facilitator Superfamily	329
AO090102000016	-1.3333	0.01642	FAD_binding_7	FAD binding domain of DNA photolyase	330
AO090113000134	-1.1209	0.01644	DSBA	DSBA-like thioredoxin domain	331
AO090026000778	-0.8872	0.01646	MFS_1	Major Facilitator Superfamily	332
AO090701000127	-0.9013	0.01648	CAS_CSE1	CAS/CSE protein, C-terminus	333
AO090003000310	-3.7892	0.01651	AOX	Alternative oxidase	334
AO090103000098	-0.9485	0.01661	Ank	Ankyrin repeat	335
AO090701000709	-0.7041	0.01668	Pkinase	Protein kinase domain	336
AO090023000035	0.6597	0.01668	HisKA	His Kinase A (phosphoacceptor) domain	337
AO090001000121	0.7247	0.01705	Ldh_2	Malate/L-lactate dehydrogenase	338
AO090003001094	-0.7331	0.01707	Mannosyl_trans2	Mannosyltransferase (PIG-V))	339
AO090012000731	-1.3756	0.01707	Pkinase	Protein kinase domain	340
AO090005000281	1.4568	0.01720	MFS_1	Major Facilitator Superfamily	341
AO090023000039	-0.8504	0.01727	MFS_1	Major Facilitator Superfamily	342
AO090003000324	-0.6368	0.01734	Pkr1	ER protein Pkr1	343
AO090023000241	-1.8159	0.01739	Polysacc_deac_1	Polysaccharide deacetylase	344
AO090005000995	-0.643	0.01767	Sterol_desat	Sterol desaturase	345
AO090003000465	-2.7845	0.01768	Arrestin_N	Arrestin (or S-antigen), N-terminal domain	346
AO090020000068	-0.8682	0.01777	eIF2A	Eukaryotic translation initiation factor eIF2A	347
AO090009000541	0.6962	0.01777	Aldo_ket_red	Aldo/keto reductase family	348
AO090001000237	0.7614	0.01794	GTP_cyclohydrol	GTP cyclohydrolase I	349
AO090001000290	-0.7087	0.01799	Methyltransf_2	O-methyltransferase	350
AO090023000499	0.6808	0.01810	zf-C2H2	Zinc finger, C2H2 type	351
AO090023000206	0.9739	0.01812	Ligase_CoA	CoA-ligase	352
AO090011000829	0.9428	0.01818	Endonuclease_NS	DNA/RNA non-specific endonuclease	353
AO090102000622	-0.6249	0.01820	HSP90	Hsp90 protein	354
AO090011000368	-0.7181	0.01834	2-Hacid_dh_C	D-isomer specific 2-hydroxyacid dehydrogenase, NAD binding domair	355
AO090012000252	-0.7622	0.01843	MFS_1	Major Facilitator Superfamily	356
AO090011000221	-0.8005	0.01857	Fungal_trans	Fungal specific transcription factor domain	357
AO090011000134	0.8949	0.01878	ADH_zinc_N	Zinc-binding dehydrogenase	358
AO090012000537	-0.67	0.01901	PTPA	Phosphotyrosyl phosphate activator (PTPA) protein	359
AO090120000158	0.6644	0.01902	Glyco_hydro_35	Glycosyl hydrolases family 35	360
AO090009000391	-0.8833	0.01929	IU_nuc_hydro	Inosine-uridine preferring nucleoside hydrolase	361
AO090102000382	-0.6836	0.01949	p450	Cytochrome P450	362
AO090038000268	0.8055	0.01955	Ank	Ankyrin repeat	363
AO090701000321	-1.9915	0.01972	Pec_lyase_C	Pectate lyase	364
AO090012000180	0.6455	0.01984	YL1_C	YL1 nuclear protein C-terminal domain	365
AO090012001016	-0.6311	0.01992	UPF0061	Uncharacterized ACR, YdiU/UPF0061 family	366
AO090005000906	0.6263	0.01995	AMP-binding	AMP-binding enzyme	367
AO090001000619	-1.197	0.02000	DAO	FAD dependent oxidoreductase	368
AO090005001110	-0.668	0.02009	zf-C2H2	Zinc finger, C2H2 type	369
AO090102000554	-1.0496	0.02015	GIY-YIG	GIY-YIG catalytic domain	370
AO090010000217	-0.7448	0.02019	UPF0183	Uncharacterised protein family (UPF0183)	371
AO090009000374	-0.5712	0.02031	NmrA	NmrA-like family	372
AO090005000628	-0.6912	0.02045	APG6	Autophagy protein Apg6	373
AO090005000460	-0.7289	0.02053	zf-C2H2	Zinc finger, C2H2 type	374
AO090011000414	-1.2975	0.02057	Gp_dh_C	Glyceraldehyde 3-phosphate dehydrogenase, C-terminal domain	375
AO090012000103	-0.8898	0.02058	LIP	Secretory lipase	376
AO090005000250	-0.9118	0.02071	NUDIX	NUDIX domain	377
AO090023000278	0.7304	0.02080	MFS_1	Major Facilitator Superfamily	378
AO090012000139	0.5697	0.02093	DUF895	Eukaryotic protein of unknown function (DUF895)	379
AO090011000555	-0.6572	0.02097	zf-C2H2	Zinc finger, C2H2 type	380
AO090120000414	-0.6878	0.02100	ECH	Enoyl-CoA hydratase/isomerase family	381
AO090023000027	0.5629	0.02106	Sugar_tr	Sugar (and other) transporter	382
AO090009000492	-0.935	0.02118	Cyclin	Cyclin	383
AO090102000246	-0.988	0.02118	Pribosyltran	Phosphoribosyl transferase domain	384
AO090011000773	-1.9186	0.02123	DUF1605	Domain of unknown function (DUF1605)	385
AO090005000823	-0.7077	0.02128	zf-RanBP	Zn-finger in Ran binding protein and others	386
AO090012000112	-0.5711	0.02136	GST_C	Glutathione S-transferase, C-terminal domain	387
AO090103000169	-0.8887	0.02147	ECH	Enoyl-CoA hydratase/isomerase family	388
AO090026000417	-0.5847	0.02154	Na_Ca_ex	Sodium/calcium exchanger protein	389
AO090012000839	0.6021	0.02169	Peptidase_S24	Peptidase S24-like	390
AO090023000072	2.2177	0.02177	p450	Cytochrome P450	391
AO090023000163	-0.672	0.02183	tRNA-synt_1e	tRNA synthetases class I (C) catalytic domain	392
AO090012000560	0.9122	0.02198	A_deaminase	Adenosine/AMP deaminase	393
AO090010000345	-1.0363	0.02207	Transp_cyt_pur	Permease for cytosine/purines, uracil, thiamine, allantoin	394
AO090023000611	-0.8958	0.02210	DUF1772	Domain of unknown function (DUF1772)	395
AO090166000090	-0.9539	0.02225	PA14	PA14 domain	396
AO090038000181	0.568	0.02235	PALP	Pyridoxal-phosphate dependent enzyme	397
AO090102000076	-0.8871	0.02238	ADH_zinc_N	Zinc-binding dehydrogenase	398
AO090023000966	-0.6357	0.02244	Cyt-b5	Cytochrome b5-like Heme/Steroid binding domain	399
AO090020000009	-1.0519	0.02258	PCMT	Protein-L-isoaspartate(D-aspartate) O-methyltransferase (PCMT)	400

LOCUS	Coef	F.p.value	PFAM_NAME	PFAM_DESCRIPTION	
AO090005000867	-0.6781	0.02264	Sugar_tr	Sugar (and other) transporter	401
AO090009000547	0.5918	0.02270	Amino_oxidase	Flavin containing amine oxidoreductase	402
AO090012000463	-0.5606	0.02280	F-box	F-box domain	403
AO090011000883	-0.901	0.02281	MFS_1	Major Facilitator Superfamily	404
AO090026000803	-1.3336	0.02284	AAA	ATPase family associated with various cellular activities (AAA)	405
AO090012000711	-2.3494	0.02294	XFP	D-xylulose 5-phosphate/D-fructose 6-phosphate phosphoketolase	406
AO090012000956	-0.9294	0.02298	APH	Phosphotransferase enzyme family	407
AO090005001154	1.2657	0.02308	MFS_1	Major Facilitator Superfamily	408
AO090003000795	-0.5876	0.02326	DegT_DnrJ_EryC1	DegT/DnrJ/EryC1/StrS aminotransferase family	409
AO090120000236	-0.6355	0.02339	Pkinase	Protein kinase domain	410
AO090012000232	0.8851	0.02341	2-Hacid_dh_C	D-isomer specific 2-hydroxyacid dehydrogenase, NAD binding domair	411
AO090023000205	0.9383	0.02349	XAP5	XAP5 protein	412
AO090012000418	0.5697	0.02352	MS_channel	Mechanosensitive ion channel	413
AO090701000830	-1.0427	0.02362	FA_desaturase	Fatty acid desaturase	414
AO090003000627	-2.3099	0.02379	RTA1	RTA1 like protein	415
AO090020000585	-0.8155	0.02395	WW	WW domain	416
AO090003000241	-0.7358	0.02406	PGAM	Phosphoglycerate mutase family	417
AO090012001017	-0.6065	0.02411	UPF0061	Uncharacterized ACR, YdiU/UPF0061 family	418
AO090012000812	-0.5481	0.02412	Pkinase	Protein kinase domain	419
AO090003000390	-0.7548	0.02416	UCH	Ubiquitin carboxyl-terminal hydrolase	420
AO090026000443	-0.9596	0.02423	3HCDH	3-hydroxyacyl-CoA dehydrogenase, C-terminal domain	421
AO090103000384	0.9331	0.02431	CFEM	CFEM domain	422
AO090120000451	-1.0135	0.02435	Abhydrolase_1	alpha/beta hydrolase fold	423
AO090005001242	0.8587	0.02438	SPRY	SPRY domain	424
AO090001000406	-1.5961	0.02449	MFS_1	Major Facilitator Superfamily	425
AO090206000108	-1.3119	0.02465	ACPS	4'-phosphopantetheinyl transferase superfamily	426
AO090011000488	-0.6239	0.02495	FA_desaturase	Fatty acid desaturase	427
AO090009000558	-0.8184	0.02501	Gln-synt_C	Glutamine synthetase, catalytic domain	428
AO090003000557	-0.5895	0.02506	TTL	Tubulin-tyrosine ligase family	429
AO090166000068	0.5521	0.02509	Prenyltrans	Prenyltransferase and squalene oxidase repeat	430
AO090103000153	-0.9821	0.02516	Peptidase_S10	Serine carboxypeptidase	431
AO090103000244	1.6084	0.02522	Tannase	Tannase and feruloyl esterase	432
AO090103000021	0.781	0.02525	Aldedh	Aldehyde dehydrogenase family	433
AO090023000071	0.8763	0.02534	polyprenyl_synt	Polyprenyl synthetase	434
AO090038000134	0.6248	0.02540	RTA1	RTA1 like protein	435
AO090011000654	-0.953	0.02552	MR_MLE	Mandelate racemase / muconate lactonizing enzyme, C-terminal dom	436
AO090038000485	-0.6599	0.02564	MFS_1	Major Facilitator Superfamily	437
AO090005001346	-1.2926	0.02575	TBCC	Tubulin binding cofactor C	438
AO090026000537	-0.695	0.02596	GDI	GDP dissociation inhibitor	439
AO090011000838	1.3312	0.02602	Biotin_lipoyl	Biotin-requiring enzyme	440
AO090020000162	-0.591	0.02618	BBE	Berberine and berberine like	441
AO090138000069	0.6242	0.02627	KR	KR domain	442
AO090023000013	-0.5565	0.02628	Saccharop_dh	Saccharopine dehydrogenase	443
AO090010000194	-1.0139	0.02632	Glycos_transf_1	Glycosyl transferases group 1	444
AO090138000144	-1.5895	0.02639	F-box	F-box domain	445
AO090003000209	0.5702	0.02656	Glyoxalase	Glyoxalase/Bleomycin resistance protein/Dioxygenase superfamily	446
AO090026000578	3.0084	0.02675	Transferase	Transferase family	447
AO090010000472	-1.5622	0.02697	PPR	PPR repeat	448
AO090011000203	-0.5924	0.02702	MIP	Major intrinsic protein	449
AO090012000116	-1.2209	0.02707	GST_C	Glutathione S-transferase, C-terminal domain	450
AO090102000581	-0.5516	0.02710	CRAL_TRIO	CRAL/TRIO domain	451
AO090023000185	0.6446	0.02712	Dynamin_N	Dynamin family	452
AO090701000536	0.8612	0.02727	ABC_tran	ABC transporter	453
AO090038000433	-0.9941	0.02731	HMG_box	HMG (high mobility group) box	454
AO090011000456	-0.7142	0.02731	COQ7	Ubiquinone biosynthesis protein COQ7	455
AO090011000416	-1.0151	0.02742	p450	Cytochrome P450	456
AO090010000032	1.1844	0.02763	Pec_lyase_C	Pectate lyase	457
AO090020000109	-1.6523	0.02766	Coq4	Coenzyme Q (ubiquinone) biosynthesis protein Coq4	458
AO090701000407	-0.8096	0.02774	Hydrolase	haloacid dehalogenase-like hydrolase	459
AO090003000625	-0.5534	0.02785	XFP	D-xylulose 5-phosphate/D-fructose 6-phosphate phosphoketolase	460
AO090026000255	1.7836	0.02788	K_trans	K+ potassium transporter	461
AO090001000130	0.8415	0.02789	Ribonuclease	ribonuclease	462
AO090005001295	-1.0528	0.02792	AMMECR1	AMMECR1	463
AO090673000006	-0.5577	0.02793	TPR_2	Tetratricopeptide repeat	464
AO090166000031	-0.6915	0.02796	AA_permease	Amino acid permease	465
AO090003001407	-0.5611	0.02797	ADH_zinc_N	Zinc-binding dehydrogenase	466
AO090020000195	-0.5589	0.02812	Methyltransf_12	Methyltransferase domain	467
AO090003001095	-0.6925	0.02815	Aldo_ket_red	Aldo/keto reductase family	468
AO090026000263	-1.1703	0.02826	DUF300	Domain of unknown function	469
AO090011000871	0.7679	0.02836	MFS_1	Major Facilitator Superfamily	470
AO090003000342	1.2684	0.02843	Zn_clus	Fungal Zn(2)-Cys(6) binuclear cluster domain	471
AO090038000148	0.8232	0.02852	MFS_1	Major Facilitator Superfamily	472
AO090020000141	0.5896	0.02864	MFS_1	Major Facilitator Superfamily	473
AO090023000060	0.7258	0.02865	FAD_binding_4	FAD binding domain	474
AO090023000902	1.9877	0.02866	Anp1	Anp1	475
AO090010000576	2.3212	0.02866	adh_short	short chain dehydrogenase	476
AO090009000214	-1.5726	0.02874	MFS_1	Major Facilitator Superfamily	477
AO090026000079	0.5172	0.02876	MFS_1	Major Facilitator Superfamily	478
AO090003001208	-0.5668	0.02881	Fungal_trans	Fungal specific transcription factor domain	479
AO090102000352	-0.7185	0.02887	WD40	WD domain, G-beta repeat	480
AO090003000149	-0.8375	0.02891	WD40	WD domain, G-beta repeat	481
AO090701000671	-0.5827	0.02893	SH3_1	SH3 domain	482
AO090012000459	0.5855	0.02912	Pyridoxal_deC	Pyridoxal-dependent decarboxylase conserved domain	483
AO090005000295	1.0125	0.02915	MFS_1	Major Facilitator Superfamily	484
AO090005001065	0.527	0.02938	Thioredoxin	Thioredoxin	485
AO090020000197	-0.5477	0.02939	Methyltransf_12	Methyltransferase domain	486
AO090003000919	-2.5094	0.02939	Ribosomal_S8e	Ribosomal protein S8e	487
AO090120000493	-0.5926	0.02946	TIM	Triosephosphate isomerase	488
AO090011000322	-0.77	0.02952	Fungal_trans	Fungal specific transcription factor domain	489
AO090011000391	-0.8571	0.02956	CASP_C	CASP C terminal	490
AO090012000554	-0.7331	0.02958	PMI_typeI	Phosphomannose isomerase type I	491
AO090010000753	-0.8407	0.02963	Glyco_hydro_28	Glycosyl hydrolases family 28	492
AO090003000722	-0.7018	0.02963	Homoserine_dh	Homoserine dehydrogenase	493
AO090120000476	-1.0668	0.02971	Zn_clus	Fungal Zn(2)-Cys(6) binuclear cluster domain	494
AO090003000430	-0.6264	0.02972	WD40	WD domain, G-beta repeat	495
AO090020000455	0.6572	0.02981	PHD	PHD-finger	496
AO090003001500	0.7077	0.02981	Glyco_transf_5	Starch synthase catalytic domain	497
AO090003000779	-0.5362	0.02982	Cation_efflux	Cation efflux family	498
AO090010000390	0.7413	0.02984	adh_short	short chain dehydrogenase	499
AO090005000439	-0.8894	0.02987	AAA	ATPase family associated with various cellular activities (AAA)	500

LOCUS	Coef	F.p.value	PFAM_NAME	PFAM_DESCRIPTION	
AO090701000750	-0.6707	0.02997	Init_tRNA_PT	Initiator tRNA phosphoribosyl transferase	501
AO090010000350	-0.8802	0.03000	MFS_1	Major Facilitator Superfamily	502
AO090102000018	-1.2969	0.03005	FAD_binding_7	FAD binding domain of DNA photolyase	503
AO090003000055	-0.6417	0.03012	Enolase_C	Enolase, C-terminal TIM barrel domain	504
AO090113000007	-1.1313	0.03012	GMC_oxred_C	GMC oxidoreductase	505
AO090020000072	-1.6104	0.03032	Glyoxalase	Glyoxalase/Bleomycin resistance protein/Dioxygenase superfamily	506
AO090701000576	-0.5624	0.03046	Glyco_transf_8	Glycosyl transferase family 8	507
AO090011000219	-0.5512	0.03047	Fungal_trans	Fungal specific transcription factor domain	508
AO090038000561	0.8712	0.03048	C2	C2 domain	509
AO090005000060	-1.6889	0.03057	AA_permease	Amino acid permease	510
AO090012000633	-0.788	0.03062	Iso_dh	Isocitrate/isopropylmalate dehydrogenase	511
AO090009000079	-0.5888	0.03085	ADH_N	Alcohol dehydrogenase GroES-like domain	512
AO090038000303	-1.1138	0.03088	ABC2_membrane	ABC-2 type transporter	513
AO090010000526	-0.8692	0.03099	Aa_trans	Transmembrane amino acid transporter protein	514
AO090009000130	-0.5224	0.03108	p450	Cytochrome P450	515
AO090038000504	-0.8278	0.03134	Pectate_lyase	Pectate lyase	516
AO090012000233	0.5596	0.03143	2-Hacid_dh_C	D-isomer specific 2-hydroxyacid dehydrogenase, NAD binding domair	517
AO090011000022	-0.7652	0.03152	AOX	Alternative oxidase	518
AO090012000947	0.909	0.03154	VWA	von Willebrand factor type A domain	519
AO090012000823	-0.6811	0.03163	Sds3	Sds3-like	520
AO090020000258	-0.6469	0.03178	Pyr_redox_2	Pyridine nucleotide-disulphide oxidoreductase	521
AO090020000650	1.5041	0.03180	BBE	Berberine and berberine like	522
AO090009000457	-0.9438	0.03181	STAS	STAS domain	523
AO090102000173	-2.1691	0.03192	DAO	FAD dependent oxidoreductase	524
AO090701000642	-1.3797	0.03194	Pkinase	Protein kinase domain	525
AO090038000206	-0.8648	0.03211	p450	Cytochrome P450	526
AO090001000279	-0.5166	0.03216	Ketoacyl-synt_C	Beta-ketoacyl synthase, C-terminal domain	527
AO090009000472	-0.513	0.03216	Bac_rhamnosid	Bacterial alpha-L-rhamnosidase	528
AO090038000182	0.6476	0.03218	PALP	Pyridoxal-phosphate dependent enzyme	529
AO090003000575	1.0834	0.03219	MFS_1	Major Facilitator Superfamily	530
AO090026000639	-1.4447	0.03229	Dioxygenase_C	Dioxygenase	531
AO090011000344	-0.6151	0.03229	Helicase_C	Helicase conserved C-terminal domain	532
AO090003001502	2.5753	0.03233	Glyco_transf_5	Starch synthase catalytic domain	533
AO090124000033	0.5565	0.03233	LysM	LysM domain	534
AO090003001146	-0.7294	0.03236	Fe-S_biosyn	Iron-sulphur cluster biosynthesis	535
AO090005000879	-0.5694	0.03253	F-box	F-box domain	536
AO090701000440	-0.7145	0.03253	MFS_1	Major Facilitator Superfamily	537
AO090010000531	-0.6521	0.03253	Transp_cyt_pur	Permease for cytosine/purines, uracil, thiamine, allantoin	538
AO090011000126	0.8478	0.03261	Na_Ca_ex	Sodium/calcium exchanger protein	539
AO090003000334	0.5955	0.03266	Transferase	Transferase family	540
AO090011000452	0.9047	0.03267	Chitin_synth_1	Chitin synthase	541
AO090701000806	-0.79	0.03274	CinA	Competence-damaged protein	542
AO090120000003	0.9373	0.03275	Aldo_ket_red	Aldo/keto reductase family	543
AO090701000146	-0.5298	0.03275	Mak16	Mak16 protein	544
AO090001000174	0.5949	0.03277	Glyco_hydro_88	Glycosyl Hydrolase Family 88	545
AO090003001529	0.4899	0.03291	COesterase	Carboxylesterase	546
AO090003000457	-2.6235	0.03291	DUF1960	Domain of unknown function (DUF1960)	547
AO090011000716	-1.4537	0.03292	DUF833	Protein of unknown function (DUF833)	548
AO090026000652	-0.5042	0.03306	Myb_DNA-binding	Myb-like DNA-binding domain	549
AO090003000793	0.8284	0.03311	Formyl_trans_C	Formyl transferase, C-terminal domain	550
AO090701000751	-1.4788	0.03315	Aldo_ket_red	Aldo/keto reductase family	551
AO090003001503	3.2559	0.03320	Glyco_transf_5	Starch synthase catalytic domain	552
AO090010000477	-1.3487	0.03325	UPF0057	Uncharacterized protein family UPF0057	553
AO090023000217	-0.6822	0.03331	DNA_pol_delta_4	DNA polymerase delta, subunit 4	554
AO090003000402	-0.6955	0.03333	Pkinase	Protein kinase domain	555
AO090102000065	-2.4123	0.03338	Aldedh	Aldehyde dehydrogenase family	556
AO090009000495	-0.8736	0.03341	Cyclin	Cyclin	557
AO090001000678	-0.77	0.03357	YL1_C	YL1 nuclear protein C-terminal domain	558
AO090003001092	-0.4854	0.03367	Mannosyl_trans2	Mannosyltransferase (PIG-V))	559
AO090003001277	-0.5293	0.03385	Sugar_tr	Sugar (and other) transporter	560
AO090120000006	3.0559	0.03388	Peptidase_A4	Peptidase A4 family	561
AO090020000336	-1.401	0.03392	NIPSNAP	NIPSNAP	562
AO090026000379	0.5592	0.03395	Condensation	Condensation domain	563
AO090102000050	-0.6195	0.03396	AAA	ATPase family associated with various cellular activities (AAA)	564
AO090010000338	-0.5529	0.03403	Fungal_trans	Fungal specific transcription factor domain	565
AO090026000820	-1.3229	0.03416	Trehalose_PPase	Trehalose-phosphatase	566
AO090102000053	0.7003	0.03417	Abhydrolase_4	TAP-like protein	567
AO090138000033	1.0827	0.03421	Glycos_transf_2	Glycosyl transferase family 2	568
AO090001000544	-1.0872	0.03428	Glyco_hydro_3_C	Glycosyl hydrolase family 3 C terminal domain	569
AO090010000031	0.5604	0.03431	Pec_lyase_C	Pectate lyase	570
AO090003000489	-0.4843	0.03434	Methyltransf_12	Methyltransferase domain	571
AO090206000119	-0.8295	0.03443	WD40	WD domain, G-beta repeat	572
AO090020000503	-1.2117	0.03444	KR	KR domain	573
AO090020000618	-0.6604	0.03476	IDO	Indoleamine 2,3-dioxygenase	574
AO090120000485	-0.5678	0.03481	Snf7	Snf7	575
AO090701000398	-1.4412	0.03485	Helicase_C	Helicase conserved C-terminal domain	576
AO090023000073	2.1132	0.03502	p450	Cytochrome P450	577
AO090701000303	0.5157	0.03505	MFS_1	Major Facilitator Superfamily	578
AO090038000090	0.5214	0.03508	Sugar_tr	Sugar (and other) transporter	579
AO090023000531	-0.6198	0.03513	TauD	Taurine catabolism dioxygenase TauD, TfdA family	580
AO090010000344	0.5602	0.03519	Pyridoxal_deC	Pyridoxal-dependent decarboxylase conserved domain	581
AO090003001077	0.5893	0.03524	Aminotran_1_2	Aminotransferase class I and II	582
AO090005000162	-0.7165	0.03531	Evr1_Alr	Erv1 / Alr family	583
AO090026000365	-0.5719	0.03540	MFS_1	Major Facilitator Superfamily	584
AO090003001108	-0.952	0.03550	C2	C2 domain	585
AO090011000404	0.6869	0.03558	COesterase	Carboxylesterase	586
AO090120000287	-1.2625	0.03573	DSPc	Dual specificity phosphatase, catalytic domain	587
AO090020000502	-1.6761	0.03579	KR	KR domain	588
AO090023000021	-2.3076	0.03598	Methyltransf_12	Methyltransferase domain	589
AO090701000827	-1.276	0.03600	adh_short	short chain dehydrogenase	590
AO090001000260	1.996	0.03601	p450	Cytochrome P450	591
AO090102000422	0.5597	0.03602	Ank	Ankyrin repeat	592
AO090020000005	-0.7577	0.03613	Peptidase_C54	Peptidase family C54	593
AO090003000648	-0.8853	0.03616	Pex19	Pex19 protein family	594
AO090009000559	-1.3993	0.03630	adh_short	short chain dehydrogenase	595
AO090005000602	-1.3905	0.03634	Peptidase_C1_2	Peptidase C1-like family	596
AO090103000216	-2.102	0.03634	GMC_oxred_C	GMC oxidoreductase	597
AO090020000489	-0.496	0.03637	PRP38	PRP38 family	598
AO090011000876	-1.6976	0.03639	Malic_M	Malic enzyme, NAD binding domain	599
AO090003000289	-1.1585	0.03688	Rad4	DNA repair protein Rad4	600

LOCUS	Coef	F.p.value	PFAM_NAME	PFAM_DESCRIPTION	
AO090005000818	1.0589	0.03697	Asparaginase	Asparaginase	601
AO090003001294	-0.6283	0.03700	Zn_clus	Fungal Zn(2)-Cys(6) binuclear cluster domain	602
AO090005001525	-1.4232	0.03707	Memo	Memo-like protein	603
AO090011000646	0.7716	0.03714	NDT80_PhoG	NDT80 / PhoG like DNA-binding family	604
AO090001000113	0.9477	0.03754	GDPD	Glycerophosphoryl diester phosphodiesterase family	605
AO090023000371	0.9547	0.03764	Acyl_transf_3	Acyltransferase family	606
AO090701000260	0.5336	0.03765	Aegerolysin	Aegerolysin	607
AO090009000299	-0.7075	0.03770	GATA	GATA zinc finger	608
AO090038000462	0.6885	0.03773	MFS_1	Major Facilitator Superfamily	609
AO090012000003	-0.5404	0.03787	Glyco_hydro_3_C	Glycosyl hydrolase family 3 C terminal domain	610
AO090005000426	-0.5771	0.03789	Methyltransf_12	Methyltransferase domain	611
AO090701000199	-0.9719	0.03791	DUF167	Uncharacterised ACR, YggU family COG1872	612
AO090020000049	0.5009	0.03791	Isochorismatase	Isochorismatase family	613
AO090009000628	-0.8721	0.03803	MFS_1	Major Facilitator Superfamily	614
AO090102000309	-1.3158	0.03806	Methyltransf_12	Methyltransferase domain	615
AO090003001099	-0.7664	0.03809	Ald_Xan_dh_C	Aldehyde oxidase and xanthine dehydrogenase, a/b hammerhead do	616
AO090005000959	-0.4858	0.03810	WD40	WD domain, G-beta repeat	617
AO090005000075	0.6379	0.03820	MFS_1	Major Facilitator Superfamily	618
AO090023000082	0.9546	0.03821	NAD_binding_4	Male sterility protein	619
AO090003000024	-2.1402	0.03834	WW	WW domain	620
AO090003001387	0.7153	0.03841	MFS_1	Major Facilitator Superfamily	621
AO090701000831	-1.4522	0.03846	Acyl_transf_1	Acyl transferase domain	622
AO090005000809	-0.9301	0.03846	WD40	WD domain, G-beta repeat	623
AO090005001636	0.6108	0.03849	zf-C3HC4	Zinc finger, C3HC4 type (RING finger)	624
AO090010000406	0.5815	0.03865	Mito_carr	Mitochondrial carrier protein	625
AO090012000592	-0.5349	0.03871	efhand	EF hand	626
AO090020000567	0.5863	0.03872	AA_permease	Amino acid permease	627
AO090003001315	0.7742	0.03879	Lipase_3	Lipase (class 3)	628
AO090005001066	-0.4997	0.03889	ABC_tran	ABC transporter	629
AO090003001542	-0.5728	0.03896	MFS_1	Major Facilitator Superfamily	630
AO090701000110	1.3641	0.03898	GIDA	Glucose inhibited division protein A	631
AO090005001454	-0.5509	0.03900	NUDIX	NUDIX domain	632
AO090102000538	-1.1072	0.03903	Helicase_C	Helicase conserved C-terminal domain	633
AO090001000710	-0.4786	0.03910	Hexokinase_2	Hexokinase	634
AO090020000665	2.6576	0.03913	Fungal_trans	Fungal specific transcription factor domain	635
AO090701000685	-1.349	0.03915	SE	Squalene epoxidase	636
AO090003000984	-3.5383	0.03920	Aldedh	Aldehyde dehydrogenase family	637
AO090103000099	-0.8618	0.03925	MFS_1	Major Facilitator Superfamily	638
AO090012000264	-1.0878	0.03939	LuxC	Acyl-CoA reductase (LuxC)	639
AO090026000382	0.473	0.03948	TRI5	Trichodiene synthase (TRI5)	640
AO090011000108	-1.2931	0.03955	Abhydrolase_1	alpha/beta hydrolase fold	641
AO090701000280	-0.5727	0.03971	UBA_3	Fungal ubiquitin-associated domain	642
AO090005001467	-0.6143	0.03973	PWI	PWI domain	643
AO090011000917	-0.5971	0.03976	AMP-binding	AMP-binding enzyme	644
AO090009000114	0.4887	0.03989	Ldl_recept_b	Low-density lipoprotein receptor repeat class B	645
AO090026000037	1.1507	0.03989	MFS_1	Major Facilitator Superfamily	646
AO090701000175	-0.4666	0.03999	MmgE_PrpD	MmgE/PrpD family	647
AO090003000832	0.4782	0.04002	MFS_1	Major Facilitator Superfamily	648
AO090005000243	-0.6377	0.04016	Thioredoxin	Thioredoxin	649
AO090020000603	0.535	0.04042	FGGY_C	FGGY family of carbohydrate kinases, C-terminal domain	650
AO090010000219	0.9667	0.04044	ABC2_membrane	ABC-2 type transporter	651
AO090023000786	-1.258	0.04046	NPD	2-nitropropane dioxygenase	652
AO090011000712	-0.9046	0.04063	p450	Cytochrome P450	653
AO090023000136	-1.4426	0.04065	HEAT	HEAT repeat	654
AO090009000286	-0.6466	0.04065	DUF1771	Domain of unknown function (DUF1771)	655
AO090010000534	0.9258	0.04077	Peptidase_S10	Serine carboxypeptidase	656
AO090005001116	0.7982	0.04084	Adap_comp_sub	Adaptor complexes medium subunit family	657
AO090005000972	0.5599	0.04085	UDPG_MGDP_dh_C	UDP-glucose/GDP-mannose dehydrogenase family, UDP binding dor	658
AO090012000837	-0.7203	0.04095	UQ_con	Ubiquitin-conjugating enzyme	659
AO090001000684	0.5606	0.04101	RRM_1	RNA recognition motif. (a.k.a. RRM, RBD, or RNP domain)	660
AO090020000352	-0.7579	0.04101	HET	Heterokaryon incompatibility protein (HET)	661
AO090701000046	-0.9604	0.04107	2-Hacid_dh_C	D-isomer specific 2-hydroxyacid dehydrogenase, NAD binding domair	662
AO090010000014	0.5214	0.04108	ACOX	Acyl-CoA oxidase	663
AO090020000571	-1.931	0.04109	CN_hydrolase	Carbon-nitrogen hydrolase	664
AO090026000507	-1.4573	0.04113	MFS_1	Major Facilitator Superfamily	665
AO090003001412	-1.5055	0.04121	Amidase	Amidase	666
AO090011000722	-0.7205	0.04122	Usp	Universal stress protein family	667
AO090005001209	-1.1825	0.04131	Clp_N	Clp amino terminal domain	668
AO090011000659	-0.7909	0.04154	PGI	Phosphoglucose isomerase	669
AO090026000629	-0.5853	0.04190	Yippee	Yippee putative zinc-binding protein	670
AO090010000164	-0.612	0.04195	Ank	Ankyrin repeat	671
AO090012000670	-1.6865	0.04203	CsbD	CsbD-like	672
AO090011000167	0.4555	0.04217	DUF1212	Protein of unknown function (DUF1212)	673
AO090701000002	-0.7118	0.04223	Asp	Eukaryotic aspartyl protease	674
AO090026000607	-1.0517	0.04233	GATase	Glutamine amidotransferase class-I	675
AO090102000621	-1.0093	0.04235	HSP90	Hsp90 protein	676
AO090020000704	0.5041	0.04238	4HBT	Thioesterase superfamily	677
AO090005001228	-0.7494	0.04239	AMP-binding	AMP-binding enzyme	678
AO090038000234	0.5473	0.04240	Alpha-amylase	Alpha amylase, catalytic domain	679
AO090701000656	0.5077	0.04252	adh_short	short chain dehydrogenase	680
AO090020000572	0.4837	0.04254	ABC_tran	ABC transporter	681
AO090010000239	-0.5263	0.04268	Fungal_trans	Fungal specific transcription factor domain	682
AO090023000518	-1.062	0.04274	NAD_binding_2	NAD binding domain of 6-phosphogluconate dehydrogenase	683
AO090012000768	0.8069	0.04277	GATA	GATA zinc finger	684
AO090138000154	-0.5756	0.04293	HET	Heterokaryon incompatibility protein (HET)	685
AO090206000117	-1.2858	0.04296	Methyltransf_12	Methyltransferase domain	686
AO090023000772	-0.5353	0.04298	cobW	CobW/HypB/UreG, nucleotide-binding domain	687
AO090038000505	0.825	0.04313	Acetyltransf_1	Acetyltransferase (GNAT) family	688
AO090009000015	0.9793	0.04325	Aa_trans	Transmembrane amino acid transporter protein	689
AO090012000942	-0.5412	0.04329	Abhydrolase_1	alpha/beta hydrolase fold	690
AO090124000083	0.7673	0.04331	Ketoacyl-synt_C	Beta-ketoacyl synthase, C-terminal domain	691
AO090026000062	-0.4628	0.04332	PALP	Pyridoxal-phosphate dependent enzyme	692
AO090026000712	0.6306	0.04335	MHYT	Bacterial signalling protein N terminal repeat	693
AO090003000252	-0.4671	0.04337	Abhydrolase_1	alpha/beta hydrolase fold	694
AO090701000599	-0.7558	0.04345	tRNA-synt_1c_C	tRNA synthetases class I (E and Q), anti-codon binding domain	695
AO090020000495	-1.2402	0.04347	Biotin_carb_C	Biotin carboxylase C-terminal domain	696
AO090005000808	-1.5799	0.04349	WD40	WD domain, G-beta repeat	697
AO090005001510	-0.4684	0.04359	Oxysterol_BP	Oxysterol-binding protein	698
AO090103000494	-3.6999	0.04365	p450	Cytochrome P450	699
AO090023000927	1.4245	0.04366	adh_short	short chain dehydrogenase	700

LOCUS	Coef	F.p.value	PFAM_NAME	PFAM_DESCRIPTION	
AO090038000302	-0.9215	0.04400	DUF1604	Protein of unknown function (DUF1604)	701
AO090011000220	0.4447	0.04401	Fungal_trans	Fungal specific transcription factor domain	702
AO090012000813	0.4677	0.04409	Glyco_hydro_72	Glycolipid anchored surface protein (GAS1)	703
AO090701000093	0.6604	0.04410	Ribosomal_S9	Ribosomal protein S9/S16	704
AO090003001027	-0.4953	0.04410	LRR_1	Leucine Rich Repeat	705
AO090003000594	-0.6694	0.04410	Glycos_transf_2	Glycosyl transferase family 2	706
AO090010000533	-0.7346	0.04412	NmrA	NmrA-like family	707
AO090005000166	-0.7526	0.04426	MFS_1	Major Facilitator Superfamily	708
AO090005001512	-0.5217	0.04431	Oxysterol_BP	Oxysterol-binding protein	709
AO090701000526	1.717	0.04444	KR	KR domain	710
AO090003001362	0.4502	0.04445	Zn_clus	Fungal Zn(2)-Cys(6) binuclear cluster domain	711
AO090020000611	-0.4773	0.04454	MFS_1	Major Facilitator Superfamily	712
AO090005000650	-0.5555	0.04464	AA_permease	Amino acid permease	713
AO090113000104	-0.4503	0.04472	adh_short	short chain dehydrogenase	714
AO090120000293	-0.8474	0.04479	AAA_5	ATPase family associated with various cellular activities (AAA)	715
AO090023000591	0.5777	0.04479	Fungal_trans	Fungal specific transcription factor domain	716
AO090003001243	-0.9045	0.04484	DUF77	Domain of unknown function DUF77	717
AO090138000024	-1.6036	0.04510	HisKA	His Kinase A (phosphoacceptor) domain	718
AO090005001479	-0.7588	0.04532	Met_10	Met-10+ like-protein	719
AO090005001009	0.7068	0.04538	Mtc	Tricarboxylate carrier	720
AO090103000442	-0.4498	0.04539	p450	Cytochrome P450	721
AO090701000518	-0.443	0.04539	HATPase_c	Histidine kinase-, DNA gyrase B-, and HSP90-like ATPase	722
AO090003001501	2.0936	0.04539	Glyco_transf_5	Starch synthase catalytic domain	723
AO090102000117	-0.6286	0.04543	NOC3p	Nucleolar complex-associated protein	724
AO090010000633	-0.7147	0.04544	Cupin_2	Cupin domain	725
AO090001000077	-0.5683	0.04547	S1-P1_nuclease	S1/P1 Nuclease	726
AO090005001564	-0.6729	0.04554	Iso_dh	Isocitrate/isopropylmalate dehydrogenase	727
AO090012000397	2.8423	0.04554	2OG-FeII_Oxy	2OG-Fe(II) oxygenase superfamily	728
AO090010000574	1.8176	0.04559	adh_short	short chain dehydrogenase	729
AO090003000526	0.5362	0.04560	TauD	Taurine catabolism dioxygenase TauD, TfdA family	730
AO090005000216	0.5151	0.04562	NAD_binding_4	Male sterility protein	731
AO090003000246	0.49	0.04563	Pkinase	Protein kinase domain	732
AO090023000444	0.5522	0.04570	PP-binding	Phosphopantetheine attachment site	733
AO090011000600	0.4588	0.04573	Aminotran_4	Aminotransferase class IV	734
AO090012000788	-0.4979	0.04587	Band_7	SPFH domain / Band 7 family	735
AO090120000492	-0.9833	0.04590	Pro_isomerase	Cyclophilin type peptidyl-prolyl cis-trans isomerase/CLD	736
AO090009000066	1.4099	0.04600	Aldolase_II	Class II Aldolase and Adducin N-terminal domain	737
AO090120000377	1.8606	0.04612	AMP-binding	AMP-binding enzyme	738
AO090005000613	-0.6659	0.04612	HEAT	HEAT repeat	739
AO090005001128	-0.5075	0.04617	Pkinase	Protein kinase domain	740
AO090020000170	-0.609	0.04625	TPR_2	Tetratricopeptide repeat	741
AO090020000096	-0.5596	0.04647	Dabb	Stress responsive A/B Barrel Domain	742
AO090124000004	-0.9553	0.04653	adh_short	short chain dehydrogenase	743
AO090026000225	-0.503	0.04664	Sec1	Sec1 family	744
AO090012000476	-0.817	0.04666	TFIID-18kDa	Transcription initiation factor IID, 18kD subunit	745
AO090012000143	3.9351	0.04669	DUF895	Eukaryotic protein of unknown function (DUF895)	746
AO090005000805	-1.1444	0.04671	Helicase_C	Helicase conserved C-terminal domain	747
AO090102000184	0.7718	0.04676	RTA1	RTA1 like protein	748
AO090003000896	-0.4495	0.04682	PSP1	PSP1 C-terminal conserved region	749
AO090003000548	-1.0999	0.04691	Methyltransf_12	Methyltransferase domain	750
AO090001000124	0.5571	0.04697	MFS_1	Major Facilitator Superfamily	751
AO090206000020	-0.7266	0.04701	Na_Ca_ex	Sodium/calcium exchanger protein	752
AO090003000693	-0.8677	0.04711	Asp	Eukaryotic aspartyl protease	753
AO090701000525	2.347	0.04713	FAD_binding_4	FAD binding domain	754
AO090020000536	0.4387	0.04717	adh_short	short chain dehydrogenase	755
AO090003001336	-2.051	0.04725	Acid_phosphat_A	Histidine acid phosphatase	756
AO090011000447	-0.6671	0.04726	AMP-binding	AMP-binding enzyme	757
AO090010000340	0.7638	0.04737	Amino_oxidase	Flavin containing amine oxidoreductase	758
AO090102000377	-1.3537	0.04742	Sulfatase	Sulfatase	759
AO090701000583	-0.6719	0.04781	PALP	Pyridoxal-phosphate dependent enzyme	760
AO090012000721	-0.4715	0.04802	Palm_thioest	Palmitoyl protein thioesterase	761
AO090102000135	-1.0092	0.04809	MFS_1	Major Facilitator Superfamily	762
AO090012000754	-1.0297	0.04840	Fungal_trans	Fungal specific transcription factor domain	763
AO090005000355	1.0186	0.04843	TRP	Transient receptor potential (TRP) ion channel	764
AO090010000492	-0.7278	0.04850	DPBB_1	Rare lipoprotein A (RlpA)-like double-psi beta-barrel	765
AO090005000577	0.6938	0.04853	Myosin_TH1	Myosin tail	766
AO090120000463	-0.6527	0.04857	MFS_1	Major Facilitator Superfamily	767
AO090001000617	-3.4842	0.04858	BBE	Berberine and berberine like	768
AO090009000209	1.0716	0.04868	WSC	WSC domain	769
AO090120000165	-0.7882	0.04869	FMN_dh	FMN-dependent dehydrogenase	770
AO090020000137	0.5648	0.04871	Fungal_trans	Fungal specific transcription factor domain	771
AO090003000748	-0.4662	0.04876	GFO_IDH_MocA	Oxidoreductase family, NAD-binding Rossmann fold	772
AO090103000407	-0.8702	0.04876	UQ_con	Ubiquitin-conjugating enzyme	773
AO090011000676	0.456	0.04877	Pec_lyase_C	Pectate lyase	774
AO090012000119	-0.4777	0.04890	F420_oxidored	NADP oxidoreductase coenzyme F420-dependent	775
AO090038000623	-0.4321	0.04893	Malic_M	Malic enzyme, NAD binding domain	776
AO090020000634	-0.4823	0.04896	AhpC-TSA	AhpC/TSA family	777
AO090011000215	-3.1095	0.04898	HLH	Helix-loop-helix DNA-binding domain	778
AO090020000203	-0.5621	0.04911	DFP	DNA / pantothenate metabolism flavoprotein	779
AO090026000516	-0.645	0.04911	E1_DerP2_DerF2	ML domain	780
AO090010000237	-0.4973	0.04915	Fungal_trans	Fungal specific transcription factor domain	781
AO090001000350	-0.5935	0.04939	Glyco_hydro_7	Glycosyl hydrolase family 7	782
AO090012000807	-0.451	0.04947	XPG_I	XPG I-region	783
AO090003000942	-2.0179	0.04961	Methyltransf_12	Methyltransferase domain	784
AO090701000172	-0.6434	0.04969	Aldedh	Aldehyde dehydrogenase family	785
AO090010000129	0.4425	0.04982	Bac_luciferase	Luciferase-like monooxygenase	786
AO090005001079	0.4814	0.04988	ADH_zinc_N	Zinc-binding dehydrogenase	787
AO090012000219	-0.85	0.04990	Biotin_lipoyl	Biotin-requiring enzyme	788
AO090103000002	-0.5199	0.04996	Pro_isomerase	Cyclophilin type peptidyl-prolyl cis-trans isomerase/CLD	789
AO090038000350	-0.7544	0.05002	Ank	Ankyrin repeat	790
AO090012000029	-0.7426	0.05002	Methyltransf_12	Methyltransferase domain	791
AO090012000843	0.5792	0.05004	ChAPs	ChAPs (Chs5p-Arf1p-binding proteins)	792
AO090020000561	0.4772	0.05006	Opi1	Transcription factor Opi1	793
AO090020000508	0.5176	0.05017	Lipase_GDSL	GDSL-like Lipase/Acylhydrolase	794
AO090020000531	0.4739	0.05029	DUF1479	Protein of unknown function (DUF1479)	795
AO090026000627	-1.4048	0.05043	Yippee	Yippee putative zinc-binding protein	796

Appendix II

Table A.II: List of 19 *A. oryzae* genes with significantly changed expression indices with bidirectional best hits in *A. niger* which are also significantly changed. The *A. oryzae* test is RJH vs. Intermig impellers, while the *A. niger* is increased impeller speed.

A. oryzae		*A. niger*			SwissProt best hit		
ID	Fold change	ID	Fold change	Same direction?	Organism	Recommended name	PubMed IDs
AO090003000246	0.490	52941	1.132	Yes	-	-	-
AO090011000337	-2.397	184932	-1.340	Yes	-	-	-
AO090011000876	-1.698	211661	-1.161	Yes	Neocallimastix frontalis (Rumen fungus)	Malic enzyme, hydrogenosomal	9004216
AO090023000318	-1.667	193984	-0.734	Yes	Schizosaccharomyces pombe (Fission yeast)	Malic acid transport protein	8750236 11859360 18257517
AO090001000290	-0.709	40478	3.098	No	-	-	-
AO090001000692	-1.236	131319	1.089	No	Emericella nidulans (Aspergillus nidulans)	Siderophore iron transporter mirC	12487628 16372000
AO090003001112	-0.844	214348	0.460	No	Emericella nidulans (Aspergillus nidulans)	Acetyl-coenzyme A synthetase	1972535 16372000
AO090003001501	2.094	212954	-0.709	No	-	-	-
AO090005001449	-0.940	50467	1.638	No	Schizosaccharomyces pombe (Fission yeast)	Pyridoxal reductase	9501991 11859360 10438489 10705982 18257517
AO090005001454	-0.551	124393	4.139	No	-	-	-
AO090011000646	0.772	48934	-0.564	No	-	-	-
AO090011000659	-0.791	210433	0.544	No	Aspergillus oryzae	Glucose-6-phosphate isomerase	16372010
AO090012000788	-0.498	172938	1.125	No	-	-	-
AO090020000072	-1.610	178371	1.137	No	-	-	-
AO090038000395	-1.264	208318	0.525	No	Aspergillus oryzae	Phosphoglycerate kinase	16372010
AO090120000260	-0.909	209490	0.305	No	-	-	-
AO090120000463	-0.653	49380	0.873	No	Aspergillus fumigatus (Sartorya fumigata)	Probable transporter mch1	16372009
AO090701000175	-0.467	53423	0.635	No	Saccharomyces cerevisiae (Baker's yeast)	Probable 2-methylcitrate dehydratase	9169875 14562106
AO090701000353	-1.778	204315	2.169	No	-	-	-

Appendix III

A. oryzae		*A. niger*		SwissProt Best hits			
ID	Corr	ID	Corr	Organism	Recommended full name	ECs	
AO090010000753	-0.8407	191158	1.292453	Saccharomyces cerevisiae (Baker's yeast)	Uncharacterized membrane protein YCR061W	-	1
AO090003000149	-0.8375	178051	0.512337	Schizosaccharomyces pombe (Fission yeast)	Leptomycin B resistance protein pmd1	-	2
AO090020000119	-0.823	209098	1.10254	Aspergillus fumigatus (Sartorya fumigata)	Uncharacterized protein AFUA_6G02800	-	3
AO090012000476	-0.817	176339	0.521319	Schizosaccharomyces pombe (Fission yeast)	Uncharacterized protein C17G6.02c	-	4
AO090011000659	-0.7909	210433	0.15526	Saccharomyces cerevisiae (Baker's yeast)	Siderophore iron transporter 1	-	5
AO090120000165	-0.7882	49535	0.473744	Saccharomyces cerevisiae (Baker's yeast)	Ubiquinone biosynthesis protein COQ4, mitochondrial	-	6
AO090026000514	-0.7824	36816	0.737902	Schizosaccharomyces pombe (Fission yeast)	Probable mitochondrial phosphate carrier protein	-	7
AO090005001641	-0.7646	177851	0.683728	Schizosaccharomyces pombe (Fission yeast)	Pentatricopeptide repeat-containing protein C1093.01	-	8
AO090020000005	-0.7577	178675	0.964595	Schizosaccharomyces pombe (Fission yeast)	Uncharacterized protein C1840.09	-	9
AO090012000554	-0.7331	55763	1.526833	Schizosaccharomyces pombe (Fission yeast)	UPF0613 protein PB24D3.06c	-	10
AO090005000460	-0.7289	209881	1.154909	Schizosaccharomyces pombe (Fission yeast)	UPF0103 protein C4H3.04c	-	11
AO090206000020	-0.7266	184561	0.848915	Emericella nidulans (Aspergillus nidulans)	Uncharacterized protein AN7484	-	12
AO090012000837	-0.7203	174644	1.269098	Schizosaccharomyces pombe (Fission yeast)	Probable mitochondrial chaperone bcs1	-	13
AO090102000352	-0.7185	129928	0.642833	Emericella nidulans (Aspergillus nidulans)	**30 kDa heat shock protein**	-	14
AO090011000368	-0.7181	43297	1.089011	Emericella nidulans (Aspergillus nidulans)	Siderophore iron transporter mirC	-	15
AO090005000162	-0.7165	54806	1.549978	Schizosaccharomyces pombe (Fission yeast)	Protein psi1	-	16
AO090011000456	-0.7142	39912	0.476278	Penicillium chrysogenum (strain ATCC 28089 /	Autophagy-related protein 8	-	17
AO090701000002	-0.7138	53364	0.194951	Neurospora crassa	**Heat shock protein HSP98**	-	18
AO090701000709	-0.7041	50680	2.875663	Schizosaccharomyces pombe (Fission yeast)	**DNA repair protein rhp41**	-	19
AO090003000402	-0.6955	207710	1.582268	Candida albicans (Yeast)	ABC transporter CDR4	-	20
AO090026000537	-0.695	197123	0.507973	Gibberella zeae (Fusarium graminearum)	Protein RDR1	-	21
AO090003001095	-0.6925	45408	0.291377	Schizosaccharomyces pombe (Fission yeast)	Uncharacterized MFS-type transporter C530.15c	-	22
AO090023000163	-0.672	211236	0.280583	Saccharomyces kluyveri (Yeast) (Saccharomyce	Cell division control protein 25	-	23
AO090701000750	-0.6707	54713	2.14299	Schizosaccharomyces pombe (Fission yeast)	Meiotically up-regulated gene 190 protein	-	24
AO090012000537	-0.67	52653	0.169879	Saccharomyces cerevisiae (Baker's yeast)	Mitochondrial clpX-like chaperone MCX1	-	25
AO090011000447	-0.6671	121695	0.003212	Emericella nidulans (Aspergillus nidulans)	Tubulin alpha-2 chain	-	26
AO090005000613	-0.6659	194073	1.573735	Schizosaccharomyces pombe (Fission yeast)	Uncharacterized transporter C1529.01	-	27
AO090020000618	-0.6604	212549	0.04974	Schizosaccharomyces pombe (Fission yeast)	Uncharacterized AIM2 family protein C30D10.14	-	28
AO090120000463	-0.6527	49380	2.070895	Saccharomyces cerevisiae (Baker's yeast)	**Drug resistance protein YOR378W**	-	29
AO090026000516	-0.645	206645	0.642227	Cochliobolus carbonum (Bipolaris zeicola)	Putative HC-toxin efflux carrier TOXA	-	30
AO090005000995	-0.643	51801	0.193145	Emericella nidulans (Aspergillus nidulans)	Catabolite repression protein creC	-	31
AO090003000055	-0.6417	202692	0.373659	Aspergillus oryzae	Mediator of RNA polymerase II transcription subunit 12	-	32
AO090012001016	-0.6311	120955	1.138564	Schizosaccharomyces pombe (Fission yeast)	Protein spt3	-	33
AO090023000531	-0.6198	46465	0.961278	Cochliobolus heterostrophus (Drechslera maye	Fatty acid transporter protein	-	34
AO090011000917	-0.5971	185892	0.368533	Schizosaccharomyces pombe (Fission yeast)	Meiotic recombination protein rec14	-	35
AO090001000350	-0.5935	208139	0.352979	Schizosaccharomyces pombe (Fission yeast)	Zinc finger protein C1039.05c	-	36
AO090120000493	-0.5926	56602	0.29821	Saccharomyces cerevisiae (Baker's yeast)	Putative cation exchanger YNL321W	-	37
AO090701000280	-0.5727	57253	0.368106	Schizosaccharomyces pombe (Fission yeast)	Uncharacterized WD repeat-containing protein C343.04c	-	38
AO090120000485	-0.5678	211200	0.648189	Saccharomyces cerevisiae (Baker's yeast)	Catabolite repression protein CAT5	-	39
AO090003001407	-0.5611	177276	1.945962	Schizosaccharomyces pombe (Fission yeast)	Ankyrin repeat-containing protein C1827.04	-	40
AO090012000592	-0.5349	52670	0.803796	Saccharomyces cerevisiae (Baker's yeast)	Rab GDP-dissociation inhibitor	-	41
AO090026000225	-0.503	206787	0.76635	Schizosaccharomyces pombe (Fission yeast)	Uncharacterized protein C3F10.06c	-	42
AO090005001066	-0.4997	184552	0.578163	Aspergillus fumigatus (Sartorya fumigata)	FAS1 domain-containing protein AFUA_8G05360	-	43
AO090020000634	-0.4823	199434	0.873358	Aspergillus fumigatus (Sartorya fumigata)	Probable transporter mch1	-	44
AO090001000710	-0.4786	55651	0.635564	Aspergillus oryzae	Phosphatidylglycerol/phosphatidylinositol transfer protein	-	45
AO090701000175	-0.4666	53423	1.787078	Schizosaccharomyces pombe (Fission yeast)	UPF0061 protein C20G4.05c	-	46
AO090038000623	-0.4321	203210	0.669416	Schizosaccharomyces pombe (Fission yeast)	UPF0675 protein C2D10.04	-	47
AO090012000813	0.4677	207134	1.043915	Saccharomyces cerevisiae (Baker's yeast)	DOA4-independent degradation protein 4	-	48
AO090166000068	0.5521	189003	1.199825	Aspergillus oryzae	Actin cytoskeleton-regulatory complex protein end3	-	49
AO090023000444	0.5522	51499	0.522565	Schizosaccharomyces pombe (Fission yeast)	Vacuolar protein sorting-associated protein 33	-	50
AO090012000418	0.5697	210182	2.826443	Saccharomyces cerevisiae (Baker's yeast)	ABC transporter ATP-binding protein ARB1	-	51
AO090005001636	0.6108	52839	0.536479	Saccharomyces cerevisiae (Baker's yeast)	Protein MSS51, mitochondrial	-	52
AO090001000634	0.6549	39382	-0.453909	Saccharomyces cerevisiae (Baker's yeast)	Glycolipid-anchored surface protein 2	-	53
AO090120000158	0.6644	46429	-0.490305	Schizosaccharomyces pombe (Fission yeast)	Uncharacterized msc5 family protein C2C4.17c	-	54
AO090003001387	0.7153	54095	-0.199771	Schizosaccharomyces pombe (Fission yeast)	Uncharacterized RING finger protein C2F3.16	-	55
AO090124000083	0.7673	55511	-0.244866	Saccharomyces cerevisiae (Baker's yeast)	Vacuolar calcium ion transporter	-	56
AO090011000126	0.8478	184679	-0.581807	Emericella nidulans (Aspergillus nidulans)	Quinate permease	-	57
AO090010000534	0.9258	56161	-0.579606	Saccharomyces cerevisiae (Baker's yeast)	Vacuolar calcium ion transporter	-	58
AO090005001154	1.2657	170261	-0.29937	Saccharomyces cerevisiae (Baker's yeast)	Uncharacterized membrane protein YCR023C	-	59
AO090012000168	1.2855	211068	-0.00751	Schizosaccharomyces pombe (Fission yeast)	Uncharacterized protein C691.05c	-	60
AO090026000255	1.7836	175333	-0.280316	Debaryomyces occidentalis (Yeast) (Schwanni	High affinity potassium transporter	-	61
AO090005000114	1.8991	204165	-1.941995	Saccharomyces cerevisiae (Baker's yeast)	General amino-acid permease GAP1	-	62
AO090003001112	-0.844	214348	0.226539	Schizosaccharomyces pombe (Fission yeast)	Uncharacterized hydroxylase C887.15c	1.-.-.-	63
AO090120000293	-0.8474	56770	2.376564	Schizosaccharomyces pombe (Fission yeast)	Putative 2-hydroxyacid dehydrogenase UNK4.10	1.-.-.-	64
AO090023000039	-0.8504	121822	0.555242	Schizosaccharomyces pombe (Fission yeast)	Uncharacterized oxidoreductase C2F3.05c	1.-.-.-	65
AO090103000099	-0.8618	131508	0.497932	Saccharomyces cerevisiae (Baker's yeast)	Inositolphosphorylceramide-B C-26 hydroxylase	1.-.-.-	66
AO090003000693	-0.8677	37080	0.678298	Schizosaccharomyces pombe (Fission yeast)	Putative aryl-alcohol dehydrogenase C977.14c	1.1.1.-	67
AO090103000407	-0.8702	52536	0.081093	Schizosaccharomyces pombe (Fission yeast)	2-hydroxyacid dehydrogenase homolog 2	1.1.1.-	68
AO090090000495	-0.8736	56645	1.309455	Schizosaccharomyces pombe (Fission yeast)	Alcohol dehydrogenase	1.1.1.1	69
AO090026000778	-0.8872	132595	0.044534	Emericella nidulans (Aspergillus nidulans)	Alcohol dehydrogenase 2	1.1.1.1	70
AO090103000169	-0.8887	191350	0.076226	Aspergillus flavus (strain ATCC 200026 / NRRL	Alcohol dehydrogenase 1	1.1.1.1	71
AO090005001111	-0.9375	205375	1.637565	Schizosaccharomyces pombe (Fission yeast)	Pyridoxal reductase	1.1.1.65	72
AO090012000417	-0.9382	56329	1.174034	Candida boidinii (Yeast)	Alcohol oxidase	1.1.3.13	73
AO090005000882	-0.9386	131120	3.927212	Pichia angusta (Yeast) (Hansenula polymorpha	Alcohol oxidase	1.1.3.13	74
AO090005001449	-0.9398	50467	0.359067	Saccharomyces cerevisiae (Baker's yeast)	**Mitochondrial peroxiredoxin PRX1**	1.11.1.15	75
AO090005000630	-0.9472	214534	0.16556	Saccharomyces cerevisiae (Baker's yeast)	**Peroxiredoxin HYR1**	1.11.1.15	76
AO090003001108	-0.952	55013	1.030194	Saccharomyces cerevisiae (Baker's yeast)	Indoleamine 2,3-dioxygenase family protein	1.13.11.-	77
AO090701000046	-0.9604	124156	0.569643	Candida albicans (Yeast)	Catechol 1,2-dioxygenase	1.13.11.1	78
AO090023000932	-0.9707	213321	0.579051	Aspergillus oryzae	3-hydroxyanthranilate 3,4-dioxygenase 1	1.13.11.6	79
AO090102000246	-0.988	53518	0.778765	Ustilago maydis (Smut fungus)	L-ornithine 5-monooxygenase	1.13.12.-	80
AO090005000125	-1.0043	44729	0.616935	Schizosaccharomyces pombe (Fission yeast)	Uncharacterized lactate 2-monooxygenase PB1A11.03	1.13.12.4	81
AO090102000135	-1.0092	51421	0.078253	Schizosaccharomyces pombe (Fission yeast)	Dihydroceramide delta(4)-desaturase	1.14.-.-	82
AO090010000463	-1.0198	56583	0.055516	Cylindrocarpon tonkinense (Cylindrocarpon lic	Cytochrome P450 53A3	1.14.-.-	83
AO090102000554	-1.0496	189208	1.952682	Saccharomyces cerevisiae (Baker's yeast)	Alpha-ketoglutarate-dependent sulfonate dioxygenase	1.14.11.-	84
AO090003001209	-1.0499	214233	2.362961	Emericella nidulans (Aspergillus nidulans)	Putative sterigmatocystin biosynthesis monooxygenase stcW	1.14.13.-	85
AO090012000264	-1.0878	40734	0.855237	Saccharomyces cerevisiae (Baker's yeast)	C-4 methylsterol oxidase	1.14.13.72	86
AO090023000314	-1.0923	51281	0.900808	Saccharomyces cerevisiae (Baker's yeast)	Ferric/cupric reductase transmembrane component 2	1.16.1.-	87
AO090113000137	-1.1105	189096	0.515993	Schizosaccharomyces pombe (Fission yeast)	Putative aldehyde dehydrogenase-like protein C922.07c	1.2.1.-	88
AO090038000303	-1.1138	208246	1.249251	Emericella nidulans (Aspergillus nidulans)	Probable formate dehydrogenase	1.2.1.2	89
AO090023000893	-1.1169	213277	1.379239	Saccharomyces cerevisiae (Baker's yeast)	Potassium-activated aldehyde dehydrogenase, mitochondrial	1.2.1.3	90
AO090003000289	-1.1585	189204	1.946431	Alternaria alternata (Alternaria rot fungus)	Aldehyde dehydrogenase	1.2.1.3	91
AO090023000692	-1.1811	57027	0.399995	Saccharomyces cerevisiae (Baker's yeast)	Pyruvate dehydrogenase E1 component subunit beta, mitochon	1.2.4.1	92
AO090005001209	-1.1825	205443	0.382406	Saccharomyces cerevisiae (Baker's yeast)	Coproporphyrinogen III oxidase	1.3.3.3	93
AO090005000739	-1.1845	52326	2.101943	Magnaporthe grisea (Rice blast fungus) (Pyricu	NADH-cytochrome b5 reductase 2	1.6.2.2	94
AO090012000997	-1.1893	209252	0.397473	Aspergillus flavus	Uricase	1.7.3.3	95
AO090003000309	-1.1931	56311	0.708676	Saccharomyces cerevisiae (Baker's yeast)	FAD-linked sulfhydryl oxidase ERV2	1.8.3.2	96
AO090001000619	-1.197	208861	1.079025	Neurospora crassa	Endoplasmic oxidoreductin-1	1.8.4.-	97
AO090701000219	-1.2148	57261	-2.59234	Emericella nidulans (Aspergillus nidulans)	Conidial yellow pigment biosynthesis polyketide synthase	2.3.1.-	98
AO090001000692	-1.2357	131319	2.290126	Schizosaccharomyces pombe (Fission yeast)	Putative lysine N-acyltransferase C17G9.06c	2.3.1.-	99
AO090020000495	-1.2402	39990	-0.069164	Penicillium patulum (Penicillium griseofulvum)	Fatty acid synthase subunit alpha	2.3.1.86 1.1.1.100 2.3.1.41	100

A. oryzae		*A. niger*		SwissProt Best hits			
ID	Corr	ID	Corr	Organism	Recommended full name	ECs	
AO090038000395	-1.264	208318	0.356987	Yarrowia lipolytica (Candida lipolytica)	Acetyl-CoA acetyltransferase	2.3.1.9	101
AO090012000130	-1.293	39481	0.025364	Saccharomyces cerevisiae (Baker's yeast)	Glycogen phosphorylase	2.4.1.1	102
AO090011000149	-1.3112	40809	0.354833	Schizosaccharomyces pombe (Fission yeast)	Putative alpha,alpha-trehalose-phosphate synthase [UDP-formin	2.4.1.15	103
AO090023000349	-1.318	192202	0.289352	Schizosaccharomyces pombe (Fission yeast)	Putative uracil phosphoribosyltransferase urg2	2.4.2.9	104
AO090026000820	-1.3229	119606	0.251053	Schizosaccharomyces pombe (Fission yeast)	Aspartate aminotransferase, cytoplasmic	2.6.1.1	105
AO090701000554	-1.3302	56751	0.172053	Kluyveromyces lactis (Yeast) (Candida sphaeric	Hexokinase	2.7.1.1	106
AO090026000803	-1.3336	40569	0.397355	Saccharomyces cerevisiae (Baker's yeast)	Probable protein kinase YGL059W	2.7.11.-	107
AO090011000679	-1.386	56390	0.319897	Fusarium solani subsp. pisi (Nectria haematoc	Mitogen-activated protein kinase	2.7.11.24	108
AO090012000132	-1.4043	209473	0.525226	Aspergillus oryzae	Phosphoglycerate kinase	2.7.2.3	109
AO090001000689	-1.4129	47182	1.177414	Saccharomyces cerevisiae (Baker's yeast)	Phosphoinositide phosphatase SAC1	3.1.3.-	110
AO090005001525	-1.4232	209410	0.645359	Aspergillus oryzae	3-phytase A	3.1.3.8	111
AO090103000406	-1.4359	44808	0.048961	Aspergillus oryzae	Alpha-glucosidase	3.2.1.20	112
AO090701000398	-1.4412	213851	-0.153652	Aspergillus niger	Beta-galactosidase	3.2.1.23	113
AO090026000639	-1.4447	181179	0.344945	Emericella nidulans (Aspergillus nidulans)	Acid trehalase	3.2.1.28	114
AO090001000592	-1.4787	208917	0.403677	Aspergillus tubingensis	Exopolygalacturonase	3.2.1.67	115
AO090701000751	-1.4788	213512	-0.506165	Aspergillus niger	Serine-type carboxypeptidase F	3.4.16.-	116
AO090103000170	-1.5088	50657	0.704559	Schizosaccharomyces pombe (Fission yeast)	Putative Lon protease homolog, mitochondrial	3.4.21.-	117
AO090003001250	-1.5518	193227	0.533694	Aspergillus oryzae	Probable cysteine protease atg4	3.4.22.-	118
AO090005000804	-1.5601	171821	1.021984	Saccharomycopsis fibuligera (Yeast)	Acid protease	3.4.23.-	119
AO090010000472	-1.5622	201613	0.701738	Neurospora crassa	Vacuolar protease A	3.4.23.-	120
AO090005001430	-1.5731	52427	0.758218	Saccharomyces cerevisiae (Baker's yeast)	Histone deacetylase RPD3	3.5.1.98	121
AO090020000109	-1.6523	178864	0.078808	Schizosaccharomyces pombe (Fission yeast)	Uracil-regulated protein 1	3.5.4.-	122
AO090102000525	-1.703	212473	0.837082	Schizosaccharomyces pombe (Fission yeast)	Probable guanine deaminase	3.5.4.3	123
AO090120000052	-1.7222	52061	1.245716	Saccharomyces cerevisiae (Baker's yeast)	Structure-specific endonuclease subunit SLX1	3.6.1.-	124
AO090023000256	-1.7246	38774	0.749965	Aspergillus oryzae	ATP-dependent DNA helicase mph1	3.6.1.-	125
AO090120000179	-1.7834	42171	0.038929	Aspergillus oryzae	Pyruvate decarboxylase	4.1.1.1	126
AO090011000747	-1.8508	185794	0.611574	Saccharomyces cerevisiae (Baker's yeast)	Mitochondrial 2-methylisocitrate lyase	4.1.3.30	127
AO090005001117	-1.8999	51702	0.456925	Aspergillus oryzae	Enolase	4.2.1.11	128
AO090011000588	-1.9969	55563	0.635213	Saccharomyces cerevisiae (Baker's yeast)	Probable 2-methylcitrate dehydratase	4.2.1.79	129
AO090005000471	-2.1775	171904	0.60254	Saccharomyces cerevisiae (Baker's yeast)	Bifunctional protein GAL10	5.1.3.2 5.1.3.3	130
AO090120000176	-2.2334	42166	1.01222	Aspergillus oryzae	Serine/threonine-protein phosphatase 2A activator 2	5.2.1.8	131
AO090003000627	-2.3099	197391	0.961749	Aspergillus oryzae	Triosephosphate isomerase	5.3.1.1	132
AO090012000998	-2.4705	199734	0.153612	Aspergillus fumigatus (Sartorya fumigata)	Mannose-6-phosphate isomerase	5.3.1.8	133
AO090701000318	-2.5717	57243	0.543502	Aspergillus oryzae	Glucose-6-phosphate isomerase	5.3.1.9	134
AO090120000174	-2.5831	186088	-0.374231	Pneumocystis carinii	Lanosterol synthase	5.4.99.7	135
AO090103000166	-2.6965	191742	0.680649	Schizosaccharomyces pombe (Fission yeast)	Putative peroxisomal-coenzyme A synthetase	6.-.-.-	136
AO090011000926	-2.7726	56739	0.933964	Schizosaccharomyces pombe (Fission yeast)	Probable cysteinyl-tRNA synthetase, cytoplasmic	6.1.1.16	137
AO090023000577	-3.2002	51812	1.069692	Candida glabrata (Yeast) (Torulopsis glabrata)	Acetyl-coenzyme A synthetase 2	6.2.1.1	138
AO090003000392	-3.3587	52560	0.459999	Emericella nidulans (Aspergillus nidulans)	Acetyl-coenzyme A synthetase	6.2.1.1	139
AO090103000167	-3.863	191228	1.145585	Cochliobolus carbonum (Bipolaris zeicola)	HC-toxin synthetase	6.3.2.-	140
AO090166000070	-4.0901	48279	0.842205	Schizosaccharomyces pombe (Fission yeast)	Ubiquitin-conjugating enzyme E2 1	6.3.2.19	141
AO090012000601	-4.5329	52675	0.422687	Schizosaccharomyces pombe (Fission yeast)	Ubiquitin-conjugating enzyme E2 4	6.3.2.19	142
AO090010000667	-4.8723	44595	0.711284	Aspergillus fumigatus (Sartorya fumigata)	Ubiquitin-conjugating enzyme E2 2	6.3.2.19	143
AO090009000634	-5.0503	204476	0.619553	Schizosaccharomyces pombe (Fission yeast)	Ubiquitin-conjugating enzyme E2 8	6.3.2.19	144
AO090003000661	-6.1244	55573	0.358156	Saccharomyces cerevisiae (Baker's yeast)	Urea amidolyase	6.3.4.6 3.5.1.54	145
AO090003000770	-5.0178	52318	0.054926	-	-	-	146
AO090020000501	-3.8496	37333	0.502941	-	-	-	147
AO090012000174	-2.6367	201546	1.003311	-	-	-	148
AO090206000078	-2.3036	201359	0.61207	-	-	-	149
AO090010000203	-1.9901	53360	0.331216	-	-	-	150
AO090020000412	-2.6068	173855	0.504543	-	-	-	151
AO090120000376	2.8907	41978	-0.318715	-	-	-	152
AO090120000175	-2.5484	42165	0.919675	-	-	-	153
AO090009000496	-2.1146	119441	0.570925	-	-	-	154
AO090023000857	-1.7779	190247	0.163635	-	-	-	155
AO090003000006	-1.4452	43055	0.556137	-	-	-	156
AO090012001027	-2.1451	39560	1.182311	-	-	-	157
AO090011000699	-1.6632	56389	0.980857	-	-	-	158
AO090120000214	-2.6266	127693	1.056145	-	-	-	159
AO090001000738	-1.953	175113	0.617573	-	-	-	160
AO090003001008	-1.2902	189170	0.436021	-	-	-	161
AO090020000043	-1.5662	48178	1.316366	-	-	-	162
AO090701000273	-1.2943	213941	0.302388	-	-	-	163
AO090038000539	-1.2284	122895	0.338785	-	-	-	164
AO090103000367	-1.6766	181376	0.478399	-	-	-	165
AO090023000687	-1.5366	50466	1.524926	-	-	-	166
AO090003000141	-1.538	208713	0.225577	-	-	-	167
AO090701000353	-1.7783	204315	2.168691	-	-	-	168
AO090009000095	-1.0601	172257	0.100776	-	-	-	169
AO090010000650	-1.1322	204025	0.320672	-	-	-	170
AO090023000624	-3.5175	213016	1.58869	-	-	-	171
AO090003000316	-0.96	208826	0.566367	-	-	-	172
AO090003000624	-1.0527	206885	0.016901	-	-	-	173
AO090009000493	-2.5345	124867	0.250768	-	-	-	174
AO090003001519	-1.1893	194913	0.054633	-	-	-	175
AO090026000711	2.3163	36316	-0.192946	-	-	-	176
AO090120000103	-0.9755	211403	0.25176	-	-	-	177
AO090003000206	-1.3421	208663	1.399978	-	-	-	178
AO090026000248	-2.7055	44893	0.718817	-	-	-	179
AO090020000493	-1.0647	209685	0.245627	-	-	-	180
AO090003000980	-0.8993	56791	0.542478	-	-	-	181
AO090010000555	-1.0955	43391	0.461467	-	-	-	182
AO090023000304	-0.8748	39109	0.179493	-	-	-	183
AO090012000646	-1.5142	56914	0.118855	-	-	-	184
AO090009000516	-0.89	49499	0.904813	-	-	-	185
AO090701000639	-1.079	43342	1.620088	-	-	-	186
AO090012000787	-0.794	207158	0.967477	-	-	-	187
AO090020000504	1.1444	42809	-0.127267	-	-	-	188
AO090026000696	-1.7182	42898	1.053596	-	-	-	189
AO090038000173	-1.9255	189430	1.174767	-	-	-	190
AO090020000239	-0.8545	40693	0.150255	-	-	-	191
AO090038000427	-1.5467	52788	0.044477	-	-	-	192
AO090011000884	-1.1819	42502	1.936766	-	-	-	193
AO090010000210	-2.1089	203335	0.288141	-	-	-	194
AO090206000070	-1.204	41506	0.359268	-	-	-	195
AO090005001060	-0.8054	46416	0.45577	-	-	-	196
AO090011000751	-0.9614	41688	2.162536	-	-	-	197
AO090038000421	-1.4226	38532	0.985614	-	-	-	198
AO090026000278	-0.7549	170627	0.984307	-	-	-	199
AO090005001558	-0.8583	209363	0.207324	-	-	-	200

A0090701000534	0.745	172647	-0.292481	-	-	-
A0090012000975	-0.8597	209282	0.823726	-	-	-
A0090026000570	0.7819	180728	-0.394426	-	-	-
A0090005000775	-0.8318	206058	0.64053	-	-	-
A0090003001184	-1.0652	39083	0.897805	-	-	-
A0090003000593	-0.8933	210529	0.164655	-	-	-
A0090120000370	-0.8864	41983	1.426107	-	-	-
A0090003000869	-0.7771	55451	0.972615	-	-	-
A0090001000419	-1.0699	123517	0.542492	-	-	-
A0090003001376	0.808	195091	-1.113034	-	-	-
A0090020000199	-0.6723	47166	1.169158	-	-	-
A0090026000230	-0.9339	206799	0.408819	-	-	-
A0090003000979	-1.4648	42852	0.07415	-	-	-
A0090003000497	-0.7626	213437	0.196209	-	-	-
A0090701000791	1.743	191577	-0.868483	-	-	-
A0090120000256	-1.1848	53210	0.313087	-	-	-
A0090023000114	-1.5288	36654	0.011987	-	-	-
A0090026000168	1.568	36928	-0.470608	-	-	-
A0090023000883	-1.0157	57089	0.173427	-	-	-
A0090005000796	-1.2536	51952	0.787112	-	-	-
A0090005001229	-1.0855	202668	1.592593	-	-	-
A0090120000260	-0.9087	209490	0.304537	-	-	-
A0090005001300	-0.8892	210655	0.728623	-	-	-
A0090026000164	-0.9035	172999	0.326369	-	-	-
A0090102000483	-0.805	54341	0.502616	-	-	-
A0090005001429	-0.8137	173936	0.627251	-	-	-
A0090120000334	-1.0366	54106	0.394643	-	-	-
A0090113000134	-1.1209	42619	0.701664	-	-	-
A0090701000127	-0.9013	182845	0.79752	-	-	-
A0090003001094	-0.7331	55020	1.910087	-	-	-
A0090023000241	-1.8159	52865	0.910947	-	-	-
A0090003000465	-2.7845	207787	0.283158	-	-	-
A0090020000068	-0.8682	199618	0.620685	-	-	-
A0090001000237	0.7614	55789	-0.145291	-	-	-
A0090001000290	-0.7087	40478	3.097606	-	-	-
A0090102000622	-0.6249	50015	0.454469	-	-	-
A0090009000374	-0.5712	45032	3.371022	-	-	-
A0090023000278	0.7304	47819	-0.018512	-	-	-
A0090120000414	-0.6878	184554	0.725492	-	-	-
A0090009000492	-0.935	53931	0.521729	-	-	-
A0090005000823	-0.7077	46645	0.733686	-	-	-
A0090011000773	-1.9186	211565	0.895683	-	-	-
A0090023000611	-0.8958	213011	1.989694	-	-	-
A0090012000463	-0.5606	205573	1.505283	-	-	-
A0090012000956	-0.9294	56125	1.141147	-	-	-
A0090120000236	-0.6355	48323	4.925651	-	-	-
A0090003000241	-0.7358	38927	0.685941	-	-	-
A0090026000443	-0.9596	175251	0.213732	-	-	-
A0090206000108	-1.3119	185605	0.114424	-	-	-
A0090011000488	-0.6239	209561	0.536193	-	-	-
A0090009000558	-0.8184	48679	0.145373	-	-	-
A0090103000244	1.6084	131536	-0.59076	-	-	-
A0090005001346	-1.2926	53653	0.664069	-	-	-
A0090138000069	0.6242	174212	-1.053366	-	-	-
A0090003000209	0.5702	38852	-0.672178	-	-	-
A0090102000581	-0.5516	56877	0.469984	-	-	-
A0090038000433	-0.9941	124094	0.467538	-	-	-
A0090005001295	-1.0528	201122	0.791397	-	-	-
A0090023000060	0.7258	173459	-1.187277	-	-	-
A0090010000576	2.3212	193675	-1.726743	-	-	-
A0090003001208	-0.5668	139793	0.384785	-	-	-
A0090701000671	-0.5827	200638	0.12138	-	-	-
A0090020000197	-0.5477	37531	0.462476	-	-	-

CMB is an Engineering Center of Excellence funded by the Danish Research Agency. It is a collaboration between an acknowledged research manager, his/her institute and university, and the Research Agency. An Engineering Center of Excellence is a research institute of first-class quality with tradition for cooperation with industry.

Center for Microbial Biotechnology
Department of Systems Biology
Technical University of Denmark

Building 223
DK-2800 Kgs. Lyngby
Denmark

Phone: +45 4525 2690
Fax: +45 4588 4148

www.cmb.dtu.dk

ISBN-nr: 9788791494918